Seismic Safety Enhancement of Cable-stayed Bridges with Pseudo Negative Stiffness Dampers

Mulyo Harris Pradono

May 2003

Seismic Safety Enhancement of Cable-stayed Bridges with Pseudo Negative Stiffness Dampers

A Dissertation

Submitted to

the Graduate School of Engineering of Kyoto University

In Partial Fulfillment

of the Requirements for the Degree of

Doctor of Engineering

by

Mulyo Harris Pradono

May 2003

Summary

A rapid growing of cable-stayed bridges throughout the world spurred recent efforts on seismic protection of these structures. These flexible structures raise many concerns about their behavior under environmental dynamic loads such as wind, earthquake, and vehicular traffic-loads. The fact that these structures possess little damping characteristics to help alleviate vibration under severe ground motions, wind turbulence, and traffic loadings needed research to enhance the technology of structural control, because the control of these structures is a unique and challenging problem.

Due to recent development of sensoring and digital control techniques, active control methods of dynamic response of structures are developed and some are implemented to buildings and bridges. The merit of the active control is that they are effective for a wide-frequency range and also for the transient vibration. However, the active control methods needs a large amount of external energy supply which is not always available during strong earthquake attack and also a high level of maintenance. On the other hand, appropriately implemented semi-active systems which operate by using significantly small energy supply perform significantly better than passive devices and have the potential to achieve the majority of the performance of fully active systems. Moreover, in contrast to active control devices, semi-active control devices do not have the potential to destabilize (in the bounded input/bounded output sense) the structural system.

Recognizing the above facts, newly developed semi-active control that uses less sensors and much simpler control algorithm than commonly semi-active control is presented. The semi-active control produces pseudo negative stiffness hysteretic loop. Combination of this hysteretic loop with structure's elastic stiffness produces artificial hysteretic loop that approaches rigid-perfectly plastic force-deformation characteristics with large energy absorption. The practical advantage of this method is that sensors are put only at the dampers to measure relative displacement and velocity so that the sources of errors and uncertainties are minimized.

Application of pseudo negative stiffness control to a typical cable-stayed bridge and the benchmark cable-stayed bridge by numerical simulations shows that this control strategy is effective in reducing seismic responses of the cable-stayed bridges. The reduction is significantly better than that by linear viscous damper and is comparable to that by active control.

Acknowledgement

I would like to express my sincere gratitude to my supervisor Professor Iemura of Kyoto University, for his invaluable guidance and encouragement throughout my three and a half years of study and research at Kyoto University. I really feel privileged to work in his Structural Dynamics Laboratory.

I would like to express my sincere appreciation to Professor Matsuhisa and Professor Matsumoto of Kyoto University for their invaluable suggestions and critical readings of my dissertation.

I would like to greatly appreciate Dr. Igarashi, Associate Professor and Dr. Takahashi, Research Associate in the Laboratory for their invaluable comment and suggestions during the development of this research. Also, I would like to appreciate Er. Nakanishi for his support and affection.

I would like to express my thanks to all the lab mates who have kindly supported me both in my research and daily life. Especially, Dr. Toyooka (now in Japan Railway Technical Research Institute), Mr. Nakata (now in the University of Illinois), Mr. Mizutani (now in Compaq) and Mr. Sogabe deserve all commendation for constructive criticism, fruitful discussion, and ready help at all times. Supports from Mr. Taghikany, Mr. Kalantari, and Dr. Sarvesh Jain are greatly appreciated.

Dr. Shirley Dyke of Washington University at Saint Louis is gratefully acknowledged for her support during author's participation in the benchmark control problem for cable-stayed bridges. I would like to thank Dr. Adachi (Hanshin Highway Public Corporation) and Dr. Okashiro (Newjec Company) for providing data of the Tempozan Cable-stayed Bridge.

Financial assistance from the Ministry of Education, Science and Culture (Monbukagakusho) of the Japanese Government during my stay in Japan is gratefully acknowledged. I am highly thankful to Dr.-Ing. Amir Partowiyatmo, Head of Laboratory for the Strength of Materials, Components, and Structures, Indonesia, for granting me study leave for completion of this dissertation.

Last but not least, I would like to thank to my parents, my sister and brother, my wife Ariefianti Nugroheni and my son Alifindra Nabil Anargya for their inspiration, understanding, and encouragement.

Table of Contents

List of Figures

List of Tables

Chapter 1

Introduction

1.1 Seismic Safety Enhancement of Structures

Natural hazard mitigation is one of the most important issues facing civil engineers today. In structural engineering, one of the constant challenges is to find new and better means of protecting existing and new civil structures from the damaging effects of destructive environmental forces, such as wind, waves, and earthquakes.

Earthquakes are considered the most destructive environmental forces for civil engineering structures. How this damaging force devastated some parts of the earth leads us to recall, for instance, the Northridge earthquake that struck the densely populated San Fernando Valley in northern Los Angeles on January 17, 1995. Damage to several major freeways serving Los Angeles choked the traffic system in the days following the earthquake. Collapses and other severe damage forced closure of portions of 11 major roads to downtown Los Angeles **(Scawthorn, 2002)**.

Moreover, the following year, on January 17, earthquake occurred at about 20 km southwest of downtown Kobe, Japan, which left 6,427 people died. The fault rupture was 30 to 50 km in length, bilateral strike-slip, and ran directly through central Kobe, which contributed to the high level of destruction **(EERI, 1995; AIJ, 1995).** The number of buildings destroyed by the earthquake exceeded 100,000, or approximately one in five buildings in the strongly shaken area. Mid-rise commercial buildings, generally 6 to 12 stories high, collapsed on virtually every block in the highest concentration of damaged buildings. The elevated Hanshin expressway which mostly supported by single, large

reinforced concrete piers, many of which failed in shear or bending over a 20-km length. Elevated railroad and structures and railway stations were particularly hard hit. All had elevated structure and embankment failures, overpass collapses, distorted rails, and other severe damage.

The above are just about two recent historical earthquakes ever happened on earth, not to mention other historical earthquakes that took million or perhaps billion of lives because of structural failure. Therefore the need for structural safety enhancement during earthquakes is an emerging issue.

1.1.1 Seismic Safety Enhancement using Ductility Demand Method

One method of enhancing seismic safety of structures is to design structures with conventional ductility demand (inelastic) method. The basic concept of the method is to provide a structure sufficient dynamic strength and ductility, enabling the structural system as a whole to absorb the seismic energy. Detailing of structural member becomes an important issue in the design. When large earthquake strikes, some designated locations **(Paulay and Priestley, 1992)** should become plastic hinges **(Figure 1-1)** with stable hysteretic loop so that large seismic energy can be absorbed by the structure.

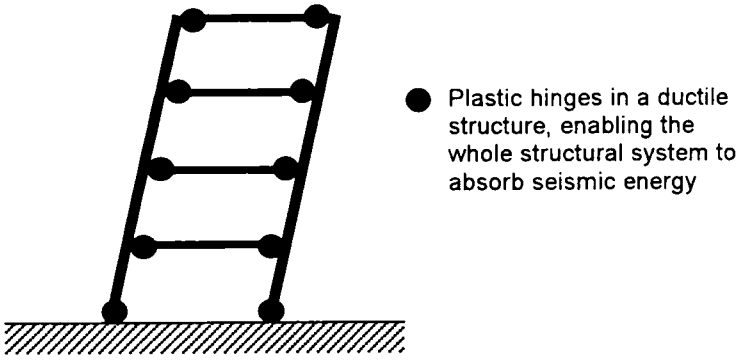

Figure 1-1. Schematic of a structure designed with ductility demand method

With the method, structures can be designed with relatively low elastic strength assuming high ductility. Although some damages will occur, such as the cracking of concrete and yielding of steel materials, the structure should not suffer major collapse.

However, once structural response goes deeply into the plastic range, structures may

not be operational nor repairable. From serious lessons of severe damage of civil infrastructures in Kobe area, public opinion has been demanding higher performance of the infra-systems. Therefore, for higher reliability of structures even under a very severe earthquake motion, structural control techniques which effectively reduce seismic force to structures shall be developed **(Iemura, 1999)**.

1.1.2 Seismic Safety Enhancement using Structural Control Technologies

The seismic safety enhancement of structures using structural control technologies can be categorized as passive, semi-active, or active controls. The control of structural responses produced by earthquake can be done by various means such as modifying stiffness, mass, and damping, and by providing passive or active counter forces **(Housner et al., 1997)**. To date, some methods of structural control have been used successfully and newly proposed methods offer the possibility of extending applications and improving efficiency. **Figure 1-2** shows the schematic diagram of structural control technologies in a civil structure.

Due to recent development of sensoring and digital control techniques, active control methods of dynamic response of structures are developed and some are implemented to buildings and bridges. The merit of the active control is that they are effective for a wide-frequency range and also for the transient vibration **(Iemura, 1999)**. However, the active control needs a large amount of external energy supply which is not always available during strong earthquake attack and also a high level of maintenance.

In an attempt to solve large amount of external energy supply, Spencer and Sain **(1997)** found that many active control systems for civil engineering applications operate primarily to modify structural damping. They claimed that preliminary studies indicate that appropriately implemented semi-active systems perform significantly better than passive devices and have the potential to achieve the majority of the performance of fully active systems, thus allowing for the possibility of effective response reduction during a wide array of dynamic loading conditions. In other words, semi-active control devices offer the adaptability of active control devices without requiring the associated large power sources **(Spencer and Sain, 1997)**.

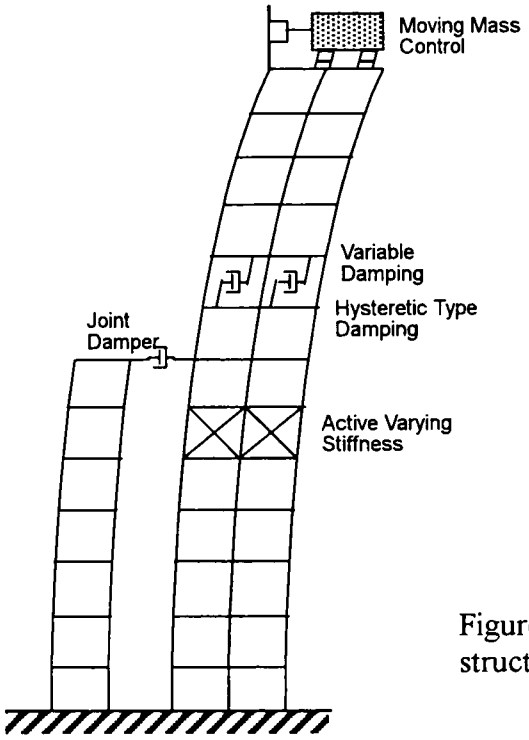

Figure 1-2. Schematic diagram of structural control in a civil structure

Moreover, according to presently accepted definitions **(Housner et al., 1997)**, a semi-active control device is one which cannot inject mechanical energy into the controlled structural system (i.e., including the structure and the control device), but has properties which can be controlled optimally to reduce the responses of the system. Therefore, in contrast to active control devices, semi-active control devices do not have the potential to destabilize (in the bounded input/bounded output sense) the structural system. In favor to these facts, semi-active control technologies have recently been widely investigated to reduce the dynamic response of structures subjected to earthquake and wind excitations **(Spencer et al., 1997; Housner et al., 1997; Jung et al., 2001; He et al., 2001; Patten 1998; Kurata et al., 1999, Iemura et al., 2001b)**.

1.2 Background of Research

The control of very flexible structures such as cable-stayed bridges is a unique and challenging problem. A vast growing of cable-stayed bridges throughout the world needs more research on the seismic protection of such structures. Flexible structures such as cable-stayed bridges raise many concerns about their behavior under environmental

dynamic loads such as wind, earthquake, and vehicular traffic-loads **(Dyke et al., 2000)**. The fact that cable-stayed bridges possess little damping characteristics to help alleviate vibration under severe ground motions, wind turbulence, and traffic loadings spurred recent efforts to enhance the technology of structural control, whether it is passive, active, semi-active or combination thereof to alleviate dynamic responses **(Abdel-Ghaffar, 1991)**.

Control strategies based on semi-active devices appear to give a promising future as the devices combine the best feature of both active and passive control systems. The typical strategy for semi-active structural control is that an "ideal" actively controlled device is firstly assumed and appropriate *primary* controller designs for this active device is designed. Then, *secondary* controller which clips the optimal control force so it is dissipative in a manner consistent with the physical nature of the device is used. This strategy has been widely used (eg., **Dyke et al., 1996ab; Jung et al., 2001**). However, as the strategy uses active controller, then the number of sensors are the same as those for active control, plus additional force sensors to make the actual force track the desired force commanded by the primary controller.

In an attempt to overcome these problems, another type of semi-active control that uses less sensors and much simpler control algorithm has been proposed in **(Iemura et al., 2001; Iemura et al., 2002, Iemura and Pradono, 2002)**. The strategy is to create pseudo negative stiffness hysteretic loop which is effective in reducing seismic responses. The advantage of this hysteretic loop over the one produced by linear viscous damper is that the combination of this hysteretic loop with elastic force will produces artificially rigid-perfectly plastic force-deformation characteristics which have large energy absorption with no residual displacement. The advantage of this method is that sensors are put only at the dampers to measure relative displacement. Moreover, since the algorithm is very simple, the sources of uncertainties and errors can be minimized.

1.3 Objective of Research

The objective of this research is to study the efficiency of structural control technologies in the form of passive and semi-active control systems in reducing seismic responses of cable-stayed bridges. The passive control systems is in form of elastic bearings plus linear

viscous damper or in the form of hysteretic bearing. The semi-active control is in the form of elastic bearing plus pseudo negative stiffness (PNS) controlled damper.

Applications of these control systems to a single degree of freedom (SDOF) system, an existing cable-stayed bridge model, and to the benchmark cable-stayed models are simulated numerically and the results are compared to those by passively and actively controlled ones.

1.4 Organization of this Dissertation

Chapter 1 starts the dissertation with general view on seismic safety enhancement of civil structures. It is followed by background of research, and research objectives.

Chapter 2 discusses general seismic response control approaches for cable-stayed bridges using passive, active, and semi-active systems proposed by other researchers.

Chapter 3 discusses the pseudo negative stiffness (PNS) controlled dampers in which the results are compared to those by linear viscous dampers in SDOF systems. Seismic response spectra were developed to compare PNS damper with linear viscous damper. Control algorithm and experimental result of PNS damper are shown. The damper utilized was variable orifice oil damper.

Chapter 4 discusses seismic retrofit of cable-stayed bridges by using structural control technologies. Numerical simulations are performed in which elastic bearings, viscous dampers, and hysteretic dampers are utilized as passive systems for seismic response reduction. The effect of soil-structure interaction on the controlled response is studied. The application of pseudo negative stiffness dampers is simulated numerically and the results are compared to those by the passive systems.

Chapter 5 presents the application of pseudo negative stiffness (PNS) dampers to the benchmark cable-stayed bridge. This benchmark bridge considers the issues of different earthquake excitations, multi-support excitations, earthquake incidence angles, coupling between three-dimensional modes, and control robustness. The results using PNS dampers are compared to those by passive systems and active control systems.

Chapter 6 closes the above discussions with conclusions.

Chapter 2

Seismic Response Control Approaches for Cable-stayed Bridges

2.1 General Remarks

Cable-stayed bridges are very appealing aesthetically and also very important lifeline structures. The increasing popularity of these bridges among bridge engineers can be attributed to the appealing aesthetics, full and efficient utilization of structural materials, increased stiffness over suspension bridges, efficient and fast mode of construction, and relatively small size of substructure **(Nazmy and Abdel-Ghaffar, 1987)**. However, from the structural dynamics point of view, cable-stayed bridges exhibit complex behavior in which the vertical, translational, and torsional motions are often strongly coupled **(Dyke et al., 2000)**. These flexible structures raise many concerns about their behavior under environmental dynamic loads such as wind, earthquake, and vehicular traffic-loads. From the analyses of various observational data, including ambient and forced vibration tests of cable-stayed bridges, it is known that these bridges have very small mechanical or structural damping (0.3% - 2%) **(Abdel-Ghaffar, 1991)**. The fact that cable-stayed bridges possess little damping characteristics to help alleviate vibration under severe ground motions, wind turbulence, and traffic loadings spurred recent efforts to enhance the technology of structural control.

Structural control basically involves regulation of the structural properties in order to achieve structural desirable response to a given external loads and modification of the excitation. The regulation of structural properties includes the modification of damping and stiffness of the structure so that it can respond more favorably to the external

excitation. Moreover, it is also possible to reduce the level of excitation transmitted to the structure, such as in base isolation systems.

The concept of structural control is appealing and exciting, however, the basic concepts of structural control themselves are not new, they have been the staple of electrical and control engineering for decades. They have been applied successfully in a variety of disciplines such as aerospace, electrical, and mechanical engineering. However, structural control of civil engineering structures has a more recent origin and its application to civil engineering structures is unique and presents a host of new challenges, especially for reducing earthquake structural responses, because of the uncertainties and the mighty power of earthquake forces.

The method in structural control can be divided into passive, active, semi-active or combination thereof (hybrid) to alleviate dynamic responses. Definitions of these control method is provided in **(Housner et al., 1997)** and is summarized here for convenient: (1) A passive control system does not require an external power source. Passive control devices impart forces that are developed in response to the motion of the structure. Passive control devices cannot increase the energy of the structural system. (2) An active control system is one in which an external source of powers control actuators that apply forces to the structure in a prescribed manner. These forces can be used to both add and dissipate energy in the structure. (3) Hybrid Control implies the combined use of active and passive control systems. (4) Semi-active control systems are a class of active control systems for which the external energy requirements are orders of magnitude smaller than typical active control systems. Typically semi-active control devices do not add mechanical energy to the structural system, therefore bounded-input bounded-output stability is guaranteed. Semi-active control devices are often viewed as controllable passive devices.

It is therefore important to understand the dynamic behavior of cable-stayed bridges for seismic safety enhancement by using structural control technologies. As reported in **Abdel-Ghaffar, 1991; Yamada et al., 1991; Branco et al., 2000; Iemura et al, 2001a; Iemura and Pradono, 2001**, the response of a cable-stayed bridge to applied loads is highly dependent on the manner in which the bridge deck is connected to the towers. If the deck is swinging freely at the towers, the induced seismic forces will be kept to minimum values, but the bridge may be very flexible so that the displacement response will be excessive. On the other hand, a rigid connection between the deck and the towers

will result in reduced displacement response but will attract much higher seismic forces during an earthquake. Therefore, it is extremely important to provide special bearings or devices at the deck-tower connections to absorb large seismic energy and reduce the response amplitudes. Examples on the applications of passive, active, and semi-active controls on the cable-stayed bridges are presented in subsequent chapters.

2.2 Passive Control of Cable-stayed Bridges

Yamada et al., **(Yamada et al., 1991)** studied the earthquake resistant design of the Higashi-Kobe Bridge. It is a long-span cable-stayed bridge in which the unique feature is that the main girder is supported by towers and piers in such a way that the girder is moveable in the longitudinal direction. This supporting method was adopted with the aim of lengthening the fundamental period of the bridge to a relatively longer period. By using this supporting method, the effects of the inertial forces due to the superstructure on the bridge towers and the caisson foundations will be greatly reduced, thereby resulting in a more rational and economical bridge design. General concept of the aseismic design is to keep the bridge structure flexible to a reasonable level in order to reduce seismic inertia, but provide safety devices to suppress excessive deformation.

The vane-type oil damper was selected for suppressing excessive deformation. The damper contains oil in its drum which is divided into two compartments. When the girder moves, the oil moves from one compartment to the next through an orifice in the partition. The turbulent flow generated when the oil passes through the orifice produces the power that moderates the girder movement **(Figure 2-1)**. The dampers were installed between the main girder and the end piers and the results are:

- When an earthquake 1.4 stronger than the design spectrum occurs on the bridge without the dampers (structural damping ratio of 1% is assumed), the displacement of the girder will be 102 cm. This will be over the critical displacement of 74 cm at which the tower buckles.
- If the dampers are installed, the girder displacement will be reduced to 64 cm, which is in the range of the design displacement of 61 cm. This is below the critical displacement for the tower to buckle. In this case, the equivalent damping ratio due to the damper is calculated to be approximately 6% based on the displacement response.

This technology is finally used for application **(Yamada et al., 1991)**.

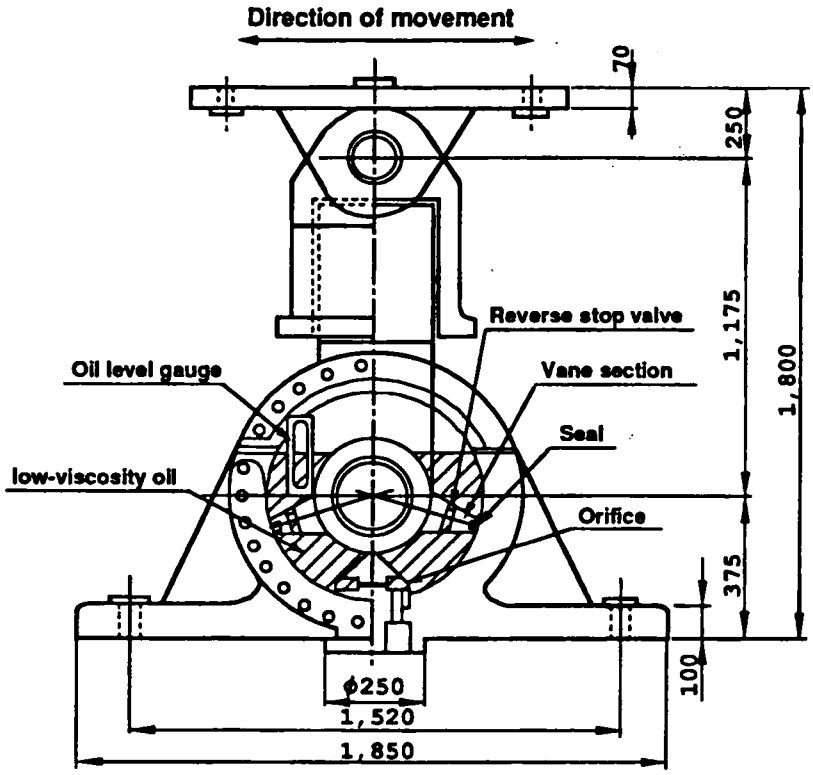

Figure 2-1 Vane-type Oil Damper used for Earthquake-resistant of the Higashi-Kobe Cable-stayed Bridge **(Yamada et al., 1991)**

Other example is attributed to the work by Branco et al **(Branco et al., 2000)**. They applied seismic displacement control of Vasco da Gama bridge by using hysteretic dampers. The dampers are put between the deck and the towers. The reason for application of this structural control technology is due to the fact that large longitudinal displacements were expected at the connections with the lateral viaducts. If no specific devices had been considered, the longitudinal displacements predicted for the design seismic action would be around 1.30 m. Hysteretic damper is mainly cheaper and needs lesser maintenance than oil damper. However, hysteretic damper produces residual displacement after an earthquake attack which needs replacement and realignment of the deck-tower connections.

A bilinear property of the hysteretic damper is assumed for the numerical simulation. The postyield stiffness of the damper was taken as 3% of initial stiffness to represent steel hysteretic dampers which is based on a work by **Blakeley et al., 1979**. A local minimum

on the displacement occurs for the yield force close to 7.5% times the total weight of the bridge. The maximum displacement obtained is between 0.85 and 0.90 m and equivalent structural damping ratio is of around 10-15%.

On the basis of this study, the construction consortium Lusoponte **(Branco et al., 2000)** then developed a hysteretic damping system that was installed in the Vasco da Gama bridge at the connections between the deck and the towers. This system is schematically illustrated in **Figure 2-2** and consists of two sets of cantilever steel beams, which will act as hysteretic dampers for the longitudinal and transverse movements. The damping is provided by the dissipation of energy due to the formation of plastic hinges in the cantilevers during any seismic excitation that is severe enough to cause yielding.

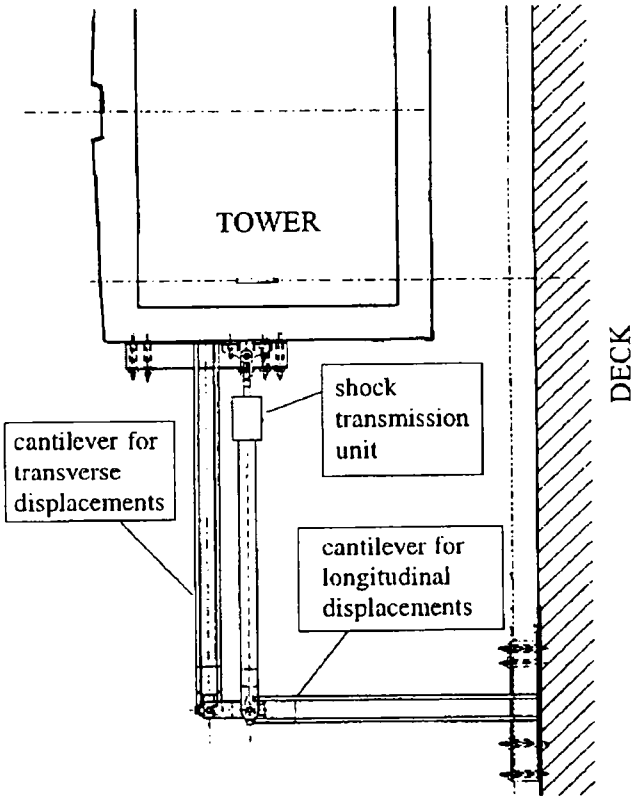

Figure 2-2 Hysteretic Damper used for Earthquake-resistant of the Vasco da Gama Cable-stayed Bridge **(Branco et al., 2000)**

As can be read above, passive control has been extensively used because the concept of seismic protection using passive devices device is simple and well known to many civil engineers. However, a passive control system is suitable only for specific design earthquake since the property cannot be adapted during a coming seismic attack. This

attracts many researcher to design active and semi-active control method for seismic protection of cable-stayed bridges as will be shown in the next subchapters. Nevertheless, these control methods are not mature enough to be applied extensively in the earthquake protection of civil engineering structures, is far from being economically competitive with passive control, and its potential has not yet been fully exploited **(Priestley et al., 1996)**. Therefore, it is the task of structural control designer to make the active and semi-active control become more economical, practical and well known to practicing engineers.

2.3 Active Control of Cable-stayed Bridges

2.3.1 Control Algorithm

The most important part of active control is the algorithm. Because the control forces are based on algorithm. Research efforts in active structural control have been focused on a variety of control algorithms based on several control design criteria. There are classical algorithms, as they are direct application of modern control theory. And, the other ones specifically proposed for civil engineering structural control applications due to the fact that they give rise to some unique control problems.

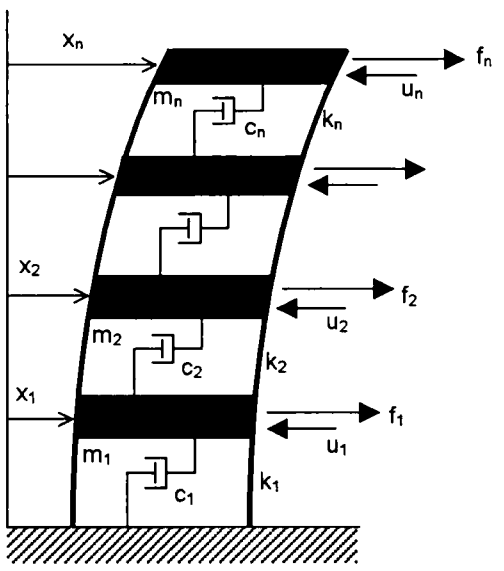

$$M = \begin{bmatrix} m_1 & & & \\ & m_2 & & \\ & & \cdots & \\ & & & m_n \end{bmatrix}$$

$$C = \begin{bmatrix} c_1 + c_2 & -c_2 & & \\ -c_2 & \cdots & \cdots & \\ & \cdots & \cdots & -c_n \\ & & -c_n & c_n \end{bmatrix}$$

$$K = \begin{bmatrix} k_1 + k_2 & -k_2 & & \\ -k_2 & \cdots & \cdots & \\ & \cdots & \cdots & -k_n \\ & & -k_n & k_n \end{bmatrix}$$

Figure 2-3. A typical civil structure with its dynamic properties

An example of famous control algorithm is linear optimal control. Because, all the control design parameters can be determined for multi-input and multi-output systems. To have better understanding on this control algorithm, let us consider a structure **(Figure 2-3)** under dynamic loading that is represented in **Equation (2.1)**,

$$\mathbf{M}\ddot{\mathbf{x}}(t) + \mathbf{C}\dot{\mathbf{x}}(t) + \mathbf{K}\mathbf{x}(t) = \mathbf{D}\mathbf{u}(t) + \mathbf{E}\mathbf{f}(t) \tag{2.1}$$

where **M**, **C**, **K** are, respectively, the $n \times n$ mass, damping, and stiffness matrices, $\mathbf{x}(t)$ is the n-dimensional displacement vector, $\mathbf{f}(t)$ is an r-vector representing applied load or external excitation, and $\mathbf{u}(t)$ is the m-dimensional control force vector. The $n \times m$ matrix **D** and $n \times r$ matrix **E** are location matrices which define locations of the control force and the excitation, respectively. The equation can be rewritten using the state-space representation in the form

$$\dot{\mathbf{z}}(t) = \mathbf{A}\mathbf{z}(t) + \mathbf{B}\mathbf{u}(t) + \mathbf{H}\mathbf{f}(t), \qquad \mathbf{z}(0) = \mathbf{z}_0 \tag{2.2}$$

where

$$\mathbf{z}(t) = \begin{bmatrix} \mathbf{x}(t) \\ \dot{\mathbf{x}}(t) \end{bmatrix} \tag{2.3}$$

is the $2n$-dimensional state vector,

$$\mathbf{A} = \begin{bmatrix} \mathbf{0} & \mathbf{I} \\ -\mathbf{M}^{-1}\mathbf{K} & -\mathbf{M}^{-1}\mathbf{C} \end{bmatrix} \tag{2.4}$$

is the $2n \times 2n$ system matrix, and

$$\mathbf{B} = \begin{bmatrix} \mathbf{0} \\ \mathbf{M}^{-1}\mathbf{D} \end{bmatrix} \quad \text{and} \quad \mathbf{H} = \begin{bmatrix} \mathbf{I} \\ \mathbf{M}^{-1}\mathbf{E} \end{bmatrix} \tag{2.5}$$

are $2n \times m$ and $2n \times r$ location matrices specifying, respectively, the locations of controllers and external excitation in the state space. In **Equations (2.4)** and **(2.5)**, **0** and **I** denote, respectively, the null matrix and the identity matrix of appropriate dimensions.

In the classical linear optimal control, the control vector $\mathbf{u}(t)$ is to be chosen in such a way that a performance index J, defined as

$$J = J_1\left[\mathbf{z}(t_o), \mathbf{z}(t_f), t_o, t_f\right] + \int_{t_o}^{t_f} J_2(\mathbf{z}, \dot{\mathbf{z}}, \mathbf{u}, \dot{\mathbf{u}}, t)\mathrm{d}t \tag{2.6}$$

is minimized subject to the constraining **Equation (2.2)**. The performance index J has

two terms. The first term, J_1, is an initial-terminal stage penalty function, which depends only on the initial and final times of the control interval $[t_o,\ t_f]$ and on the states evaluated at those two time instants. The second term of J is an integral evaluated over the control interval $[t_o, t_f]$.

In **Equation (2.6)**, J is a scalar functional which is to be minimized with respect to $\mathbf{u}(t)$ while satisfying the constraint specified by the state-space **Equation (2.2)**. Other constraints, of course, can also be introduced. For example, bounds can be placed on the allowable range of the structure's position and velocity. One thus has

$$|\mathbf{z}| \le \mathbf{b} \tag{2.7}$$

as an additional (iequality) constraint.

The form of the performance index usually chosen for study in structural control is quadratic in $\mathbf{z}(t)$ and $\mathbf{u}(t)$. Setting $t_o = 0$, it is written as

$$J = \int_0^{t_f} \left[\mathbf{z}^T(t)\mathbf{Q}\mathbf{z}(t) + \mathbf{u}^T(t)\mathbf{R}\mathbf{u}(t)\right]dt \tag{2.8}$$

In the above, the superscript ^{T} indicates vector or matrix transpose, the time interval $[0, t_f]$ is defined to be longer than that of external excitation, $\mathbf{Q}$ is a $2n\times 2n$ positive semi-definite matrix, and $\mathbf{R}$ is an $m\times m$ positive definite matrix. The matrices $\mathbf{Q}$ and $\mathbf{R}$ are referred to as weighting matrices, whose magnitudes are assigned according to the relative importance attached to the state variables and to the control forces in the minimization procedure. The assignment of large values to the elements of $\mathbf{Q}$ indicates that response reduction is given priority over the control forces required. The opposite is true when the elements of $\mathbf{R}$ are large in comparison with those of $\mathbf{Q}$. Hence, by varying the relative magnitudes of $\mathbf{Q}$ and $\mathbf{R}$, one can synthesize the controllers to achieve a proper trade off between control and effectiveness and control energy consumption.

To solve the optimal control problem with J defined by **Equation (2.8)** subject to the constraint represented by **Equation (2.2)**, the Lagrangian L is first formed by adjoining these two equations with a time-varying Lagrange multiplier $\lambda(t)$ **(Sage and White, 1977; Kwakernaak and Sivan, 1972)**, giving

$$L = \int_0^{t_f} \left\{\mathbf{z}^T(t)\mathbf{Q}\mathbf{z}(t) + \mathbf{u}^T(t)\mathbf{R}\mathbf{u}(t) + \boldsymbol{\lambda}^T(t)\left[\mathbf{A}\mathbf{z}(t) + \mathbf{B}\mathbf{u}(t) + \mathbf{H}\mathbf{f}(t) - \dot{\mathbf{z}}(t)\right]\right\}dt \tag{2.9}$$

The necessary conditions which define the optimal control can be found by taking the first variation of the Lagrangian with respect to the state and control variables and setting

it to zero. Taking the first variation of Equation (2.9) yields

$$\delta L = -\boldsymbol{\lambda}^{\mathrm{T}}(t_f)\delta\mathbf{z}(t_f) + \boldsymbol{\lambda}^{\mathrm{T}}(0)\delta\mathbf{z}(0) + \int_0^{t_f}\left[\left(\dot{\boldsymbol{\lambda}}^{\mathrm{T}} + \frac{\partial H}{\partial \mathbf{z}}\delta\mathbf{z} + \frac{\partial H}{\partial \mathbf{u}}\delta\mathbf{u}\right)\right]dt \qquad (2.10)$$

where H is the Hamiltonian defined as the integrand of **Equation (2.9)**.

Now, $\mathbf{dz}(0)=\mathbf{0}$ since $\mathbf{z}(0)=\mathbf{z}_0$ is a given constant. By requiring $\delta L = 0$, one must have

$$\frac{\partial H}{\partial \mathbf{u}} = 0, \qquad 0 \le t \le t_{\mathrm{f}} \qquad (2.11)$$

$$\dot{\boldsymbol{\lambda}}^{\mathrm{T}} + \frac{\partial H}{\partial \mathbf{z}} = \mathbf{0} \qquad (2.12)$$

with boundary condition

$$\boldsymbol{\lambda}^{\mathrm{T}}(t_f) = 0 \qquad (2.13)$$

Equations (2.11-2.13) are the necessary conditions for optimal control. Upon carrying out the necessary partial derivatives of H with respect to $\mathbf{u}$ and $\mathbf{z}$, one obtains

$$\dot{\boldsymbol{\lambda}} = -\mathbf{A}^{\mathrm{T}}\boldsymbol{\lambda} - 2\mathbf{Q}\mathbf{z}, \qquad \boldsymbol{\lambda}(t_{\mathrm{f}}) = \mathbf{0} \qquad (2.14)$$

$$\mathbf{u} = -\tfrac{1}{2}\mathbf{R}^{-1}\mathbf{B}^{\mathrm{T}}\boldsymbol{\lambda} \qquad (2.15)$$

The system of equations given by **Equations (2.2), (2.14), (2.15)** provides the optimal solution for $\mathbf{z}(t)$, $\mathbf{u}(t)$, and $\boldsymbol{\lambda}(t)$. They define a two-point boundary value problem since $\mathbf{z}(t)$ is specified at $t = 0$ and $\boldsymbol{\lambda}(t)$ is specified at $t = t_{\mathrm{f}}$.

As commonly used for civil structure application, closed-loop control is implemented. In this control method, when the control vector is regulated by the state vector, one has

$$\boldsymbol{\lambda}(t) = \mathbf{P}(t)\mathbf{z}(t) \qquad (2.16)$$

The unknown matrix $\mathbf{P}(t)$ can be determined by substituting **Equation (2.16)** into **Equations (2.2), (2.14), (2.15)**. One can show that it satisfies

$$\left[\dot{\mathbf{P}}(t) + \mathbf{P}(t)\mathbf{A} - \tfrac{1}{2}\mathbf{P}(t)\mathbf{B}\mathbf{R}^{-1}\mathbf{B}^{\mathrm{T}}\mathbf{P}(t) + \mathbf{A}^{\mathrm{T}}\mathbf{P}(t) + 2\mathbf{Q}\right]\mathbf{z}(t) + \mathbf{P}(t)\mathbf{H}\mathbf{f}(t) = \mathbf{0},$$
$$\mathbf{P}(t_f) = \mathbf{0} \qquad (2.17)$$

When $\mathbf{f}(t)$ is zero, **Equation (2.17)** reduces to

$$\dot{\mathbf{P}}(t) + \mathbf{P}(t)\mathbf{A} - \tfrac{1}{2}\mathbf{P}(t)\mathbf{B}\mathbf{R}^{-1}\mathbf{B}^{\mathrm{T}}\mathbf{P}(t) + \mathbf{A}^{\mathrm{T}}\mathbf{P}(t) + 2\mathbf{Q} = \mathbf{0}, \qquad \mathbf{P}(t_{\mathrm{f}}) = \mathbf{0} \qquad (2.18)$$

In optimal control theory, **Equation (2.18)** is referred to as the Riccati equation and

$\mathbf{P}(t)$ is the Riccati matrix. Since $\mathbf{P}(t)$ is specified at t_f, **Equation (2.18)** is solved backwards in time. Methods for solving the matrix Riccati equation are well documented in the literature **(Kwakernaak and Sivan, 1972)**.

The substitution of **Equation (2.16)** into **Equation (2.15)** shows that the control vector $\mathbf{u}(t)$ is linear in $\mathbf{z}(t)$. The *linear optimal control law* is

$$\mathbf{u}(t) = \mathbf{G}(t)z(t) = -\tfrac{1}{2}\mathbf{R}^{-1}\mathbf{B}^{\mathrm{T}}\mathbf{P}(t)z(t) \tag{2.19}$$

where $\mathbf{G}(t) = -\frac{1}{2}\mathbf{R}^{-1}\mathbf{B}^{\mathrm{T}}\mathbf{P}(t)$ is the control gain. When $\mathbf{z}(t)$ is accessible through measurement, $\mathbf{u}(t)$ can be determined from **Equation (2.19)** and it is known that the feedback controller determined in this way generates a stable closed-loop system.

We remark that, strictly speaking, the Riccati matrix $\mathbf{P}(t)$ obtained from **Equation (2.18)** does not yield an optimal solution unless the excitation term $\mathbf{f}(t)$ vanishes within the control interval $[0, t_f]$ as seen from **Equation (2.17)**, or it is a white noise stochastic process **(Sage and White, 1977; Kwakernaak and Sivan, 1972)**. It is also mentioned that, in structural applications, numerical computations have shown that the Riccati matrix $\mathbf{P}(t)$ typically remains constant over the control interval, dropping to zero rapidly near t_f **(Soong, 1990)**. Therefore, $\mathbf{P}(t)$ can in most cases be approximated by a constant matrix $\mathbf{P}$ and the Riccati **Equation (2.18)** reduces to

$$\mathbf{PA} - \tfrac{1}{2}\mathbf{PBR}^{-1}\mathbf{B}^{\mathrm{T}}\mathbf{P} + \mathbf{A}^{\mathrm{T}}\mathbf{P} + 2\mathbf{Q} = \mathbf{0} \tag{2.20}$$

The control gain $\mathbf{G}(t)$ is also constant with

$$\mathbf{G} = -\tfrac{1}{2}\mathbf{R}^{-1}\mathbf{B}^{\mathrm{T}}\mathbf{P} \tag{2.21}$$

which can be precalculated for a given structure and with prescribed weighting matrices $\mathbf{Q}$ and $\mathbf{R}$.

Upon substituting **Equation (2.19)** into **Equation (2.2)**, the behavior of the optimally controlled structure is described by

$$\dot{\mathbf{z}}(t) = (\mathbf{A} + \mathbf{BG})\mathbf{z}(t) + \mathbf{Hf}(t), \qquad \mathbf{z}(0) = \mathbf{z}_0 \tag{2.22}$$

Finally, it is emphasized that the control law given in **Equation (2.19)** requires knowledge of the entire state vector $\mathbf{z}(t)$ of the structure. Since the entire state can rarely be measured directly, it is often necessary to replace $\mathbf{z(t)}$ by $\hat{\mathbf{z}}(t)$, the state estimator determined from incomplete state measurements.

Let $\mathbf{y}(t)$ be the p-dimensional measurement (output) vector ($p \leq 2n$) with

$$\mathbf{y}(t) = \mathbf{C}\mathbf{z}(t) + \boldsymbol{\eta} \tag{2.23}$$

where $\mathbf{C}$ is the $p \times 2n$ measurement matrix and $\boldsymbol{\eta}$ is the p-vector of possible output noise. The state estimator $\hat{\mathbf{z}}(t)$ can be designed as a Luenberger observer when the signal-to-noise ratio for the output is sufficiently high and as a Kalman filter otherwise **(Kwakernaak and Sivan, 1972)**. It is given by

$$\dot{\hat{\mathbf{z}}}(t) = \mathbf{A}\hat{\mathbf{z}}(t) + \mathbf{B}\mathbf{u}(t) + \mathbf{G}^*\left[\mathbf{C}\hat{\mathbf{z}}(t) - \mathbf{y}(t)\right], \qquad \hat{\mathbf{z}}(0) = \mathbf{z}_0 \tag{2.24}$$

In the above, the estimator has an internal model of the system being estimated as indicated by the first two terms while the third term corrects the model by a linear feedback of the difference between the measurement output $\mathbf{y}(t)$ and the computed output $\hat{\mathbf{y}}(t) = \mathbf{C}\hat{\mathbf{z}}(t)$. In the Luenberger version, the estimator gain $\mathbf{G}^*$ is chosen so that the estimator error $\hat{\mathbf{z}}(t) - \mathbf{z}(t)$ decays exponentially at a prescribed rate.

2.3.2 Application to Cable-stayed Bridges

The application of active control system to a cable-stayed bridge represents a new, difficult, and unique problem, with many complexities in modeling, control design, and implementation. Cable-stayed bridges exhibit complex behavior in which the vertical, translational, and torsional motions are often strongly coupled. Clearly, the control of very flexible structures has not been studied to the same extent as buildings have.

Therefore, benchmark structural control problems for cable-stayed bridges were set by Dyke etal. **(Dyke et al., 2000)**. The goal of this benchmark study is to provide a testbed for the development strategies for the control of cable-stayed bridges. More detail about the benchmark cable-stayed bridge is shown in **Chapter 5** where the author applies pseudo negative stiffness dampers to the benchmark problem. However, for the sample active control application in phase I benchmark, some important things are shown herein.

The benchmark problem is based on the cable-stayed bridge that is currently under construction in Cape Girardeu, Missouri, USA. It is the Bill Emerson Memorial bridge spanning the Mississippi River. As shown in **Figure 2-4**, it is composed of two towers, 128 cables, and 12 additional piers in the approach bridge from the Illinois side. The

bridge has a total length of 1205.8 m. The main span is 350.6 m and the side spans are 142.7 m.

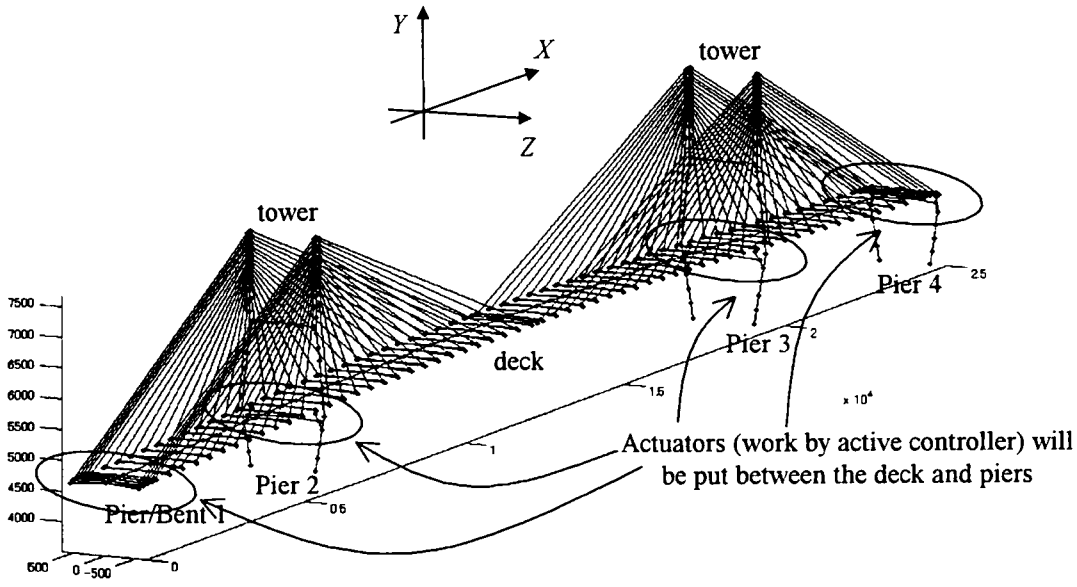

Figure 2-4 Schematic of Bill Emerson Memorial Bridge

The benchmark problem itself contains control design which is an active system designed for the linearized cable-stayed bridge model. Accelerometer and displacement transducers are used for feedback to the control algorithm. The sample control system employs a total of 24 hydraulic actuators located between the deck and abutment as well as the deck and the towers and oriented to apply forces longitudinally. The actuators have a capacity of 1000 kN. For this sample control design actuator dynamics are neglected and the actuator is considered to be ideal. To implement this controller one would replace the shock transmission devices in the bridge with hydraulic actuators. For simplicity in this sample control design, the control devices act as ideal force actuators, and actuator dynamics and control-structure interaction is neglected. A linear quadratic Gaussian algorithm is presented for this active controller.

Five accelerometers and four displacement sensors are employed in the sample control system. Four accelerometers are located on top of the tower legs, and one is located on the deck at mid span. Two displacement sensors are positioned between the deck and pier 2 and two displacement sensors are located between the deck and pier 3. All accelerometers and displacement sensors, respectively, are positioned to measure the absolute acceleration and relative displacement in the longitudinal direction to the bridge.

A reduced order model of the system is developed for control design. This model is formed from the evaluation model and has 30 states. The sample controller employs a linear quadratic Gaussian control design. For this design, input ground excitation is taken to be stationary white noise, and an infinite horizon performance index is chosen that weights the displacements of the deck at abutment. The full state feedback gain matrix for the deterministic regulator problem were done by using the MATLAB® **(Mathworks, 1997a)** routine within the control toolbox. To represent the hardware used to implement this algorithm on a digital computer, the input signal passes through a model of an analog-to-digital converter (A/D) and the output control signal passes through a model of a digital-to-analog converter (D/A).

The closed-loop response is evaluated for the three earthquakes specified. **Table 2-1** shows the values of the evaluation criteria. In each case the controlled cable tension is well within the safe bounds. The values in the evaluation criteria are unitless. The values are direct comparison with the ones produced by uncontrolled systems, except criteria number J_{16} to J_{18}.

Table 2-1. Evaluation criteria for sample controller

Evaluation Criteria	El Centro	Mexico	Gebze
J_1 (shear force at tower base)	0.387	0.458	0.454
J_2 (shear force at deck level)	1.068	1.369	1.378
J_3 (moment at tower base)	0.294	0.584	0.443
J_4 (moment at deck level)	0.625	0.614	1.225
J_5 (deviation of cable tension)	0.186	0.077	0.148
J_6 (deck displacement)	1.201	2.331	3.564
J_7 (normed shear force at tower base)	0.226	0.398	0.323
J_8 (normed shear force at deck level)	1.178	1.212	1.437
J_9 (normed moment at tower base)	0.266	0.419	0.455
J_{10} (normed moment at deck level)	0.881	1.107	1.457
J_{11} (normed deviation of cable tension)	0.023	0.010	0.017
J_{12} (force by control devices)	1.589e-3	0.574e-3	1.715e-3
J_{13} (stroke of control devices)	0.788	1.174	1.954
J_{14} (instantaneous power required)	2.701e-3	1.752e-3	7.369e-3
J_{15} (total power force required)	4.287e-4	2.334e-4	6.949e-4
J_{16} (number of control devices)	24	24	24
J_{17} (number of sensors)	9	9	9
J_{18} (resources to implement algorithm)	30	30	30

From the table, it is clear that the controlled bridge shows lower (evaluation criteria < 1.000) and yet larger (evaluation criteria > 1.000) responses than the uncontrolled one. It is shown that the controlled base shear at the towers is much lower than uncontrolled one.

On the other hand, at the expense of lower force, the displacement response is much larger for the controlled system. Because disconnecting the deck from the towers (to be replaced by actuating devices) makes the bridge become more flexible and therefore attract lower seismic induced force and yet produce larger relative displacement. This shows that the above sample controller is not exhaustive in controlling the bridge. Better results obtained by other participant for phase I benchmark problem **(Jung et al., 2001)** are shown in **Chapter 5** which are useful for direct comparison with pseudo negative stiffness control algorithm proposed in this dissertation.

2.4 Semi-active Control of Cable-stayed Bridges

2.4.1 Control Algorithm

Because of the intrinsically nonlinear nature of semi-active control devices, development of control strategies that are practically implementable and can fully utilize the capabilities of these unique devices is an important and challenging task. Various nonlinear control strategies have been developed to take advantage of the particular characteristics of the semi-active devices, including bang-bang control **(McClamroch and Gavin, 1995; Mukai, et al., 1994)**, clipped optimal control **(Patten, et al., 1994a,b; Dyke, et al., 1996a)**, bi-state control **(Patten, et al., 1994a,b)**, fuzzy control methods **(Sun and Goto, 1994)**, and adaptive nonlinear control **(Kamagata and Kobori, 1994)**. **(Caughey, 1993)** proposed a variable stiffness system that employed a semi-active implementation of the Reid spring **(Reid, 1956)** as a structural element. He et al **(He et al., 2001)** proposed a resetting semiactive stiffness dampers used for controlling seismically excited cable-stayed bridges.

2.4.2 Application of "Smart" Dampers to Cable-stayed Bridges

A "smart" damping strategy for seismic protection of cable-stayed bridges by investigating the first generation (phase I) problem for cable-stayed bridges **(Dyke et al., 2000)** is shown. Smart dampers (e.g., variable orifice damper **(Figure 2-5)**, controllable fluid damper **(Figure 2-6)**, etc.) are considered as supplemental damping devices. A clipped-optimal control algorithm is employed **(Jung et al., 2001)**. Since a smart damper is an energy-dissipative device that cannot add mechanical energy to the structural system, the control strategy guarantees the bounded-input and, bounded-output stability of the controlled structure. The bridge model used is the benchmark problem for cable-stayed bridge as the one in **Subchapter 2.3.2**.

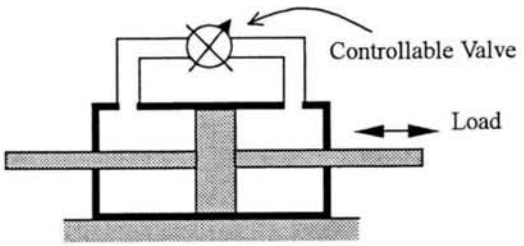

Figure 2-5. Schematic diagram of variable orifice oil damper

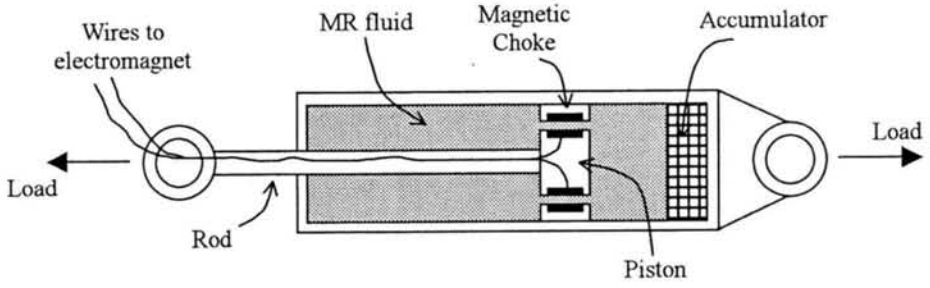

Figure 2-6. Schematic diagram of MR Damper **(Spencer et al., 1997)**

The strategy of a clipped-optimal control algorithm for seismic protection of bridges using smart dampers is as follows: First, an "ideal" active control device is assumed, and an appropriate *primary* controller for this active device is designed. Then a *secondary* bang-bang-type controller causes the smart damper to generate the desired active control force, so long as this force is dissipative. The H2/LQG control design **(Spencer et al., 1994; Zhou et al., 1996)** is adopted as the *primary* controller. The ground excitation is

taken to be a stationary white noise, and an infinite horizon performance index is chosen that weights appropriate parameters of the structure, i.e.,

$$J = \lim_{\tau \to \infty} \frac{1}{\tau} E\left[\int_0^{\tau} \left\{\mathbf{z}^{\mathrm{T}}\mathbf{Q}\mathbf{z} + \mathbf{u}^{\mathrm{T}}\mathbf{R}\mathbf{u}\right\} dt\right] \tag{2.25}$$

where **R** is chosen to be an identity matrix of order 8, and **Q** is the response weighting matrix. A stochastic response analysis has been performed to determine appropriate values of the weighting parameters. Two combinations of appropriate weighting parameters are considered as follows:

Case 1: deck displacements (q_d) and overturning moments (q_{om}),

$$\mathbf{Q}_{d\&om} = \begin{bmatrix} q_d \mathbf{I}_{4\times 4} & \mathbf{0} \\ \mathbf{0} & q_{om}\mathbf{I}_{4\times 4} \end{bmatrix} \tag{2.26}$$

Case 2: deck displacements (q_d) and moments at deck level (q_{md}),

$$\mathbf{Q}_{d\&md} = \begin{bmatrix} q_d \mathbf{I}_{4\times 4} & \mathbf{0} \\ \mathbf{0} & q_{md}\mathbf{I}_{4\times 4} \end{bmatrix} \tag{2.26}$$

By applying the above weighting matrices to the *primary* controller, the "desired" active control forces can be obtained. For the general smart damping device, the *secondary* control strategy is given by

$$f_{sa,i} = \begin{cases} f_{a,i}, & f_{a,i} \times \dot{x}_{dev} < 0 \\ 0, & \text{otherwise} \end{cases} \tag{2.27}$$

where $f_{sa,i}$ is the control force of the ith smart damper, $f_{a,i}$ is the "desired" control force of the ith device, and $\dot{x}_{dev}$ is the velocity across the ith damper. Since the smart damper is an energy-dissipative device that cannot add mechanical energy to the structural system, special care must be taken in the design of the *primary* controller so that the "desired" control force $f_{a,i}$ is dissipative during the majority of the seismic event.

The results show that smart damping strategies have nearly the same effectiveness as the active control system for seismic protection of the benchmark cable-stayed bridge model **(Jung et al., 2001)**. However, Jung et al did not compare the semi-active system results directly with that by passive system (good examples by **(Dyke et al., 1996c; Ramallo et al., 2002)** show this comparison). Because, according to the author opinion, a direct comparison with passive system will be very useful for most civil engineers (whose

acquaintance to active and semi-active control is rare) to have better understanding about structural control technologies. For this reason, the research done for this dissertation compares directly the semi-actively controlled results with those by passive system, as they are shown in **Chapter 4** and **Chapter 5**.

2.5 Summary

This chapter introduces seismic response control of cable-stayed bridges. Cable-stayed bridges, which are increasing in popularity among bridge engineers, have very small structural damping. The response of a cable-stayed bridge to seismic loads is highly dependent on the manner in which the bridge deck is connected to the towers. Therefore, the application of structural control technologies for seismic response reduction of a cable-stayed bridge is done mainly by connecting the deck and towers by control devices.

Structural control basically involves regulation of the structural properties in order to achieve desirable response to a given external loads. The regulation of structural properties includes the modification of mass, damping, and stiffness of the structure so that it can respond more favorably to the external excitation. The control method can be passive, active, semi-active, or a combination thereof.

Passive control devices are well known for many civil engineers for seismic control. However, for a wider-frequency range and also for the transient vibration, active control is now being developed for practical application. Nevertheless, active control methods needs a large amount of external energy supply which is not always available during strong earthquakes and also high level of maintenance.

To overcome the external energy problem of fully active control, semi-active control seems to be a promising method for civil structures. Semi-active control use active control algorithm as its primary controller. Then, secondary controller is used to consider the device constraints. By using these techniques, semi-active control has the potential to achieve the best feature of active control and yet requires far less energy.

So far, many researchers in structural control fields rarely compare their results with those of passive systems. Comparison is very useful for civil engineers whose knowledge on passive control is mostly in hand. Therefore, applications of pseudo negative stiffness control on cable-stayed bridges are carried out with comparing the results to those by

passive and active controls in the next chapters.

Chapter 3

Pseudo Negative Stiffness Control

3.1 General Remarks

Semi-active control in seismically excited structures is mainly to dissipate energy from the structure **(Spencer and Sain, 1997)**. Moreover, because many active control systems for civil engineering applications operate primarily to modify structural damping, preliminary studies indicate that semi-active control strategies can potentially achieve the majority of the performance of fully active systems **(Spencer et al., 1997; Jung et al., 2001)**.

Keeping in mind that the semi-active control is mainly to dissipate energy from the structure, it is thought to be significantly beneficial if the device itself is controlled, avoiding the use of many sensors and complicated active controllers. The objective of the control is then to improve the hysteretic loop of the device so that it dissipates more vibratory energy in order to reduce seismic induced displacement and forces. This will result in a practical and economical semi-active control while keeping the track of seismic safety enhancement of civil structures.

Therefore, the focus of the research shown in this dissertation is to study the pseudo negative stiffness control in improving the hysteretic loop produced by a variable damper. The applications of this control method to a typical cable-stayed bridge (**Chapter 4**) and the benchmark control problem of cable-stayed bridges (**Chapter 5**) are investigated and the results are compared to those by passive and active control. The advantages of pseudo negative stiffness control algorithm in improving seismic safety enhancement of single degree of freedom systems are illustrated in the next subchapters.

3.2 Analytical Review

Consider a steady-state motion of an SDOF system. The graphical interpretation for the energy dissipated in linear viscous damping is shown as a hysteretic loop in **Figure 3-1a (Chopra, 1995)**. It is of interest to examine the total (elastic plus damping) resisting force because additional dampers are usually put parallel to existing members that have stiffness. The plot is the hysteretic loop of **Figure 3-1a** rotated as shown in **Figure 3-1b**. Where f_D and f_S are damping and elastic forces, respectively, u and $\dot{u}$ are relative displacement and velocity, respectively, ω is excitation frequency and u_0 is maximum relative displacement. The energy dissipated by damping is still the area enclosed by the ellipse. The hysteretic loop associated with viscous damping is the result of dynamic hysteresis, therefore the loop area is proportional to excitation frequency. This has advantage over static hysteresis associated with plastic deformation since no permanent displacement is expected at the end of excitation.

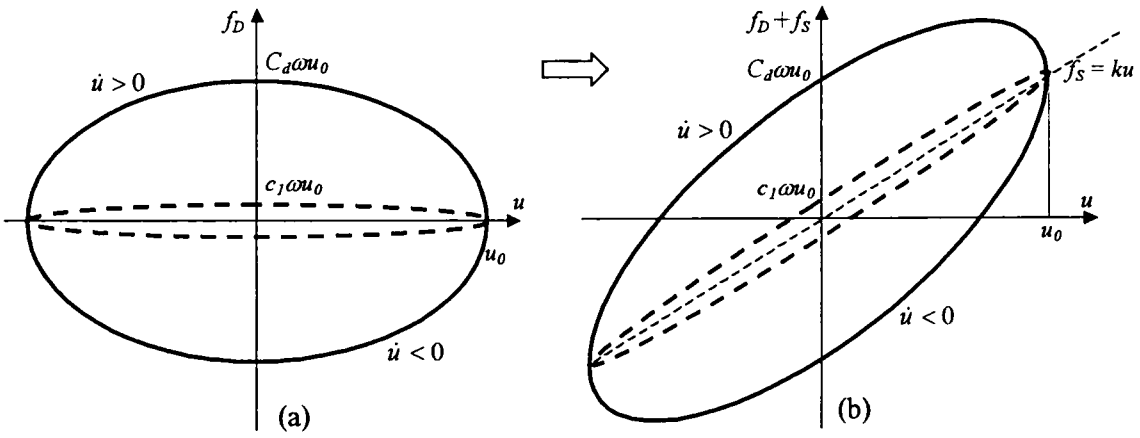

Figure 3-1. Hysteretic loop for (a) linear viscous damper;
(b) spring and viscous damper is parallel

It is clear from **Figure 3-1** that increasing the damping coefficient from c_1 to C_d will increase the energy dissipation. However, as damping coefficient increases, the maximum elastic plus damping force becomes larger than the maximum elastic force (**Figure 3-1b**). The calculation is shown below.

For hysteretic loop of a linear damper shown in **Figure 3-1b**, damping force is expressed as

$$f_D = c_{cr}\zeta\omega\sqrt{u_0^2 - u^2} \tag{3-1}$$

where ζ is damping ratio. The frequency of the excitation ω is the same as the natural frequency of the system. The critical damping coefficient c_{cr} can then be expressed as

$$c_{cr} = \frac{2k}{\omega} \tag{3-2}$$

where k is the existing elastic stiffness. Therefore, **Equation (3-1)** can be rewritten as

$$f_D = 2\zeta k\sqrt{u_0^2 - u^2} \tag{3-3}$$

The total of elastic force plus damping force is expressed as

$$f = ku + 2\zeta k\sqrt{u_0^2 - u^2} \tag{3-4}$$

Maximum total force occurs when,

$$\frac{df}{du} = k - \frac{2\zeta ku}{\sqrt{u_0^2 - u^2}} = 0 \tag{3-5}$$

or,
$$u_{f,\max} = \frac{u_0}{\sqrt{4\zeta^2 + 1}} \tag{3-6}$$

where $u_{f,\max}$ is the displacement at the maximum total force. Therefore, the ratio of maximum total force $f_{\max}$ divided by maximum elastic force $f_{s,\max}$ can then be expressed as

$$\frac{f_{\max}}{f_{s,\max}} = \frac{\frac{ku_0}{\sqrt{4\zeta^2+1}} + 2\zeta ku_0\sqrt{1 - \frac{1}{4\zeta^2+1}}}{ku_0} = \frac{1}{\sqrt{4\zeta^2+1}} + 2\zeta\sqrt{1 - \frac{1}{4\zeta^2+1}} \tag{3-7}$$

For example, if we have a damping ratio ζ of 0.5, then by using **Equation (3-7)**, the total (damping + elastic) force will be 1.414 times the elastic force. Therefore, it has been reported in **(Dyke et al., 1997; Kelly, 1999; Hall, 1999; Gavin and Aldemir, 2001)** that larger damping force does not always favorable to structures. They claimed that larger damping ratio results in larger top story acceleration and inter-story drift for an isolated structure that incorporate additional damper. This can be attributed to the fact that the

total (damping + elastic) force becomes larger than the elastic force. The force difference is significant for large damping ratio.

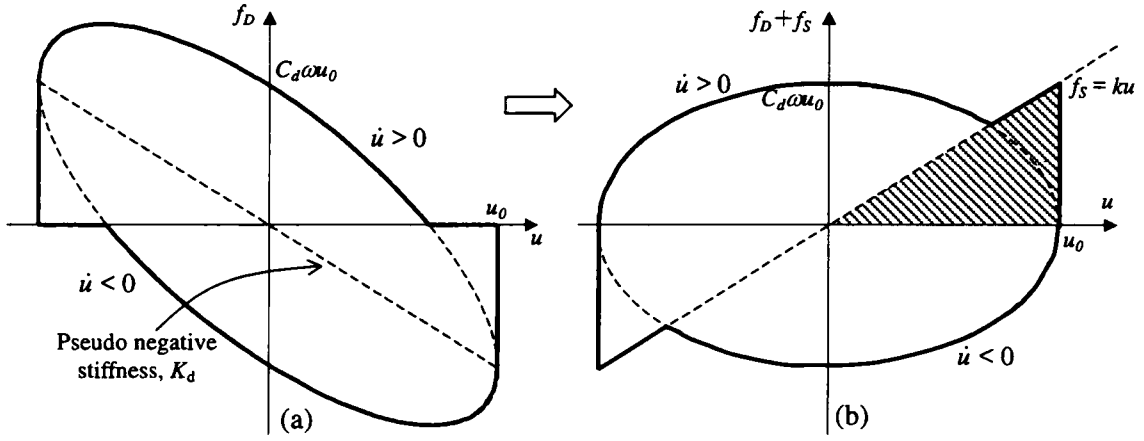

Figure 3-2. Hysteretic loop for (a) variable damper;
(b) spring and variable damper is parallel

For this reason, a new hysteretic loop produced by a variable damper will be introduced. Assume that we can produce a damping hysteretic loop shown in **Figure 3-2a** (control strategy to produce this hysteretic loop and experimental results will be shown later on in this chapter). Then, the total (elastic + damping) resisting force will be that shown in **Figure 3-2b**. It is clear from the figure that large area inside the loop (large energy dissipation) can be produced while keeping the total force the same with the elastic force.

If the maximum strain energy E_{so} of the single degree of freedom system is shown graphically as shaded area in **Figure 3-2b**, and the energy loss in a cycle of harmonic vibration E_D is shown as area inside the thick loop, then based on equivalent damping ratio ζ_{eq} equation **(Chopra, 1995)**,

$$\zeta_{eq} = \frac{1}{4\pi}\frac{E_D}{E_{so}} \tag{3-8}$$

one can calculate **Equations (3-9)** to **(3-11)** and end up with 53.4% damping ratio, which is close to 64% damping ratio of rigid-perfectly plastic force-deformation characteristics **(Priestley et al., 1996)**, of course with no residual displacement. On the other hand, for the same damping ratio as 53.4%, linear viscous damper (hysteretic loop in **Figure 3-1b**) will produce total force of 1.46 times the elastic force (calculated with **Equation (3-7)**).

$$\zeta_{eq} = \frac{\pi C_d \omega u_0^2 + C_d \omega u_0^2 - 0.25\pi C_d \omega u_0^2}{2\pi k u_0^2} \tag{3-9}$$

$$\zeta_{eq} = \frac{C_d \omega u_0^2 (0.75\pi + 1)}{2\pi c C_d u_0^2} \tag{3-10}$$

$$\zeta_{eq} = \frac{0.75\pi + 1}{2\pi} = 0.534 \tag{3-11}$$

In other words, by using pseudo negative stiffness control, one can obtain large damping ratio, above example 53.4%, while keeping the total restoring force (damping plus elastic) the same with elastic force. Whereas for the same damping ratio, linear viscous damper would produce total restoring force 1.46 times larger than the elastic force.

3.3 Control Algorithm

By using a variable damper, hysteretic loop shown in **Figure 3-2a** can be approached using the following formula:

$$F_d = K_d u + C_d \dot{u} \tag{3-12}$$

$$f_D \begin{cases} F_d & \text{if } F_d \dot{u} > 0 \\ 0 & \text{if } F_d \dot{u} \le 0 \end{cases} \tag{3-13}$$

where u and $\dot{u}$ are piston displacement and velocity, respectively. f_D is the demand force to the variable damper. For a real variable damper, when the demand force equals zero, the smallest possible force applies. Also, when the variable damper cannot achieve F_d, then the largest possible force applies. By choosing appropriate K_d (in this case $K_d = -k$) and C_d (positive value), hysteretic loop in **Figure 3-2b** can be approached under harmonic motion whose frequency is the same with natural frequency of the structure ω.

Variable dampers has been experimentally tested **(Iemura et al., 2001; Iemura et al., 2002)** to produce pseudo negative stiffness hysteretic loop. The damper used is variable orifice oil one. Opening ratio of the flow control can be changed by electric power based on signal from control PC. By changing it, quantity of flow through valve can be adjusted

and pressure loss is varied. This series of mechanism enables variable damper to generate the demanded force as close as possible. Because opening ratio can be changed at real time, this variable damping device is regarded as real time control device.

3.4 Experimental Results

The modeling of the variable damper, that is the relationship among damping force, opening ratio, and response quantities, is required for the use of it as control device **(Iemura et al., 2001)**. From the test results, it is considered that damping force of variable damper depends on the square of relative velocity and that it is possible to neglect stiffness element in modeling this variable damper. In consideration of friction element f_f, damping force of variable damper is assumed as follows.

$$F(h,\dot{u}_t) = \mathrm{sgn}(\dot{u}_t)\left\{f(h)\dot{u}_t^2 + f_f\right\} \tag{3-13}$$

where h is opening ratio of the valve. $f(h)$ and f_f are decided as follow on the basis of the regression analysis of the test results with least-squares method.

$$f(h) = \frac{159.232}{h^2} + 307.2 \ (\mathrm{kN \cdot sec^2/m^2}) \tag{3-14}$$

$$f_f = 0.6 \ (\mathrm{kN}) \tag{3-15}$$

Thus, the determined relationship among damping force, opening ratio, and relative velocity becomes

$$F(h,\dot{u}_t) = \mathrm{sgn}(\dot{u}_t)\left\{\left(\frac{159.232}{h^2} + 307.2\right)\dot{u}_t^2 + 0.6\right\} (\mathrm{kN}) \tag{3-16}$$

The range of opening ratio is between 0.05 ($h_{\min}$) and 0.8 ($h_{\max}$). The feasible region of variable damper is shown in **Figure 3-3**. Damping force of variable damper is in the same direction of relative velocity, so second and forth quadrants in the figure are impossible region of damping force. This means that variable damper will never make vibration larger if undesirable spill-over occurs. That is a characteristic of semi-active control device using variable damper. Value of opening ratio is decided at every time step on the condition as follows. (i) Case of the demanded force in the feasible region II; Opening

ratio h is calculated based on **Equation (3-16)** from the demanded force and measured relative velocity and the signal of it is set for variable damper to generate the demanded force. (ii) Case of the demanded force outside the feasible region II; When the direction of the demanded force is the same to that of relative velocity, opening ratio is chosen for variable damper to generate demanded force as close as possible. When the direction of the demanded force is against that of relative velocity, opening ratio is chosen for variable damper to generate as small force as possible. Experimental results using variable damper to produce negative stiffness hysteretic loop is shown in **Figure 3-4**. This shows that variable damper can be controlled to produce pseudo negative stiffness hysteretic loop. **Appendix E** discusses this matter in detail.

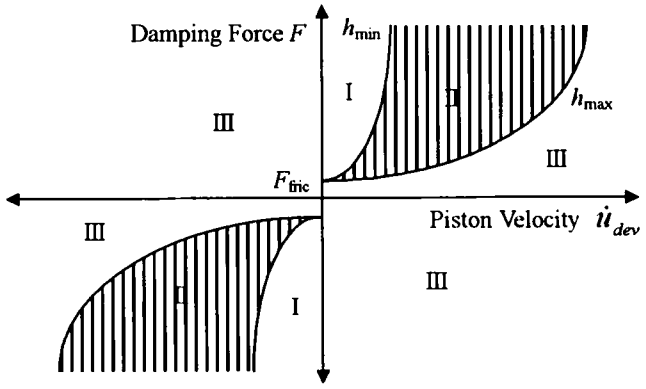

Figure 3-3 Feasible region of variable damper in relative velocity and damping force plane

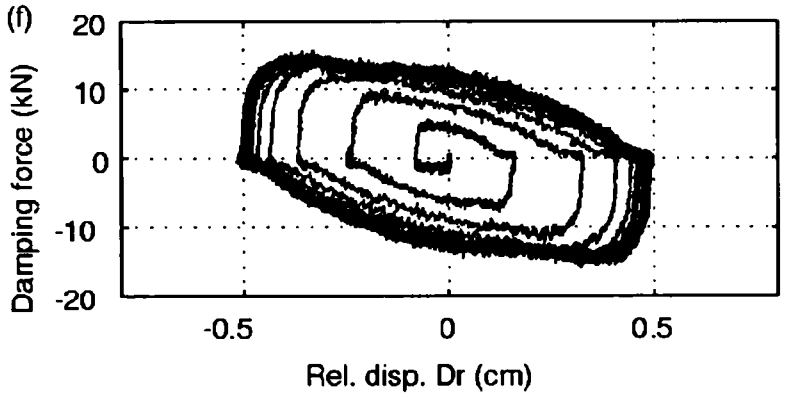

Figure 3-4 Response of variable damper controlled as pseudo negative stiffness subjected to sinusoidal input (1.8 Hz, max 10gal)

The pseudo negative stiffness algorithm has great advantage in practical application. Only relative displacement and velocity (which actually can be derived from relative

displacement) are used for feedback and sensor is required only at damper place. The algorithm is such simple and clear, so that sources of errors and uncertainties can be minimized.

3.5 Simple Pseudo Negative Stiffness Damper

Moreover, there is a much simpler approach to produce pseudo negative stiffness hysteretic loop. The damper should have damping coefficient as shown in **Figure 3-5a**. As shown in the figure, the damping coefficient is only the function of displacement and sign of velocity (forward or reverse).

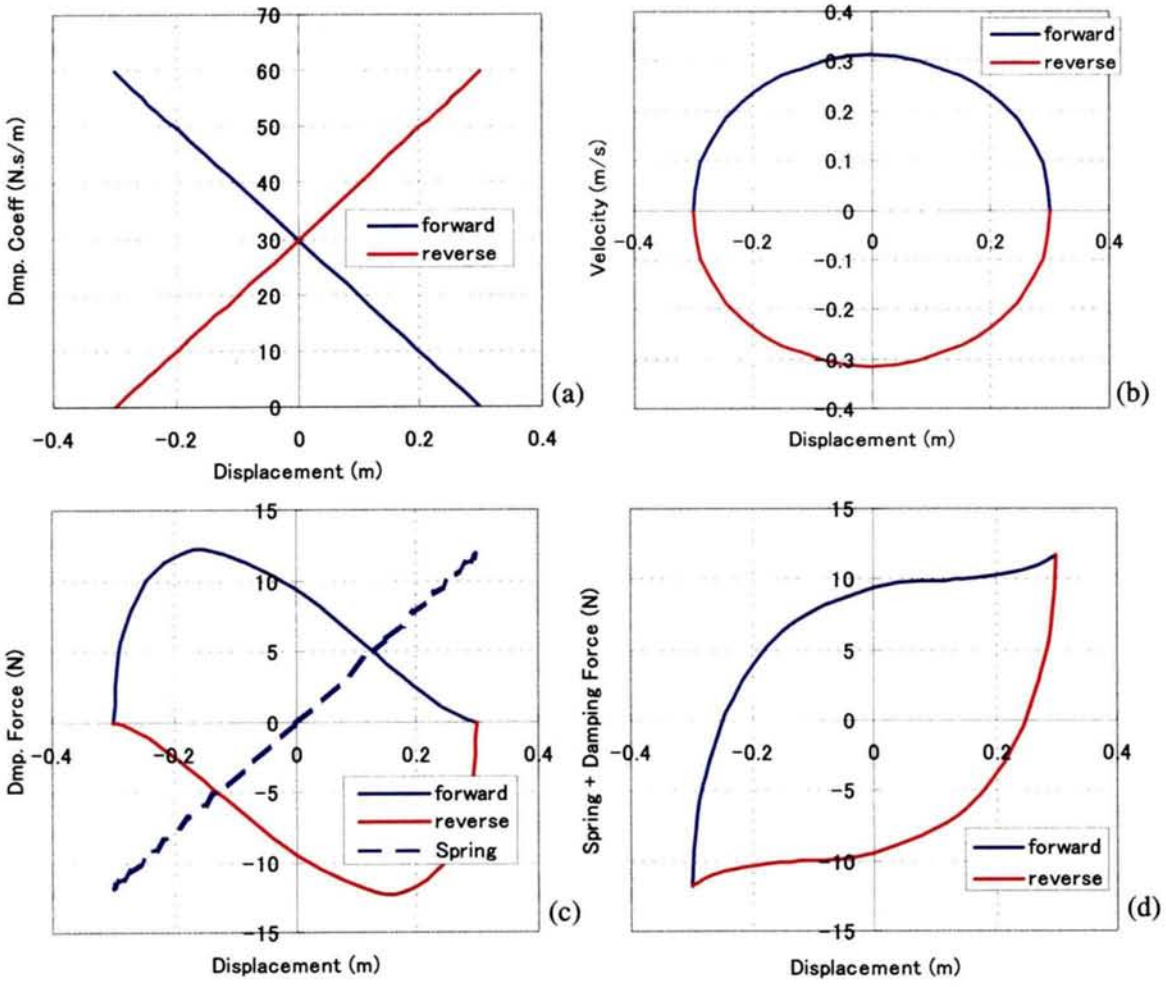

Figure 3-5 (a) damping coefficient, (b) piston velocity, (c) damping force, (d) total restoring (spring + damping) force

For example, for a steady state motion, the velocity of the piston is shown in **Figure 3-5b**. Then, by multiplying the damping coefficient with the piston velocity, hysteretic loop shown in **Figure 3-5c** is obtained. The total restoring (spring+damping) force is shown **Figure 3-5d**. Again, this shows large energy absorption with smaller restoring force than the elastic force.

The efficacy of this simple pseudo negative stiffness (PPNS) damper over linear viscous (LIN) damper is shown in the next subchapter by using response spectra.

3.6 Seismic Response Spectra

Seismic response spectra for a single degree of freedom system employing linear (LIN) viscous damper (53.4% damping ratio), pseudo negative stiffness (PNS) damper (also 53.4% damping ratio), and *simple* pseudo negative stiffness (PPNS) damper were developed. The first results shown in **Figure 3-6** are for PNS damper that is compared with linear viscous (LIN) damper.

It is clear from the figure that PNS damper results in lower absolute acceleration and relative velocity than those by linear viscous (LIN) damper although damping ratios for both systems are the same. This is because the total (damping + elastic) force is smaller for PNS damper. Hysteretic loops for both linear (LIN) and pseudo negative stiffness (PNS) damper are shown in **Figure 3-7** at a natural period of 6.3 second, which is a typical natural period for retrofitted cable-stayed bridges (shown in **Chapters 4** and **5**). The hysteretic loops show clearly the concept of pseudo negative stiffness damper in increasing the loop area of a variable damper.

Seismic response spectra for *simple* pseudo negative stiffness (PPNS) damper were developed and the results are shown in **Figure 3-8**. It is clear from the figures that PPNS damper is significantly better than linear viscous (LIN) damper and has the potential to achieve the effectiveness of PNS damper in reducing seismic responses. Hysteretic loops for both linear (LIN) and passive pseudo negative stiffness (PPNS) damper are shown in **Figure 3-9** for the natural period of 6.3 second.

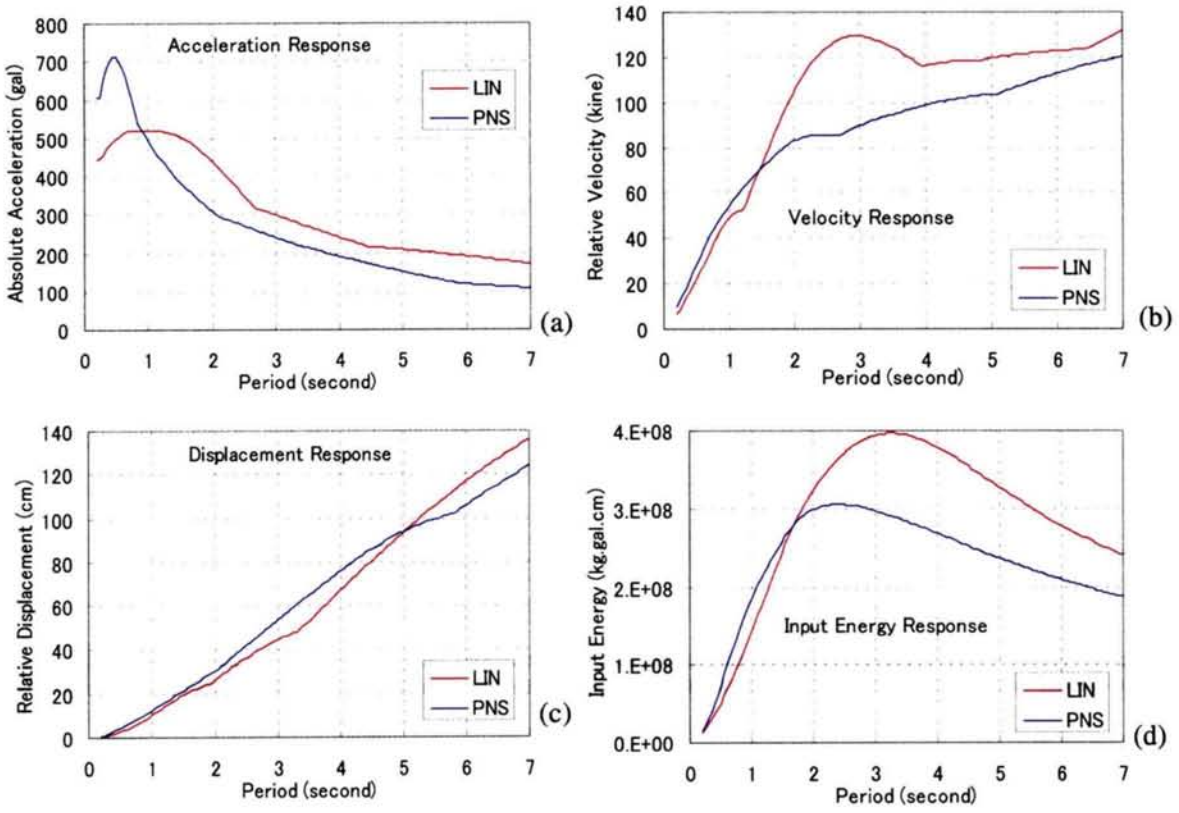

Figure 3-6 (a) acceleration, (b) velocity, (c) displacement,
and (d) input energy response spectra
for linear viscous (LIN) and pseudo negative stiffness (PNS) dampers
(damping ratio for both 53.4%) (Type 1-III-1 earthquake)

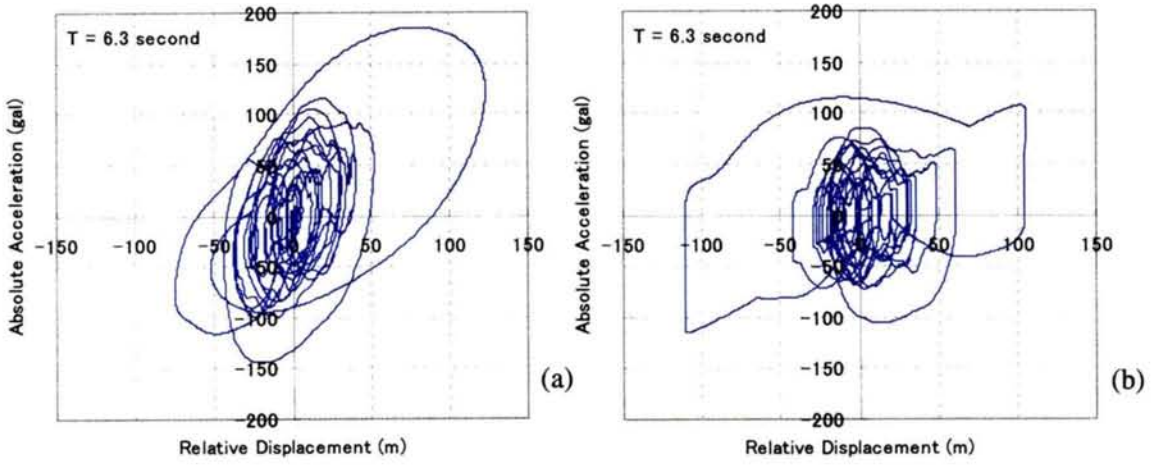

Figure 3-7 (a) total (spring + damping) hysteretic loop for linear viscous damper system,
(b) total (spring + damping) hysteretic loop for variable damper system,
(Type 1-III-1 earthquake)

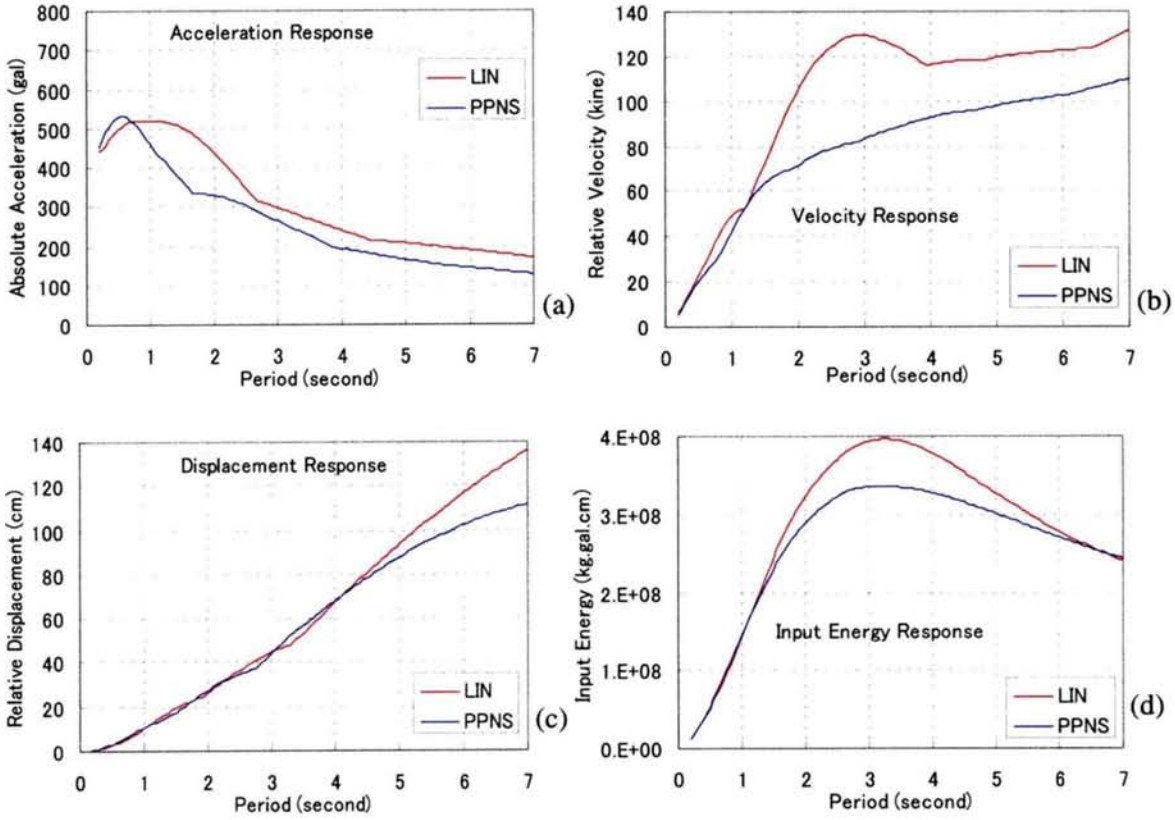

Figure 3-8 (a) acceleration, (b) velocity, (c) displacement,
and (d) input energy response spectra
for linear viscous (LIN) and *simple* pseudo negative stiffness (PPNS) dampers
(damping ratio for both 53.4%) (Type 1-III-1 earthquake)

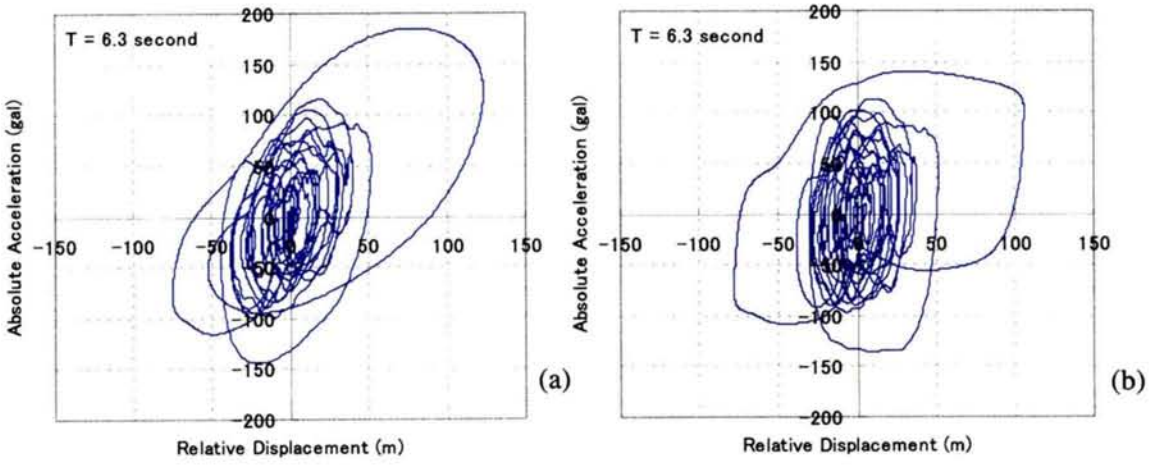

Figure 3-9 (a) total (spring + damping) hysteretic loop for linear viscous damper system,
(b) total hysteretic loop for *simple* pseudo negative stiffness damper system,
(Type 1-III-1 earthquake)

3.7 Summary

This chapter shows the method for producing pseudo negative stiffness hysteretic loop and the advantage of pseudo negative stiffness damper over linear viscous damper. In contrast to the linear viscous damper, the increase of damping ratio does not make the total damper plus elastic force exceeds the elastic force. This is because the hysteretic loop produced by variable damper and elastic force approaches that of rigid-perfectly plastic force-deformation characteristics. Or in other words, the pseudo negative control algorithm produces desirable artificial hysteretic loop by using variable dampers.

Comparison of response spectrum between linear viscous damper and pseudo negative stiffness damper shows that significant reduction of absolute acceleration and relative velocity can be obtained by using pseudo negative stiffness damper while keeping the displacement response similar to that of the linear viscous damper. Moreover, the input earthquake energy becomes smaller for pseudo negative stiffness damper.

The method is also advantageous over active controller or commonly semi-active controller because lesser sensors are needed and very simple algorithm is incorporated. Less sensors and simple algorithm minimizes the source of errors and uncertainties.

Chapter 4

Seismic Retrofit of a Cable-stayed Bridge

4.1 General Remarks

Due to severe damages of many bridges caused by the Hyogo-ken Nanbu Earthquake in Kobe area in 1995, very high ground motion (level II design) is now required in the new bridge design specification set in 1996 **(Japan Roadway Association, 1996)** in Japan, in addition to the relatively frequent earthquake motion (level I design) by which old structures were designed and constructed. Hence, seismic safety of cable-stayed bridges, including the Tempozan Bridge, which were built before the present specification has to be reviewed and seismic retrofit has to be done, if it is found necessary.

The basic concept of retrofit by using structural control technology is to make the structure flexible and highly damped. This can be achieved by replacing the fixed-hinge connections between the deck and towers with flexible bearings so that the induced seismic forces will be kept to minimum values, and to add energy absorbing devices set parallel to the bearings to absorb large seismic energy and reduce the seismic response amplitudes.

4.1.1 The Bridge for Study

Tempozan Bridge, built in 1988, is a three-span continuous steel cable-stayed bridge which is situated on the reclaimed land and crosses the mouth of the Aji River, Osaka, Japan **(Hanshin Highway Public Corporation, 1992)**. The total length of the bridge is

640 m with a center span of 350 m, and the length of side spans are 170 m and 120 m reflecting the alignment and site conditions (see **Figures 4-1** and **4-2**). The height clearance of the deck is as high as 50 m above the sea level to secure a large and high clearance under the bridge. As for the geological condition, the bridge is supported on 35m-thick soft layer.

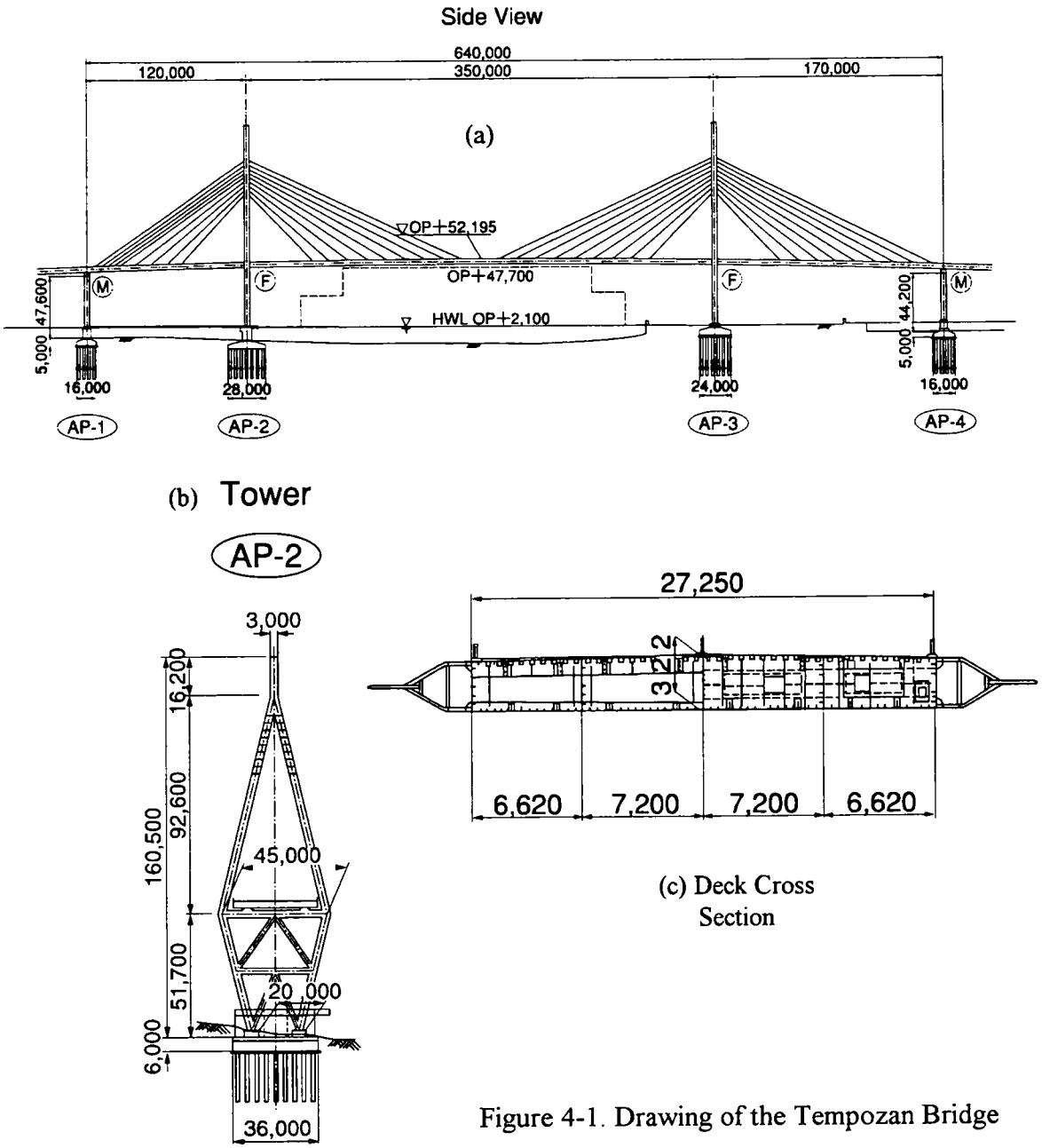

Figure 4-1. Drawing of the Tempozan Bridge

Because of severe wind, seismic, and geological conditions, the design problems such as wind stability, earthquake resistant property, and the construction method were fully investigated and studied in the construction design. The cable in the superstructure is

2-plane fan pattern multi-cable system with 9 stay cables each plane. The main deck was designed to be a flat hexagonal box deck to improve its wind stability. The main towers, standing with flexibility on the foundation footings, are A-shaped to have a good appearance and to improve the torsional rigidity. The foundation consists of cast-in-place RC piles of 2 m in diameter, and the bearing capacity was decided from the results of a loading test at the site.

Figure 4-2. Aerial view of the Tempozan Bridge

As to the seismic design in the longitudinal direction, the main deck is fixed at both towers to resist horizontal seismic forces. The bridge is relatively flexible with a predominant period of 3.7 seconds. Because of the flexibility of the tower, the stress due to temperature is comparatively small compared to that due to seismic action. As to the seismic design in transverse direction, the main deck is fixed at the towers and the end piers. Another method to reduce seismic forces to the bridge is to take soil-structure interaction effect into the design. The seismic design is made by dynamic analysis using an acceleration response spectrum analysis and the behavior at the time of earthquakes is examined by a time history analysis in order to consider the dynamic soil-structure interaction.

Due to severe damages of many bridges caused by the Hyogo-ken Nanbu Earthquake in 1995, new bridge design specification was set in 1996. The new specification requires very high ground motion (level II design) in addition to the relatively frequent earthquake motion (level I design) by which old structures were designed and constructed. **Figure 4-3** shows the original design spectrum used for designing the Tempozan Bridge and new design spectrum specified in the bridge design specification set in 1996 for level I and level II earthquake **(Japan Roadway Association, 1996)**. Level II earthquake has Type I (inter plate type) and Type II (intra plate type). As can be seen in the figure, the new design spectrum show higher acceleration response in all period ranges than the original one.

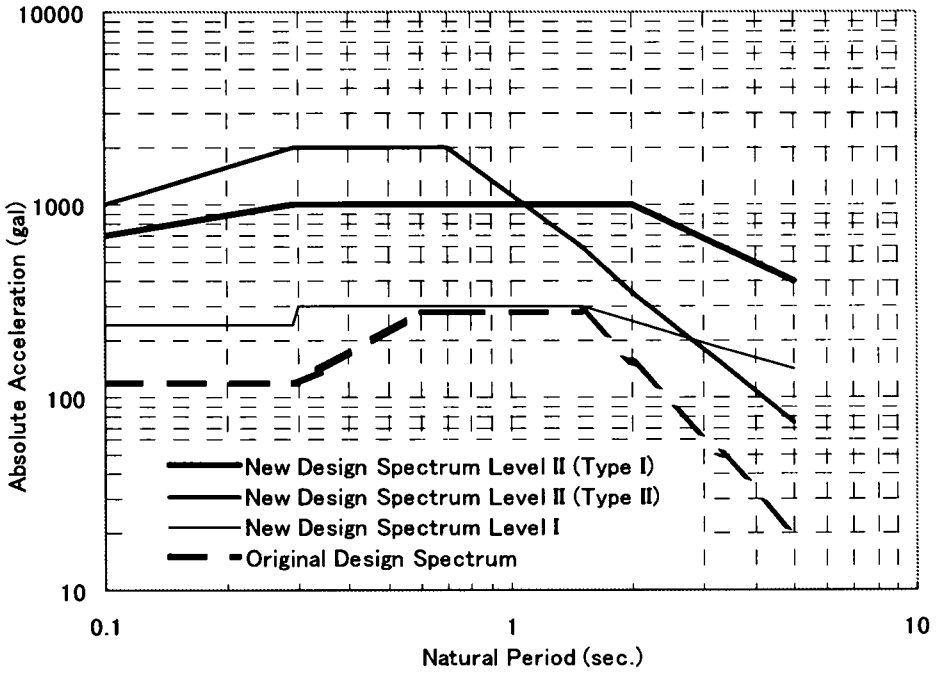

Figure 4-3. Design spectra for bridges

4.1.2 Objective

The objective of the research in this chapter is firstly to review the response of the Tempozan Bridge under new seismic design spectrum earthquake inputs. Secondly, the application of seismic response control technologies to seismic retrofit of the bridge is studied. The technologies are in the form of passive and semi-active controls to reduce the bridge seismic responses.

4.2 Structural Modeling

The Tempozan Bridge is modeled for seismic review by using finite element model. The cables are modeled by truss elements, towers and deck by beam elements, and the isolation bearings by spring elements. Moment-curvature relationship of the members is calculated based on member sectional properties and materials (**Appendix B**).

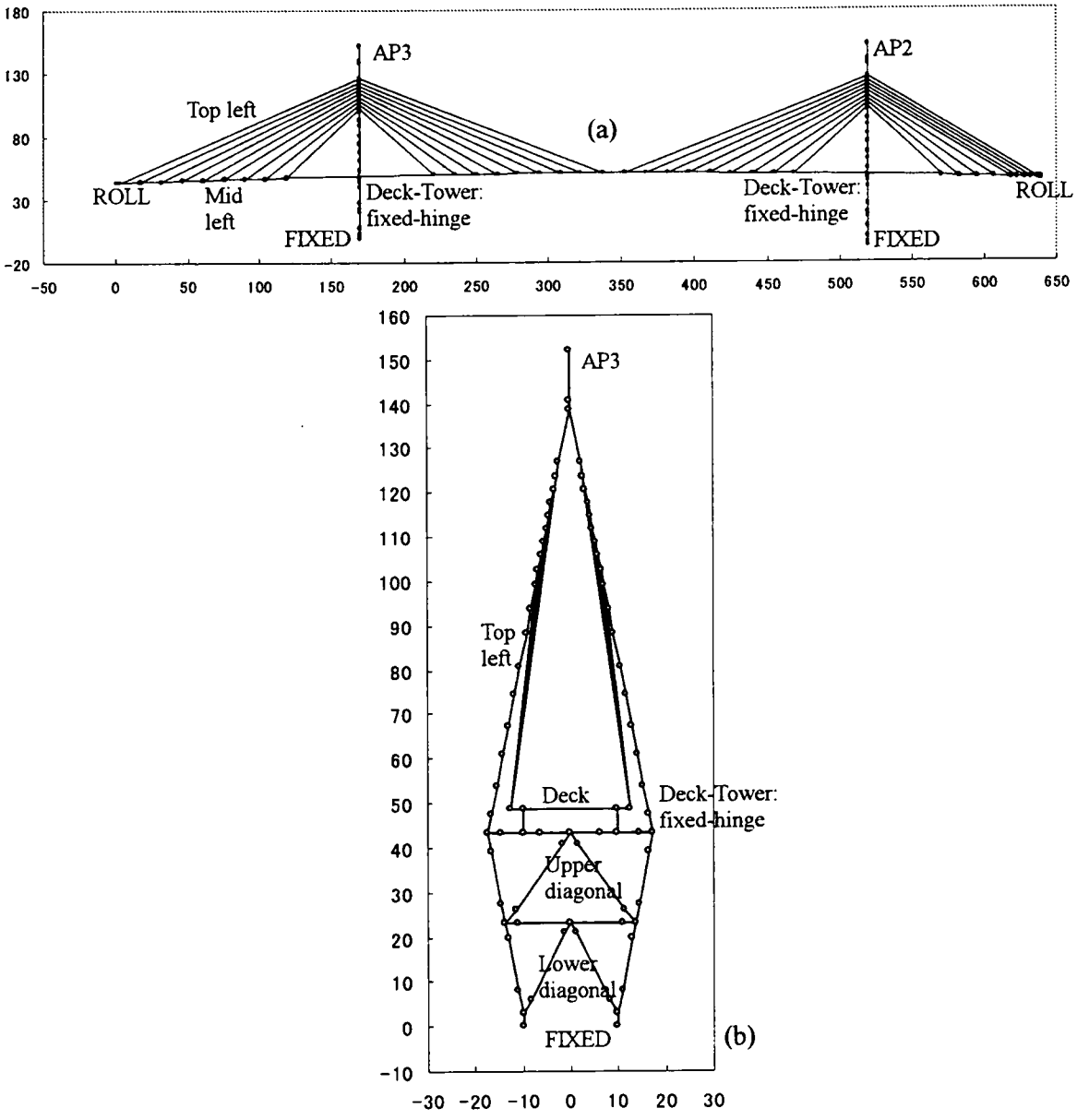

Figure 4-4. The Tempozan Bridge model in (a) longitudinal and (b) lateral directions

The plots of the model are shown in **Figure 4-4**. **Figure 4-4a** shows the model in the longitudinal direction. **Figure 4-4b** shows the tower in the transversal direction.

The original structure system has fixed-hinge connections between the towers and the deck and rollers connection between the deck-ends and piers, so that the deck longitudinal movement is constrained by the towers. The total mass of 25,354 tons is distributed appropriately at each node as lumped masses. The tower base is assumed to be fixed at the ground. Later on, the effect of flexible foundation and radiation of energy from foundation is studied in this chapter. The deck ends are moving freely at longitudinal direction.

The models were then analyzed by a commercial finite element program **(Prakash and Powell, 1993)**. Firstly, the model was analyzed two dimensionally in longitudinal and transversal directions. Then, effects of three dimensional model was also studied. The damping model used for the analysis is proportional to mass and stiffness so that damping ratio at each mode can be calculated. Numerical integration method is Newmark's constant acceleration method (beta equals one forth). The integration method is unconditionally stable, therefore integration time step of 0.01 second is assumed to be appropriate to obtain reliable numerical results.

From the analysis of the model, mode shapes and natural periods of each mode shape can be obtained. The amount of the mode shapes in longitudinal direction model is 190 in total. First ten mode shapes, natural periods, and effective modal mass ratio as a fraction of total mass in longitudinal direction are shown in **Figures 4-5** and **4-6**. From the figures, it is clear that the first mode is important during longitudinally seismic attack since the effective modal mass as a fraction of total mass in this direction is 84%. The first mode corresponds to 3.75 second of natural period.

For the lateral model, the amount of mode shapes is 144 in total. First two important mode shapes are shown in **Figure 4-7** for Tower AP3. It is clear from the figure, that the first mode in the lateral direction is important during laterally seismic attack, since the effective modal mass as a fraction of total mass is 81%. The first mode corresponds to 1.79 second of natural period.

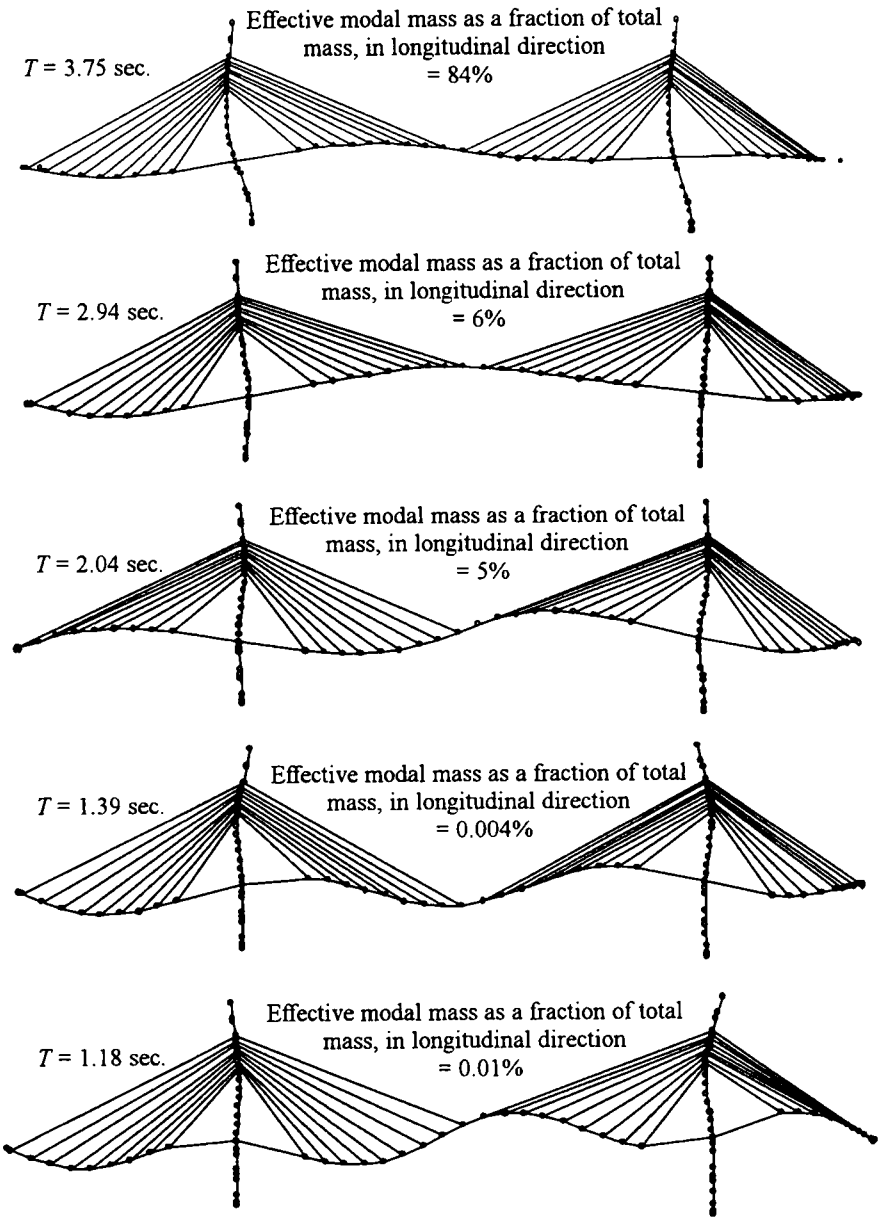

Figure 4-5. First to fifth modes of the Tempozan Bridge model in longitudinal direction (displacement is exaggerated; 190 modes in total)

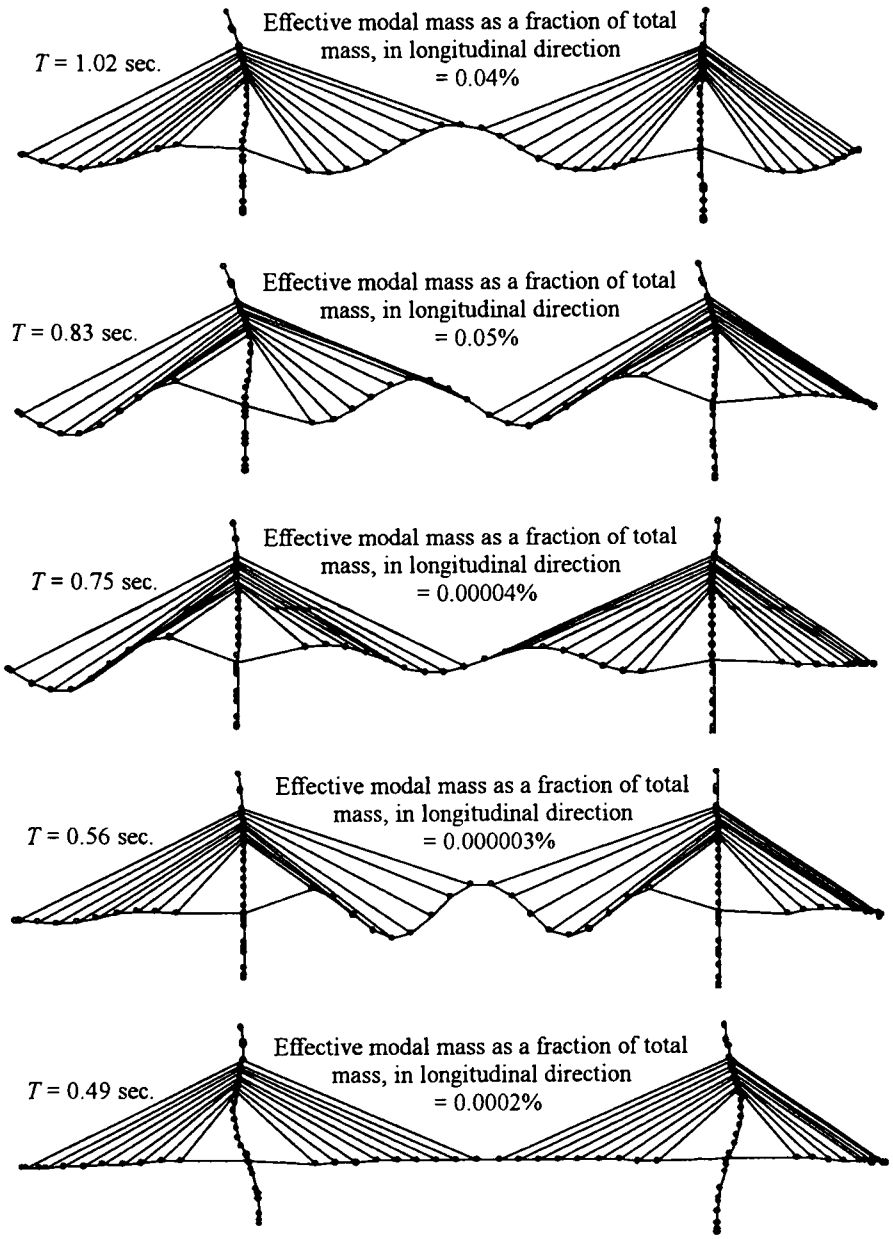

Figure 4-6. Sixth to tenth modes of the Tempozan Bridge model in longitudinal direction (displacement is exaggerated; 190 modes in total)

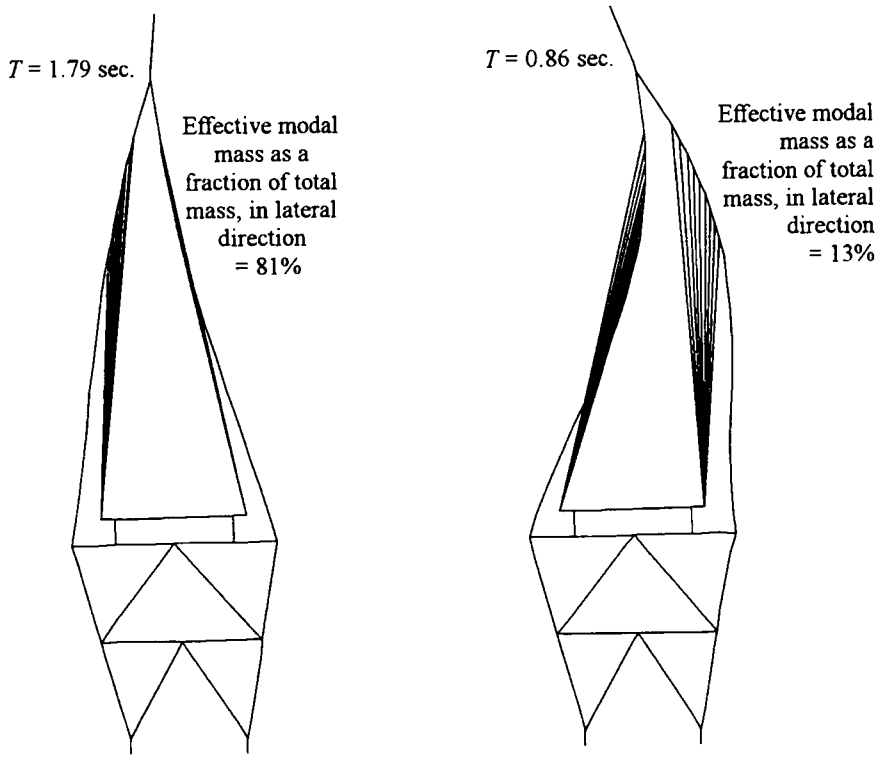

Figure 4-7. First and second modes of the Tempozan Bridge model in lateral direction (displacement is exaggerated; Tower AP3, 144 modes in total)

4.3 Seismic Response under Original and New Design Earthquakes

To derive earthquake motions that fit to the original design spectrum at period of interest, three well-known earthquake records were scaled up or down to fit the original design spectrum at the period of interest at damping ratio of 5%. The three records are: El Centro NS 1940, Parkfield NE, and Pacoima Dam SW. The response spectra of those earthquake records fitted to the original design spectrum are shown in **Figures 4-8** and **4-9**. **Figure 4-8** shows the earthquake response spectra that are fitted to the original design spectrum at the natural period of 3.75 second. This is the natural period of the bridge model in longitudinal direction at first mode (which is the main mode, because effective modal

mass as a fraction of total mass is 84%). **Figure 4-9** shows that the earthquake response spectra are fitted to the original design spectrum at the natural period of 1.79 second. This is the natural period of the bridge model in lateral direction at first mode (also the main mode, since effective modal mass as a fraction of total mass is 81%).

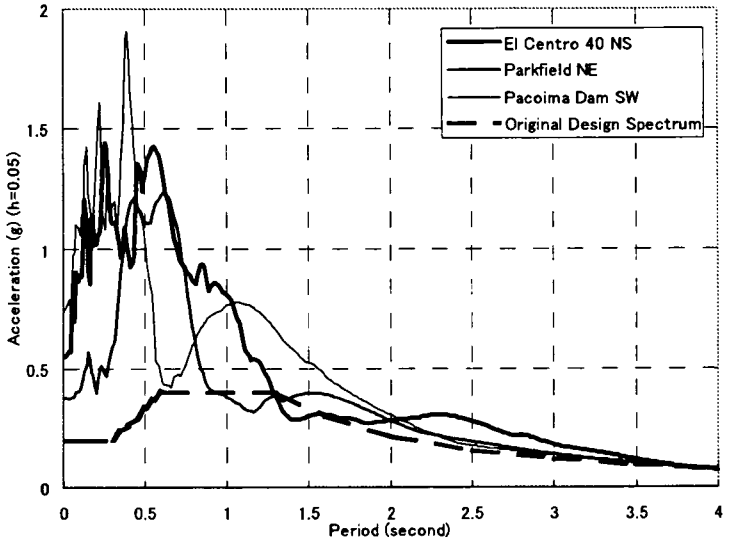

Figure 4-8. Response spectra of earthquake records fitted to original design spectrum at $T = 3.75$ second (damping ratio = 5%).

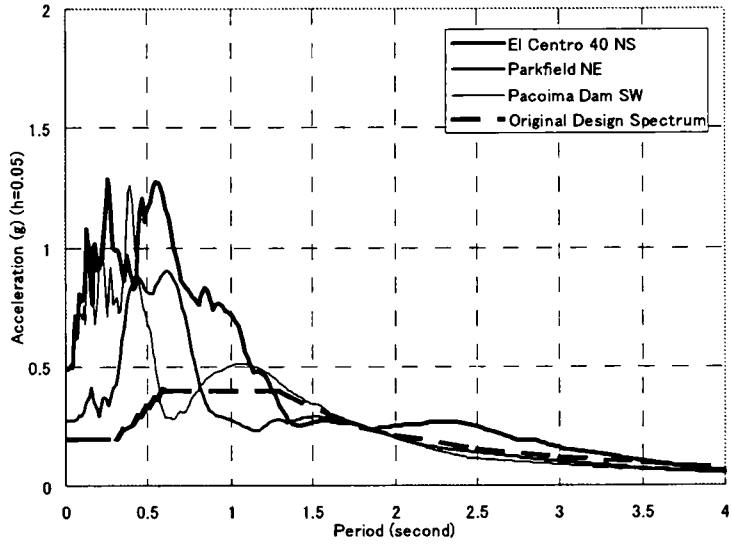

Figure 4-9. Response spectra of earthquake records fitted to original design spectrum at $T = 1.79$ second (damping ratio = 5%).

The new design earthquake data are called Type I-III-1, I-III-2, and I-III-3. These are artificial acceleration data used for design in Japan for soft soil condition. They are Level II Type 1 which are inter-plate type earthquakes. The acceleration records and their response spectra are shown in **Figures 4-10** to **4-12**.

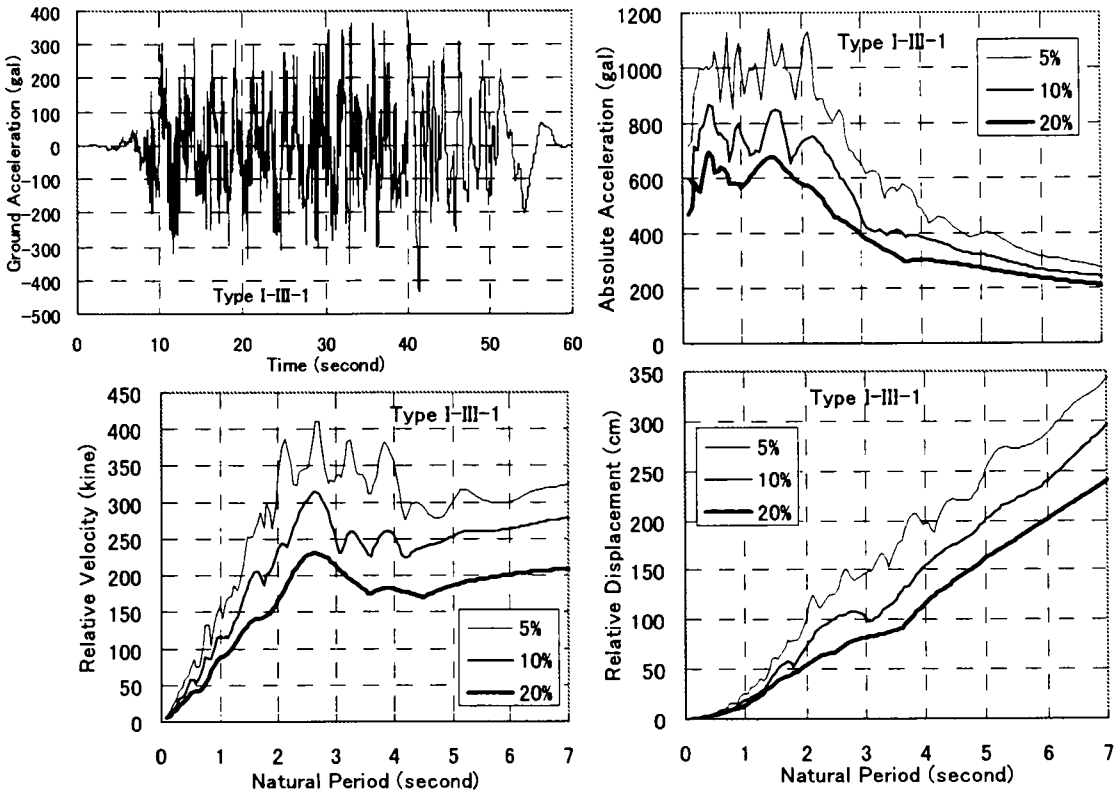

Figure 4-10. New design earthquake and its spectra (Type 1-III-1)

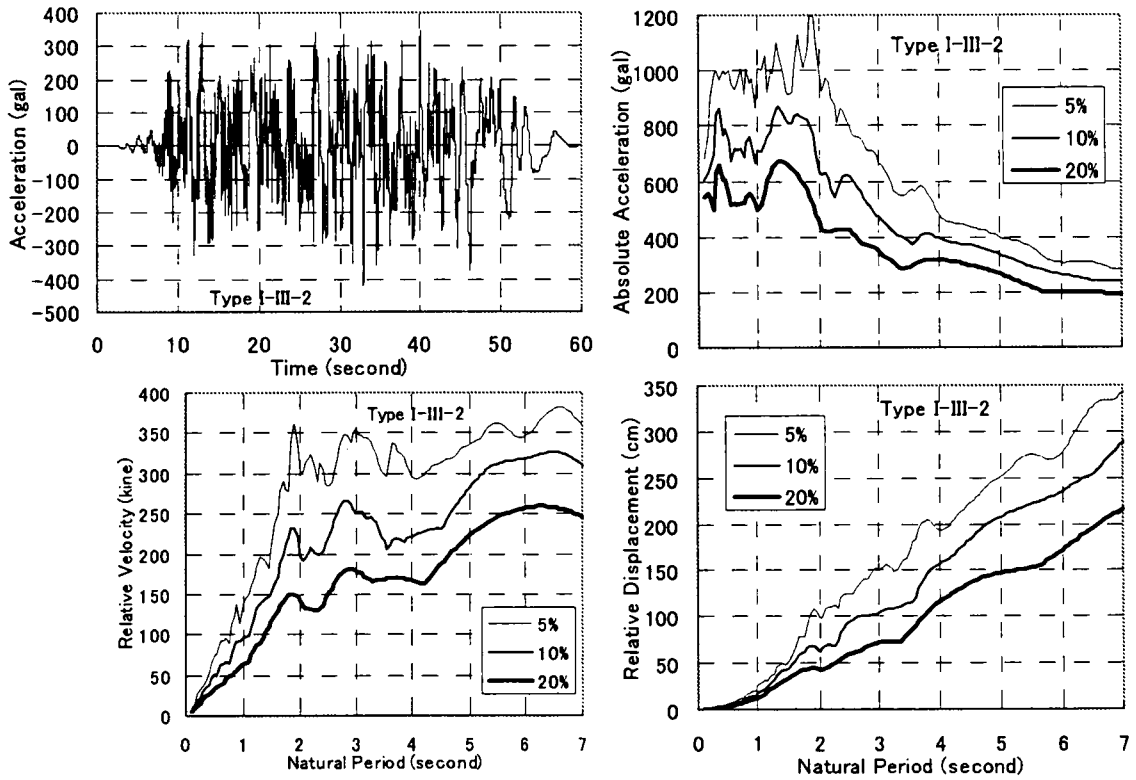

Figure 4-11. New design earthquake and its spectra (Type 1-III-2)

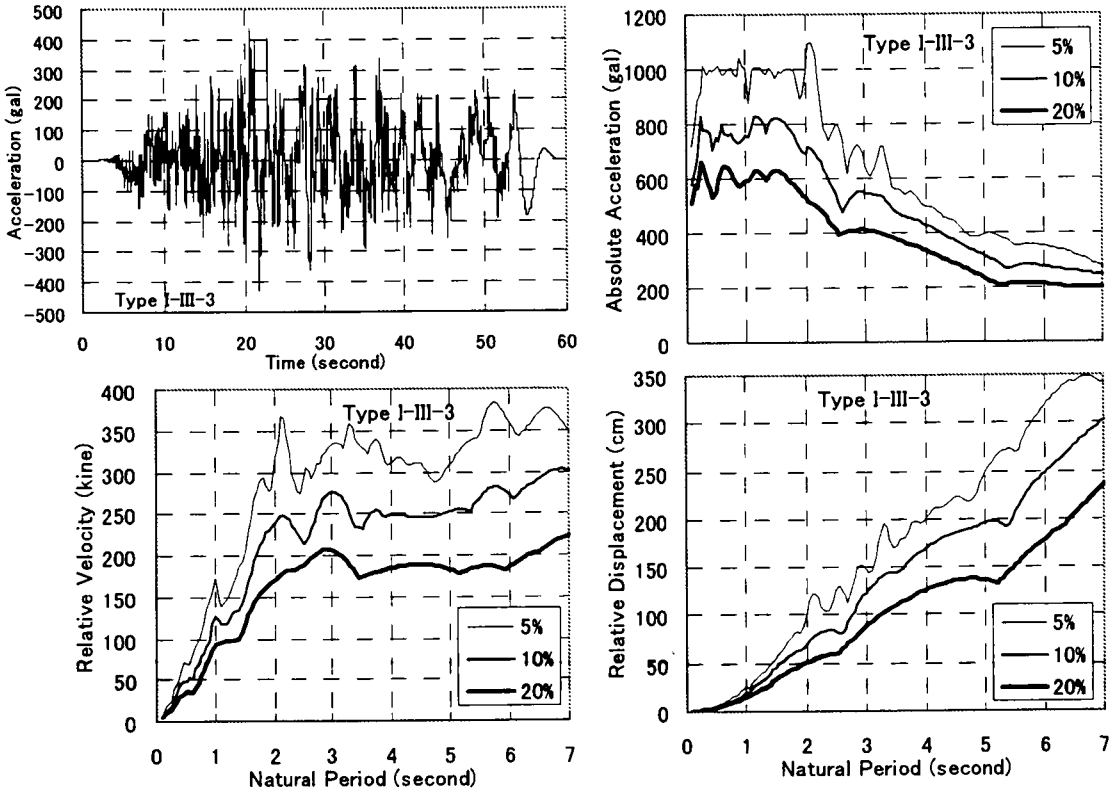

Figure 4-12. New design earthquake and its spectra (Type 1-III-3)

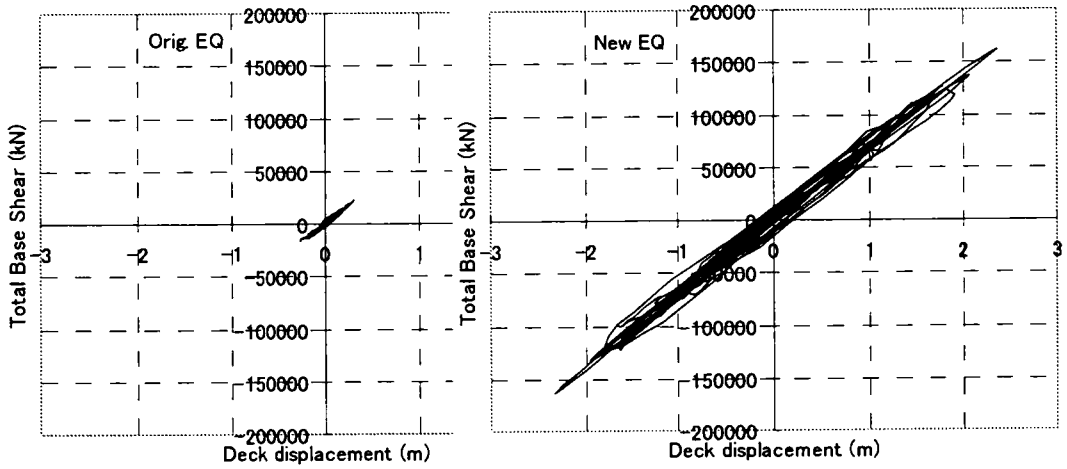

Figure 4-13. Deck displacement – base shear relationship of the Tempozan Bridge model under original (scaled Parkfield NE) and new (Type 1-III-3) design earthquakes in the longitudinal direction (First mode natural period $T = 6.31$ second)

Figure 4-13 shows the deck-displacement – base-shear relationship under original and new design earthquake inputs in the longitudinal direction. **Figure 4-14** shows the displacement time history of the deck. From the figures, it is clear that the Tempozan

Bridge response in the longitudinal direction is governed by the first mode, since there is clear relationship between deck displacement and base shear, as shown in **Figure 4-13**.

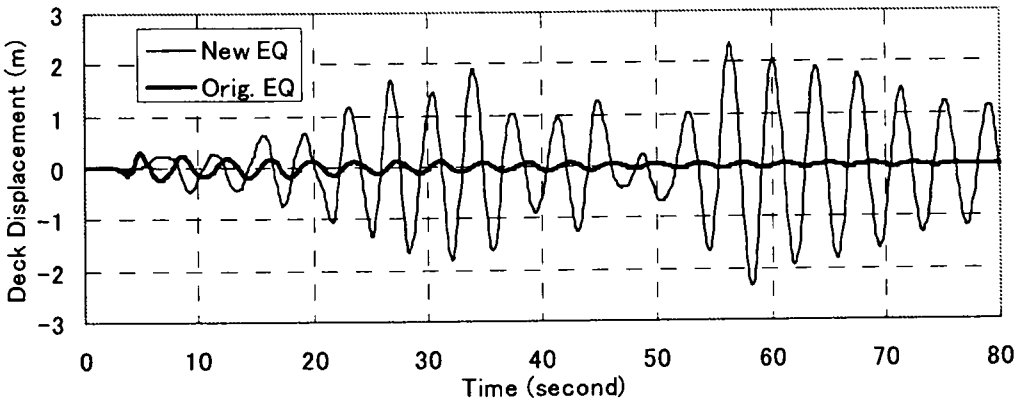

Figure 4-14. Deck displacement time history of the Tempozan Bridge model under original (scaled Parkfield NE) and new (Type 1-III-3) design earthquakes in the longitudinal direction (First mode natural period $T = 6.31$ second)

The new design earthquake results in significant increase in base shear and deck displacement. The mean increase is about 717%. Maximum responses of the Tempozan Bridge model are shown in **Table 4-1**.

In the lateral direction, the deck displacement time history is shown in **Figure 4-15** and the maximum responses are shown in **Table 4-2**. The new design earthquake results in significant increase in seismic response. The mean increase is about 394%.

Table 4-1. Maximum Responses of the Original Bridge in Longitudinal Direction

Members	Original Design Earthquake [1)]	New Design Earthquake [2)]	Percentage [3)]
Deck Displacement	0.25 m	2.37 m	948 %
Tower Base Moment [4)]	400 MN.m	3100 MN.m	775 %
Tower Base Shear [4)]	12400 kN	88500 kN	714 %
Tower Base Axial Force [4)]	9000 kN	48000 kN	533 %
Cable Force [5)]	3500 kN	24000 kN	685 %
Bearing Force [6)]	15800 kN	94000 kN	595 %
Deck Moment [7)]	58 MN.m	370 MN.m	637 %
Deck Axial Force [7)]	6600 kN	56000 kN	848 %

1) Scaled Parkfield NE earthquake
2) Type 1-III-3 earthquake
3) Mean increase of member responses ≈ 717%
4) At Tower AP3
5) At Top left in **Figure 4-4a**
6) Between tower AP3 and deck
7) At Mid left in **Figure 4-4a**

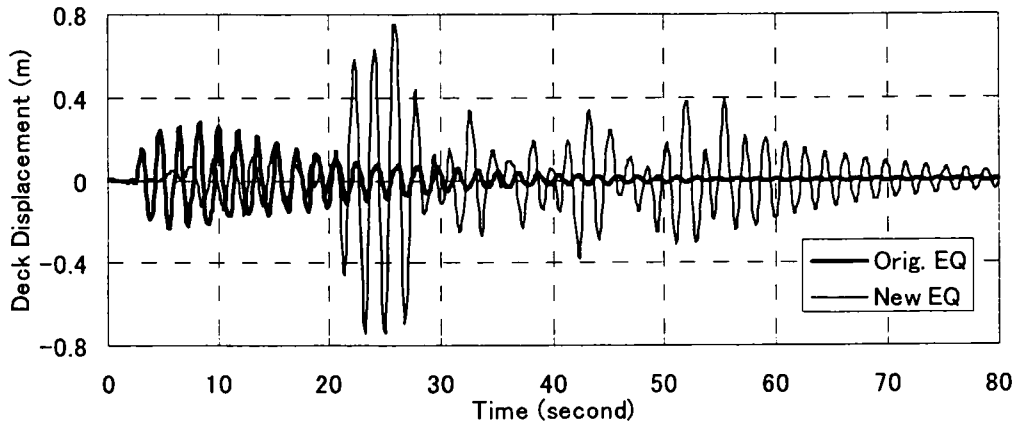

Figure 4-15. Deck displacement time history of the Tempozan Bridge model under original (scaled Parkfield NE) and new (Type 1-III-3) design earthquakes in the lateral direction (First mode natural period $T = 1.79$ second)

Table 4-2. Maximum Responses of the Original Bridge in Lateral Direction

Members	Original Design Earthquake [1)]	New Design Earthquake [2)]	Percentage [3)]
Deck Displacement	0.182 m	0.744 m	409 %
Tower Base Moment [4)]	170 MN.m	670 MN.m	394 %
Tower Base Axial Force [4)]	79100 kN	354000 kN	447 %
Cable Force [5)]	740 kN	2680 kN	362 %
Bearing Force [6)]	17600 kN	54300 kN	308 %
Upper Diagonal Axial Force [7)]	35000 kN	151000 kN	431 %
Lower Diagonal Axial Force [7)]	40300 kN	164000 kN	407 %

1) Scaled Pacoima Dam SW earthquake
2) Type 1-III-3 earthquake
3) Mean increase of member responses ≈ 394%
4) At Tower AP3
5) At Top left in **Figure 4-4b**
6) Between tower AP3 and deck
7) At Diagonal member in **Figure 4-4b**

To review whether the above member responses exceed the elastic limit of the members, static gravity analysis and member elastic limit calculation were carried out. The static gravity member forces are shown in **Table 4-3**. The elastic limit of members is calculated (**Appendix B**), and the results are shown in **Table 4-4**. It is clear by adding **Table 4-2** (seismic response) with **Table 4-3** (static gravity), and then comparing the results with **Table 4-4** (member's elastic limit), the tower base moment under new design earthquake exceeds the member elastic limit by a factor of 3. Whereas the original design

earthquake produces base moment only about half the elastic limit. The cable force induced by the new design earthquake results in large compression force in the cable, which is not allowable.

Table 4-3. Maximum Static Gravity Response of the Original Bridge in Longitudinal Direction

Members	Static force/moment
Tower Base Moment [1)]	53 MN.m
Tower Base Axial Force [1)]	118500 kN
Cable Force [2)]	8257 kN
Deck Moment [3)]	38 MN.m
Deck Axial Force [3)]	32000 kN

1) At Tower AP3
2) At Top left in **Figure 4-4a**
3) At Mid left in **Figure 4-4a**

Table 4-4. Member Elastic Limit of the Original Bridge in Longitudinal Direction

Members	Elastic limit
Tower Base Moment [1)]	950 MN.m
Tower Base Axial Force [1)]	550000 kN
Cable Force [2)]	34000 kN
Deck Moment [3)]	5770 MN.m
Deck Axial Force [3)]	404000 kN

1) At Tower AP3
2) At Top left in **Figure 4-4a**
3) At Mid left in **Figure 4-4a**

It is clear from the review above, that the new design earthquake produces large member forces, especially the tower base moment, it exceeds the elastic limit by a factor of 3. The cable suffers from compressive force which has to be avoided. Therefore, seismic retrofit of the cable-stayed bridge by the application of structural control technologies is needed.

4.4 Retrofitted with Elastomeric Bearing and Viscous Damper

For the retrofitted structure (**Figure 4-16b**), the stiffness of the bearing is an important issue as very flexible bearings produce large seismic displacement response and stiff bearings reduce the effectiveness of damper to absorb energy, as it is shown later on. Therefore, based on a study on a simplified model of the bridge under seismic motion, shown later on in this subchapter, bearing stiffness that produces retrofitted main period (T') 1.7 times the original main period (T) was finally chosen.

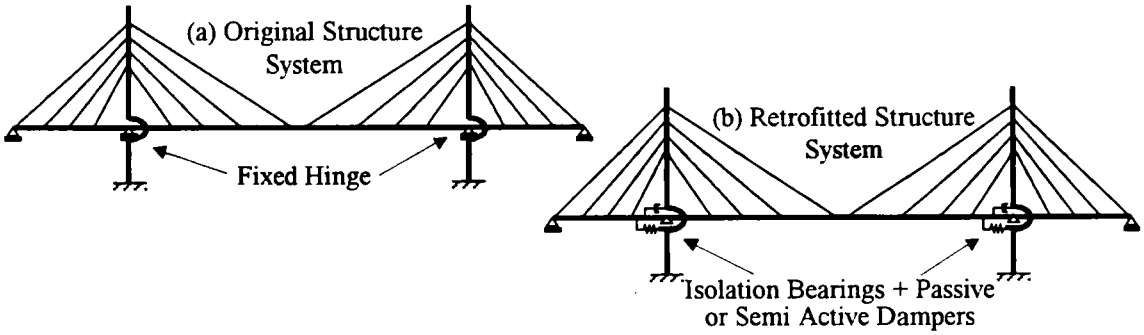

Figure 4-16. Retrofit system of the cable-stayed bridge

To obtain optimum bearing stiffness, a simplified model of the bridge is developed to study the effectiveness of bearings plus dampers in reducing cable-stayed bridge seismic responses. The simplified model represents the main mode of the bridge in the longitudinal direction **(Branco et al., 2000)**. The simplified model consists of a set of massless bar elements and one vibrating concentrated mass (**Figure 4-17b**). This mass corresponds to the mass associated with the first longitudinal vibration mode of the bridge. The lower vertical element (depicted in bold) simulates the stiffness of the bridge for a horizontal displacement of the towers at the deck level. The contribution of the cables and of the towers above the deck level to the overall longitudinal stiffness of the bridge is simulated by other vertical elements.

System in **Figure 4-17b** is further reduced to that in **Figure 4-17c** assuming that the contribution of the cable stiffness k_c, the tower above the deck level stiffness k_{tu}, and elastic bearing stiffness k_i can be represented by connecting stiffness k. This is because the system has only one mode shape, therefore the displacement resulted from the rotation

of tower at the deck level can be linearly combined with the displacement from other elastic members.

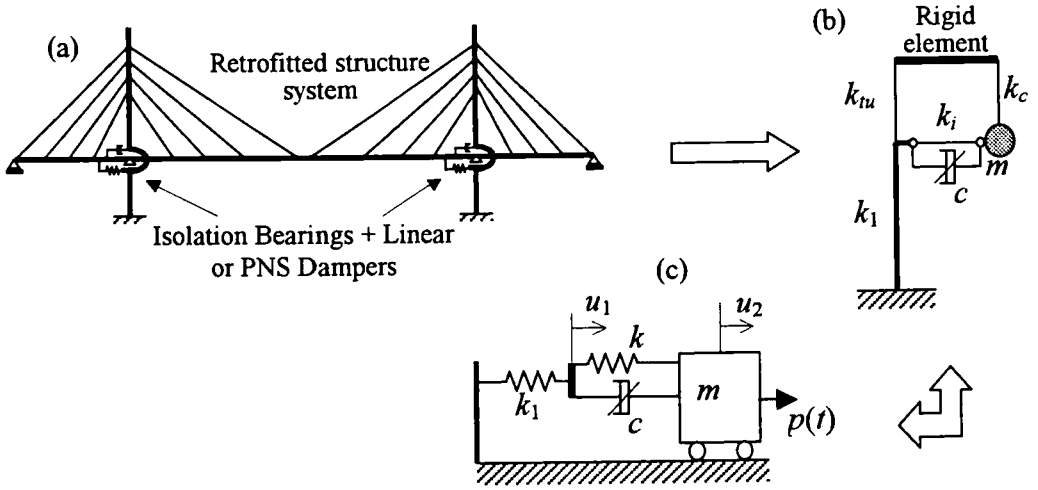

Figure 4-17. Simplified model of the cable-stayed bridge

The study used the model shown in **Figure 4-17c**. By using this model, the stiffness k was altered to produce T ranges from 3.75 to 9.0 seconds. Then, the damping coefficient c was determined by using **Equations (4-1)** to **(4-5)** so that damping ratio ζ_1 equals 20%, which is the expected damping ratio for the retrofitted bridge. For a two-spring system in **Figure 4-17c**, there is only one mass, therefore, the system has only one mode shape. **Equation (4-1)**, which is for classical damping **(Chopra, 1995)**, is used to calculate damping ratio ζ_1 of the system. The mass M, stiffness K, and damping C matrices are shown in **Equation (4-4)**.

$$\zeta_1 = \frac{C_1}{2M_1\omega_1} \tag{4-1}$$

where:

$$C_1 = \phi_1^T C \phi_1 \tag{4-2}$$

$$M_1 = \phi_1^T M \phi_1 \tag{4-3}$$

$$M = \begin{bmatrix} 0 & 0 \\ 0 & m \end{bmatrix}, \quad K = \begin{bmatrix} k_1 + k & -k \\ -k & k \end{bmatrix}, \text{ and } \quad C = \begin{bmatrix} c & -c \\ -c & c \end{bmatrix} \tag{4-4}$$

$$\phi_1 = \begin{Bmatrix} \left(\frac{k}{k_1+k}\right) \\ 1 \end{Bmatrix} \tag{4-5}$$

ϕ_1 : first mode shape, without damping

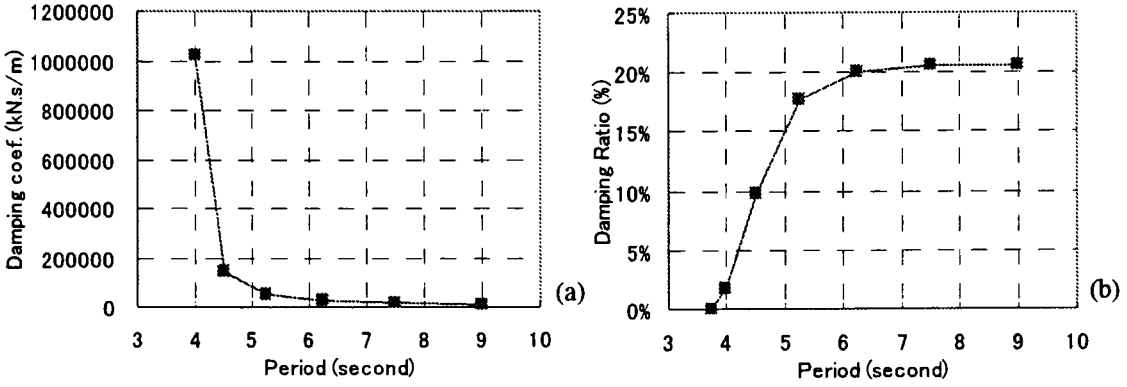

Figure 4-18. (a) Damping coefficient determined by **Equations (4-1)** to **(4-5)** for the system (b) Damping ratio determined from decaying motion of the system

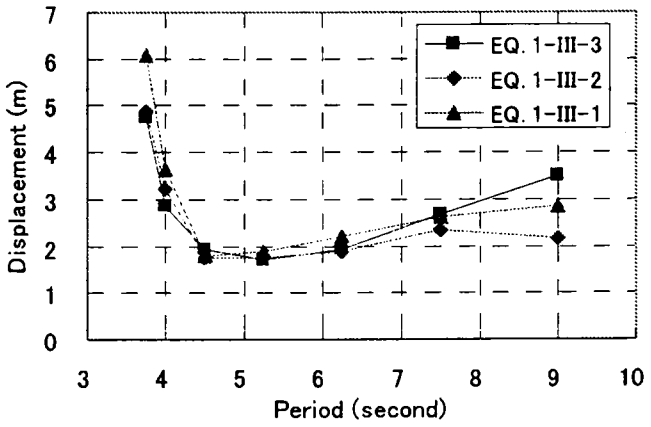

Figure 4-19. Displacement response, damping ratio $\zeta = 20\%$ (Type 1-III-3, 1-III-2, & 1-III-1: artificial ground accelerations used for design in Japan for soft soil condition)

Figure 4-18a shows the calculated damping coefficient to achieve damping ratio ζ_1 of 20%. **Figure 4-18b** shows the damping ratio of the model calculated from the decaying motion of the model. It is clear from the figures that if T' is larger than $1.7T$, expected damping ratio of the system can easily be achieved by choosing appropriate damping coefficient c (in this case, c is calculated by using **Equations (4-1)** to **(4-5)**). Up to this point, k that produce T' that is larger than $1.7T$ is appropriate so that the expected damping ratio can be achieved. However, as it is shown in **Figure 4-19**, when T' is larger than $1.7T$, for a constant damping ratio, larger seismic displacement response will occur. Therefore, k that produces $T' = 1.7T = 6.31$ second, was finally chosen for determining the stiffness of bearings for seismic retrofit of the bridge so that added damper set parallel to the bearings can effectively reduce seismic-induced displacement and forces.

4.4.1 Modal shape analysis

First modes of the original and retrofitted structures have the largest contribution to the longitudinal movement of the bridge therefore it is interesting to be shown here for analysis. The first mode shapes of the original bridge and the retrofitted bridge are shown in **Figure 4-20**.

Figure 4-20a shows the first mode shape of the original structure. Natural period (T) of this mode is 3.75 second, which is close to the design value for the bridge (3.7 second **(Hanshin Highway Public Corporation, 1992)**). This first mode has effective modal mass as a fraction of total mass of 84%. **Figure 4-20b** shows the first mode shape of the retrofitted structure. The first mode natural period (T') of the retrofitted bridge is 6.31 second and the effective modal mass as a fraction of total mass is 92%.

It is clear from the figures that smaller curvatures at the towers and the decks are found at the retrofitted structure than that in the original structure. Therefore, the retrofitted structure is expected to produce smaller moments at towers and decks than that in the original structure during earthquake excitation.

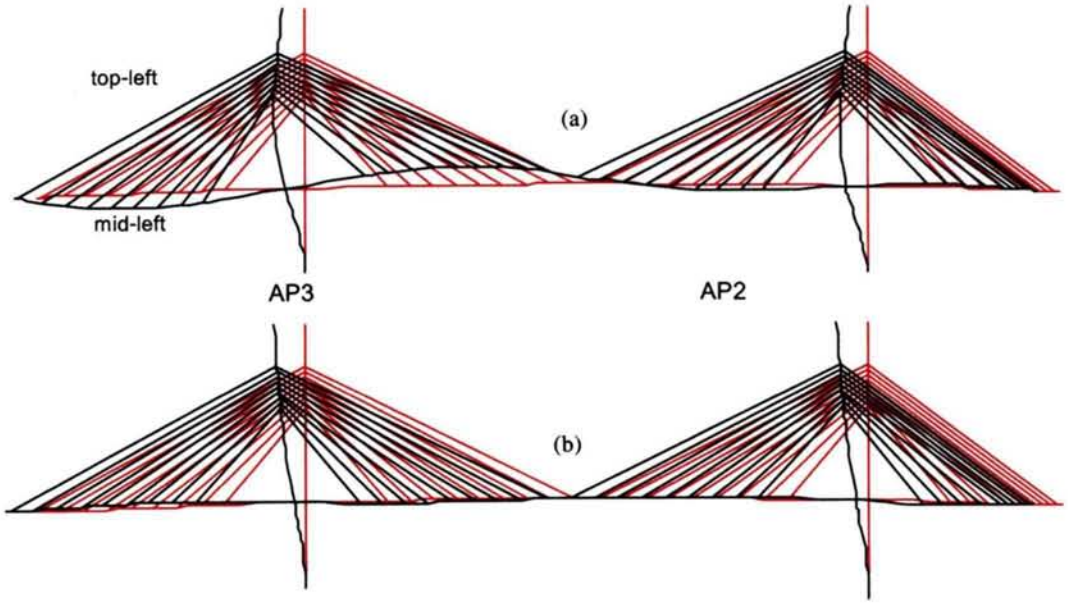

Figure 4-20. First mode shapes of (a) original and (b) retrofitted structures (deformation is exaggerated)

4.4.2 Time history analysis

The models were analyzed by a commercial finite element program **(Prakash and Powell, 1993)** which produces a piece-wise dynamic time history, using Newmark's constant average acceleration (β = 1/4) integration of the equations of motion, governing the response of a nonlinear structure to a chosen base excitation. The input motions were Type I-III-3, I-III-2, and I-III-1 earthquakes which are artificial acceleration data used for design in Japan for soft-soil condition. Those data are intended as Type I (inter plate type). With numerical comparison (see **Figure 4-3**), Type I earthquake motion gives higher effect to the bridge than Type II motion, in longer period range.

Table 4-5 shows maximum seismic response of the original bridge model and the retrofitted bridge model. The earthquake attack is in the longitudinal direction. The input is Type 1-III-3 earthquake.

Table 4-5. Maximum earthquake responses and damping ratios in longitudinal direction

Items	Original structure	Retrofitted structure		
		Elastic bearings	Elastic bearing + viscous dmp.	Hysteretic bearings
Deck displacement	2.37 m	4.17 m	1.50 m	1.58 m
Tower moment [1)]	3100 MN.m	2000 MN.m	900 MN.m	900 MN.m
Tower axial force [1)]	48000 kN	15000kN	15000 kN	21000 kN
Cable force	24000 kN	3440 kN	4000 kN	5000 kN
Bearing force [2)]	94000 kN	44000 kN	24500 kN	26500 kN
Deck moment	370 MN.m	95 MN.m	75 MN.m	95 MN.m
Deck axial force	56000 kN	21000 kN	11000 kN	15000 kN
Damping ratio	2 %	2 %	35 %	13.1 %
Natural period	3.75 s	6.31 s	6.73 s	3.86 s and 6.31 s [3)]

[1)] Base of tower AP3, [2)] At connection between deck and tower AP3,
[3)] Initial and post yielding stiffness

It is clear from the table, that if elastic bearings are used for seismic retrofit, the sectional forces are reduced to about 40% of the original ones. However, the displacement response increases up to 176% of the original one. Therefore, additional dampers are needed.

By adding viscous dampers to the elastic bearings, the sectional forces are reduced to about 25% of the original ones and the displacement response is reduced to 63% of the

original one. All member forces are lower than the member's yield forces and the cables are not under compressive force. The structural damping ratio is calculated as 35% from the decaying motion of the bridge. The natural period elongates from 6.31 second to 6.73 second because of large damping ratio. Hysteretic loops of bearing displacement as a function of bearing force and deck displacement as a function of tower base shear are shown in **Figure 4-21**. It can be seen that although the bearing hysteretic loop is "fat", the structural hysteretic loop that shows the damping ratio at the first mode is "less fat". More about this is studied in the last part of this chapter.

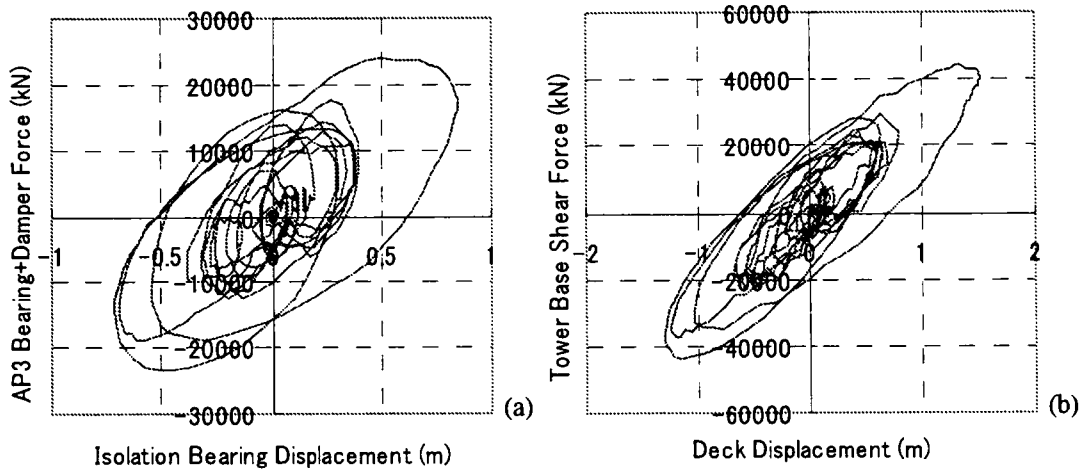

Figure 4-21. Hysteretic loops of (a) bearing plus damper and (b) structural system

4.5 Retrofitted with Steel Hysteretic Bearing

The hysteretic bearing second stiffness produces $T' = 1.7T$. Bearing initial stiffness is its second stiffness divided by 0.03 to represent a typical steel hysteretic damper **(Blakeley et al., 1979)**. The hysteretic bearing yield force is set as 10000 kN (0.04 × total weight of the bridge) at one tower.

If hysteretic bearings are used for seismic retrofit, the sectional forces are reduced to about 29% of the original ones and the displacement response is reduced to 67% of the original one. All member forces are lower than the member's yield forces and the cables are not under compressive force.

Figure 4-22 shows the hysteretic loops of bearing displacement as a function of bearing force and deck displacement as a function of tower base shear. The structural hysteretic loop is "less fat" than bearing hysteretic loop.

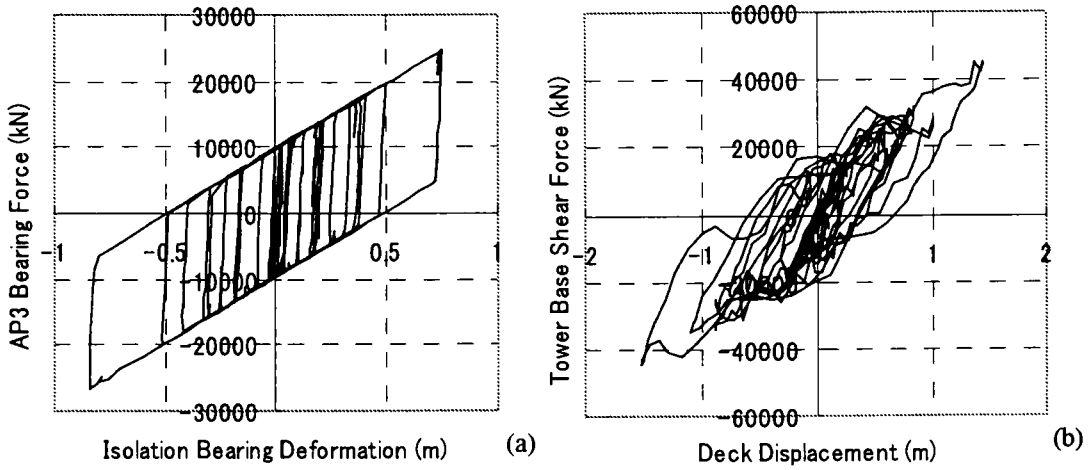

Figure 4-22. Hysteretic loops of (a) hysteretic bearing and (b) structural system

Equivalent structural damping ratio is calculated as 13.1% by using pushover analysis to obtain a back-bone curve at the main mode (**Figure 4-23**). The maximum displacement of the deck is set the same as the maximum seismic displacement. **Table 4-5** shows maximum seismic response of the original bridge model and the retrofitted bridge model by using steel hysteretic damper. The earthquake attack is in the longitudinal direction. The input is Type 1-III-3 earthquake.

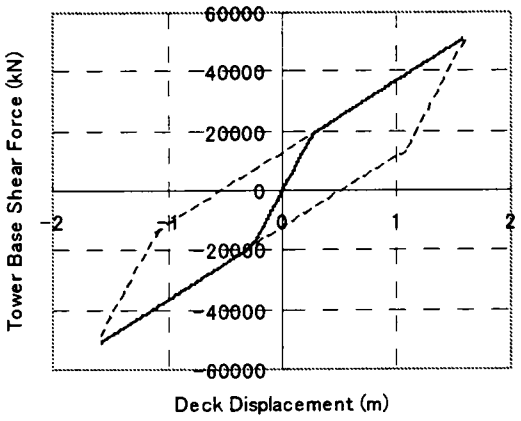

Figure 4-23. Back-bone curve of the bridge model from pushover analysis to calculate structural damping ratio

4.6 Effects of Flexible Foundation and Radiation of Energy from Foundation

One method to study the soil-structure interaction (SSI) effects on the effectiveness of the bridge seismic retrofit is to take into account the effects of flexible foundations and radiation of energy from foundations. In this method, the cable-stayed bridge is idealized as that in **Figure 4-24 (Kawashima and Unjoh, 1991)**. Subsoil supporting the foundation was assumed as an elastic half space. The subsoil was assumed elastic with no energy dissipation. The foundation was idealized as a rigid mass-less circular plate. Radius of the rigid circular plate was simply assumed so that it gives the same surface area as the foundation. Dynamic stiffness of the foundation was assumed in a frequency independent form:

$$K_x = \frac{8G_s a}{2-\upsilon} \qquad C_x = \frac{\pi G_s a^2}{V_s} \tag{4-6}$$

$$K_r = \frac{8G_s a^3}{3(1-\upsilon)} \qquad C_r = \frac{0.25\pi\sqrt{2(1-\upsilon)/(1-2\upsilon)}G_s a^4}{V_s} \tag{4-7}$$

in which K_x and C_x respresent spring and damping coefficient for sway motion, and K_r and C_r represent those for rocking motion. V_s and a represent shear wave velocity of subsoils and radius of foundation, respectively. Soil modulus of elasticity E_s was taken as 15 MPa for soft clay and Poisson ratio υ was assumed as 0.45 for clay (saturated) **(Bowles, 1982)**. Shear modulus of elasticity can then be calculated as $G_s = E_s/(2+2\upsilon)$ = 5.17 MPa. Shear wave velocity V_s is assumed as 150 m/s.

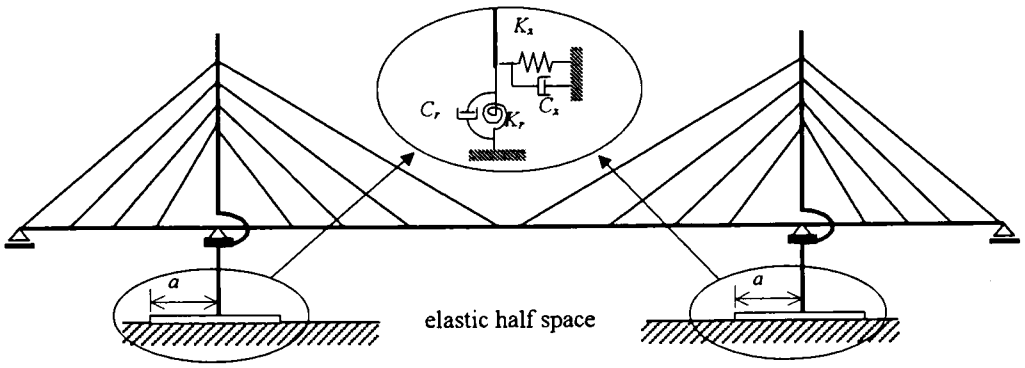

Figure 4-24. Cable-stayed bridge model studied for flexible and energy radiating foundation

The results (Type 1-III-3 input earthquake) are shown in **Table 4-6**. Comparing this table with **Table 4-5**, one can reveal that the above SSI model increases the natural period and the damping ratio of the original structure, because of additional flexibility and damping at the base of the foundation. However, for the retrofitted structure, the damping ratio is reduced and the effectiveness of bearings and dampers in reducing seismic responses is also reduced.

This is because the flexibility introduced by the above SSI model reduces the frequency of the structure and the relative movement at the bearings. These matters will reduce energy absorption by damper, because viscous damper is frequency dependent, and hysteretic damper is relative-movement dependent. Therefore, an introduction of flexibility from the above SSI model reduces the effectiveness of additional dampers put between the deck and the structure.

Table 4-6. Maximum earthquake responses and damping ratios (SSI model included)

Items	Original structure	Retrofitted structure	
		Elastic bearing + viscous damper	Hysteretic bearings
Deck displacement	2.78 m	2.57 m	2.77 m
Tower moment[1)]	1500 MN.m	800 MN.m	882 MN.m
Tower axial force [1)]	36200 kN	12500 kN	19800 kN
Cable force	12300 kN	3010 kN	4470 kN
Deck moment	228 MN.m	58 MN.m	86 MN.m
Deck axial force	31900 kN	9100 kN	12300 kN
Foundation Displ.	0.171 m	0.079 m	0.093
Damping ratio	3.1 %	23 %	9.3 %
Natural period	5.04 s	7.66 s	5.13 s and 7.46 s [3)]

[1)] Base of tower AP3, [2)] At connection between deck and tower AP3,
[3)] Initial and post yielding stiffness

4.7 Effects of Three Dimensionality

The previous study was based on a two dimensional (2D) model. To study the effectiveness of the model, a three dimensional (3D) model was analyzed to obtain important mode shapes. The results show that in the longitudinal direction, the 2D model

(**Figure 4-20a**) agrees well with the 3D model (**Figure 4-25a**). The first mode shape in 2D model has T = 3.75 seconds and effective modal mass as a fraction of total mass of 84% and those of the 3D model are T = 4.02 seconds and 88%, respectively. Therefore, the 2D analysis above is appropriate for studying the effectiveness of passive and semi-active control in this cable-stayed bridge.

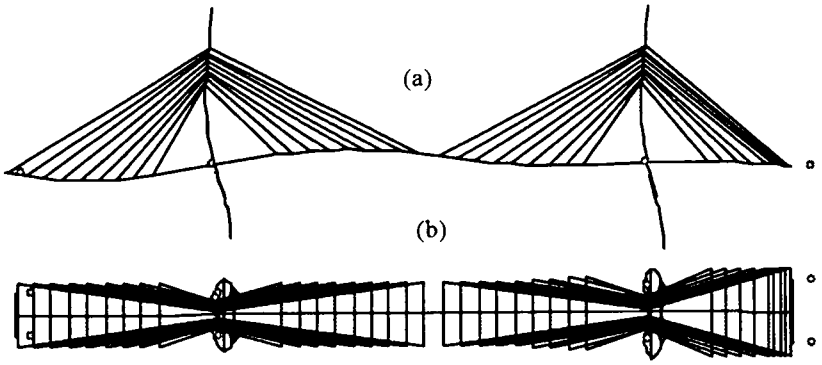

Figure 4-25. First Mode Shape of the 3D Model (a) side view (b) plan

However, because of significant coupling of motions, the 2D model is not sufficient for modeling the cable-stayed bridge in lateral direction. Examples of coupling between bending and torsion are shown in **Figures 4-26** and **4-27**. The 2D model has T = 1.79 seconds and effective modal mass as a fraction of total mass of 81%. On the other hand, those of the 3D model in the third and seventh modes are T = 2.23 seconds, 45.4%, T = 1.48 seconds, and 21.9%, respectively.

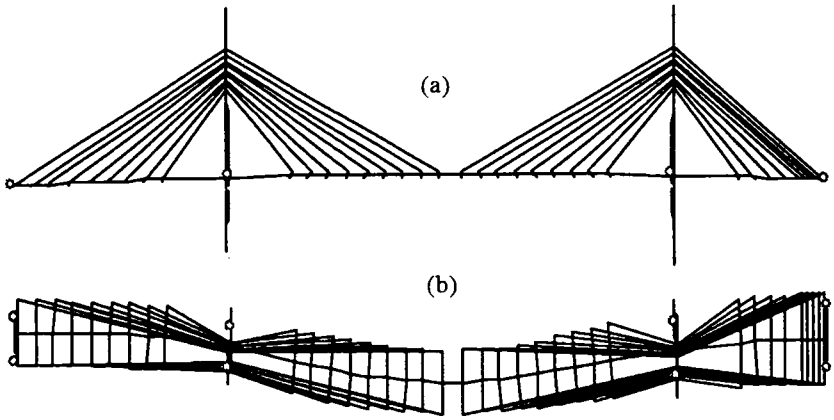

Figure 4-26. Third Mode Shape of the 3D Model (a) side view (b) plan

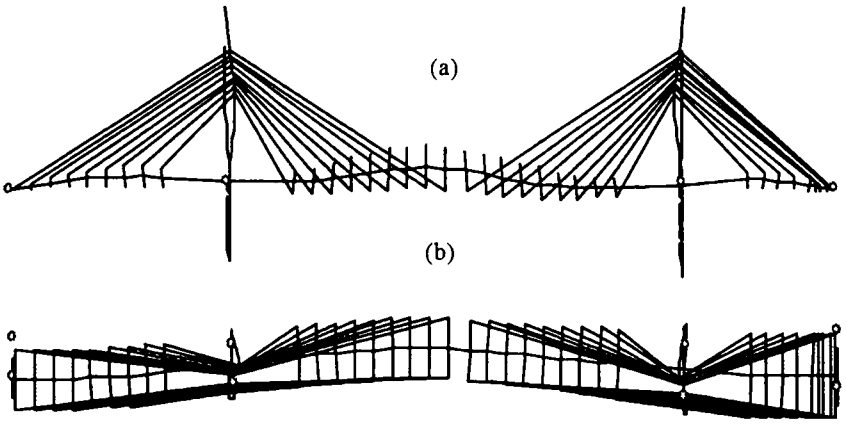

Figure 4-27. Seventh Mode Shape of the 3D Model (a) side view (b) plan

4.8 Effects of Connections with Adjacent Structures

The retrofitted bridge has natural period longer (6.31 second) than the original one. The original bridge was designed to have 3.75 second of main natural period **(Hanshin Highway Public Corporation, 1992)**. Assuming that the adjacent structures, in this case adjacent decks that approach the bridge, were also designed to have the same natural period as that of the original bridge structure, then there are differences between the retrofitted structure natural period, T = 6.31 sec., and the adjacent structures natural period (assumed to be the same as the original structure's T = 3.75 sec.). This difference in natural period between two adjacent structures will cause dynamics problem, such as pounding, error in assumptions, etc. Therefore, a study was carried out to examine the effect of connecting the bridge decks to adjacent structures. The connections is assumed to cause the retrofitted-bridge natural period return to T = 3.75 second, by giving additional spring at both ends of the deck. The additional spring represents the stiffness of adjacent structures and is set so that the retrofitted structure has natural period the same as the original one.

Figure 4-28 shows the mode shapes of the retrofitted structures. **Figure 4-28a** shows the mode shape of the retrofitted structure without any restriction at either deck end. **Figure 4-28b** shows the mode shape of the retrofitted structure with additional spring at

deck ends. From the figure, one can observe that only minor difference occurs between the mode shapes.

However, time history analysis shows that by connecting the deck to the adjacent structures, the adjacent structures resist significant amount of seismic induced force. To illustrate, the force at a connection at the end of deck is 34000 kN and the shear force at Tower AP3 base is only 11000 kN. On the other hand, for the retrofitted structure without deck end connections, Tower AP3 base shear is 24000 kN. In other words, connecting the bridge deck to adjacent structures is advantageous to the bridge, because significant amount of force is transmitted to adjacent structures. Therefore, next study about the bridge will use the retrofitted-bridge model without any connections to adjacent structures since this will give worse effect to the bridge.

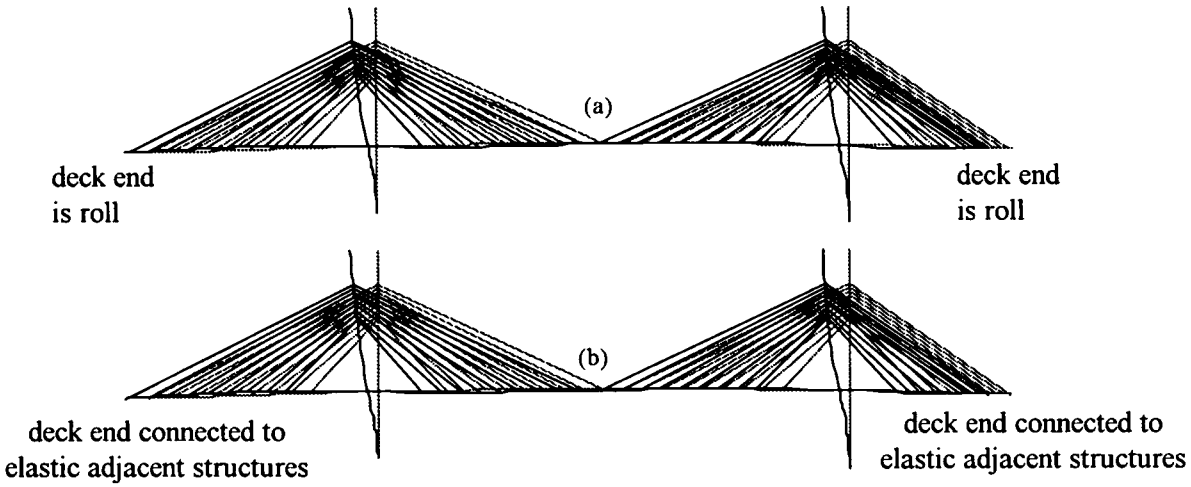

Figure 4-28. First mode shapes of retrofitted structures
(a) without deck-end connections to adjacent structures, $T = 6.31$ sec.
(b) with deck-end connections to adjacent structures, $T = 3.75$ sec.

4.9 Retrofitted with Pseudo Negative Stiffness Damper

The semi-active control proposed uses variable-orifice dampers, or shortened herein as variable damper. By using a certain algorithm shown previously in **Chapter 3**, the variable damper can produce pseudo-negative stiffness hysteretic loop. The effectiveness

of variable-orifice dampers in controlling seismically excited buildings by using pseudo negative stiffness control algorithm has been demonstrated through both simulation and full-scale experimental studies **(Iemura et al., 2001b)**.

This pseudo-negative hysteretic loop combined with connecting stiffness produces hysteretic loop that is as close as to that of rigid–perfectly plastic force–deformation characteristics (**Figure 4-29a**). **Figure 4-29** shows ideal and realistic force–deformation characteristics of connecting stiffness and variable damper when pseudo-negative stiffness algorithm is used. In this case, the connecting stiffness between the deck and the tower is a sum of bearing stiffness, upper-tower stiffness, and cable stiffness.

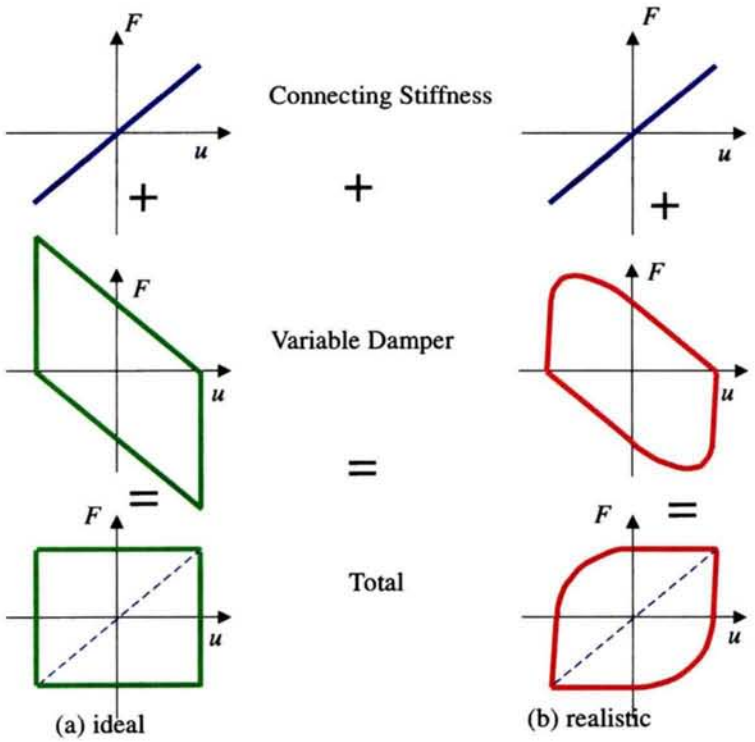

Figure 4-29. Ideal and realistic hysteretic loops
produced by pseudo-negative stiffness variable damper

4.9.1 Structural damping ratio

Because the dampers are put between the deck and the tower, the elemental damping ratio of 53.4% will not become the structural damping ratio. The structural damping ratio becomes 35.6% at the main mode. This is because of the flexibility introduced by the

tower below the deck level.

Figure 4-30 illustrates the effects of spring (set in series) to the damping ratios. Tower stiffness is k_1 and connecting stiffness is k. The strain energy of the system in one cycle (shaded area) is a summation from that of stiffness k_1 and that of stiffness k. Energy absorption of the system is only from that by the variable damper. Therefore, for the case of $k = 0.5k_1$, or retrofitted natural period equals 1.7 times original natural period, the structural damping ratio will be 2/3 of elemental damping ratio. If the variable damper was put between the deck and some stiff supports on the ground, then structural damping ratio will be the same as the elemental damping ratio.

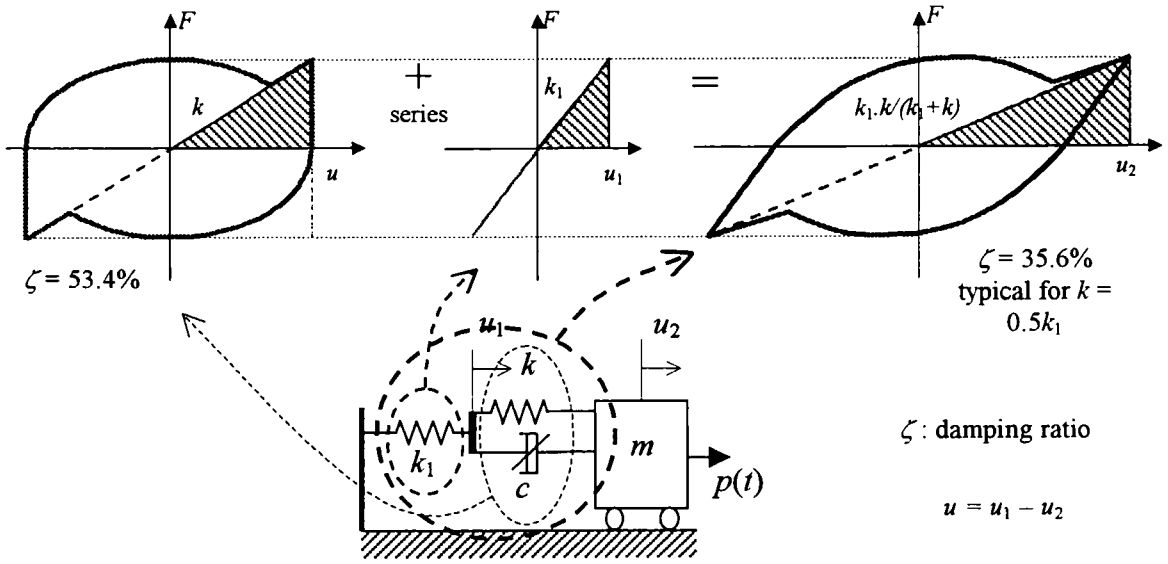

Figure 4-30. Damping ratio of a spring-damper-mass system

4.9.2 Seismic Response of the Bridge

The cable-stayed bridge model with isolation bearings and dampers (**Figure 4-16b**) was analyzed by a program developed by the authors under MATLAB environment **(Mathworks, 1997a)** which produces a piece-wise dynamic time history, using Newmark's constant average acceleration ($\beta = 1/4$) integration of the equations of motion, governing the response of a nonlinear structure to a chosen base excitation. The cable-stayed bridge model is a 76 degree of freedom system. The input motions were Type I-III-1, I-III-2, and I-III-3 earthquakes which are artificial acceleration data used for design in Japan.

The results show that the application of pseudo negative stiffness control algorithm is effective in reducing seismic response of the bridge model. **Figure 4-31** shows base shear-deck displacement relationship for both bridge with linear damper and pseudo negative stiffness damper, respectively, under Type I-III-1 earthquake input. The bridge model with pseudo negative stiffness dampers shows lower base shear than that of the bridge with linear damper.

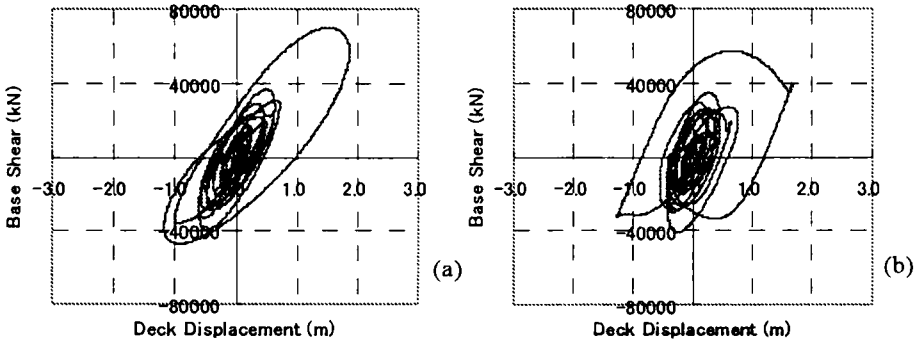

Figure 4-31. Base shear – deck displacement relationship of a cable-stayed bridge model with (a) linear dampers (b) pseudo negative stiffness dampers (Type I-III-1 earthquake)

Figure 4-32 shows the hysteretic loops produced by both linear dampers and pseudo negative stiffness dampers (at tower AP3). The damping force produced by pseudo negative stiffness damper is larger than that of linear damper. However, the total force of damping plus isolation bearing is lower for pseudo negative stiffness damper (**Figure 4-33**). Therefore the base shear of the cable-stayed bridge model is lower for the pseudo negative stiffness dampers.

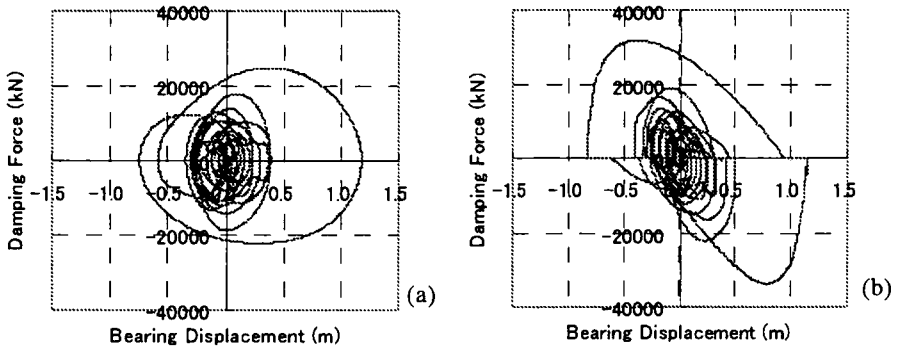

Figure 4-32. Damping force – bearing displacement relationship of a cable-stayed bridge model with (a) linear dampers (b) pseudo negative stiffness dampers (Type I-III-1 earthquake)

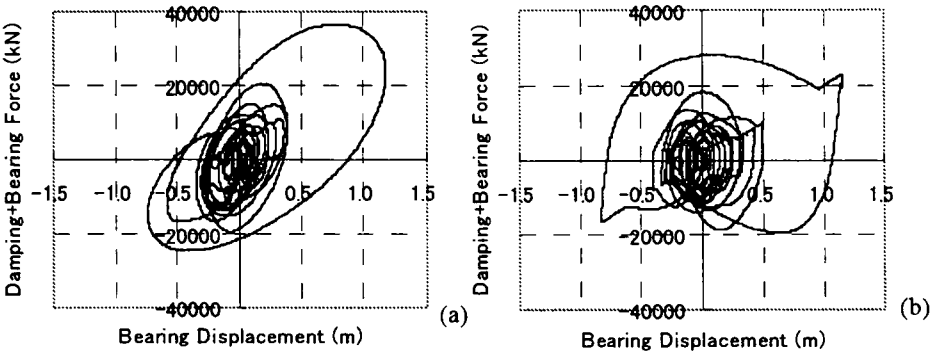

Figure 4-33. Total connection force – bearing displacement relationship of a cable-stayed bridge model with (a) linear dampers (b) pseudo negative stiffness dampers (Type I-III-1 earthquake)

4.10 Summary

This chapter presents the application of passive and pseudo negative stiffness control for seismic retrofit of a typical cable-stayed bridge. For better relation with real case, the cable-stayed bridge model is developed based on the design drawing of the Tempozan Bridge in Osaka, Japan, built in 1988 as part of Hanshin Expressway.

Very high ground motion (level II design) is now required in the new bridge design specification set in 1996 in Japan. Hence seismic safety of cable-stayed bridges built before the present specification has to be reviewed and seismic retrofit has to be done, if it is found necessary. The results show that significant increase in seismic responses of the bridge in the longitudinal and transversal direction was found when the existing bridge was simulated using new design earthquakes. On the contrary, by applying passive control for seismic retrofit of the bridge, significantly lower seismic responses were obtained so that seismic safety of the bridge could be enhanced.

Another means of seismic retrofit is by using pseudo negative stiffness control. The chapter show that pseudo negative stiffness control results in significantly better seismic responses reduction than that by passive viscous damper. The deck displacement as well as base shear force are significantly lower than those by passive viscous damper.

Chapter 5

Application of Pseudo Negative Stiffness Damper to the Benchmark Bridge

5.1 General Remarks

In the field of civil engineering, many control algorithms and devices have been investigated over the last two decades to protect structures against natural hazards such as strong earthquakes and winds. However, it is generally impossible to compare different control strategies directly because the control methods were applied to different structures. This problem can be addressed by *testbed* structures, that is by developing benchmark studies.

In recent years, benchmark problems have been recognized as a means to compare and contrast various control strategies **(Caughey, 1998)**. Benchmark control problems allow researchers to apply various control strategies, such as passive, active, semi-active, or combination thereof, to a specified problem, and to compare results directly in terms of a specified set of performance objectives. Additionally, these problems may include control constraints and hardware models to more accurately portray the types of implementation issues and constraints one must consider in reality.

One goal of a benchmark study is to direct future research efforts towards the most promising structural control strategies. In recent years, benchmark studies have been actively investigated by the International Association of Structural Control (IASC) and the ASCE Engineering Mechanics Committee **(Special Issue: Benchmark Problems, 1998; Session 10 – Benchmark Tests of Buildings, 1998)**. Until recently, all of benchmark problems considered have focused on the control of buildings **(Special Issue:**

Benchmark Problems, 1998; Session 10 – Benchmark Tests of Buildings, 1998; Spencer et al., 1999).

During the *Second International Workshop on Structural Control*, held in Hong Kong in December, 1996 **(Dyke et al., 2000)**, working groups were formed to plan the development of a series of benchmark control problems for various classes of civil engineering structures. The working group on bridge control recognized that the control of flexible bridge structures represents a new, difficult, and unique problem, with many complexities in modeling, control design, and implementation. Cable-stayed bridges exhibit complex behavior in which the vertical, translational, and torsional motions are often strongly coupled. Clearly, the control of very flexible bridge structures has not been studied to the same extent as buildings have. As a result, little expertise has been accumulated. Thus, the control of seismically excited cable-stayed bridges presents a challenging problem to the structural control community.

An analytical feasibility study was performed on a well-studied and documented bridge model in order to identify and resolve important issues associated with the control of a flexible bridge structure **(Schemmann et al., 1998)**. To effectively study the seismic response control of cable-stayed bridges, a benchmark problem for seismic protection has been developed by Dyke et al. **(Dyke et al., 2000)**.

5.2 Benchmark Problem Statement

The first generation of benchmark problems on cable-stayed bridges focused on the Bill Emerson Memorial Bridge under construction in Cape Girardeau, Missouri, USA **(Dyke et al., 2000, 2003)**. Based on the detailed drawings of the Bill Emerson Memorial Bridge, a three-dimensional evaluation model was developed to represent the complex behavior of the full scale benchmark bridge. A linear evaluation model, using the equations of motion generated around the deformed equilibrium position, was deemed appropriate. Because the structure is attached to bedrock, the effects of soil-structure interaction were neglected. To simplify the phase I problem, two assumptions were made regarding the excitation. This problem focused on a one dimensional ground acceleration applied in the longitudinal direction, and uniformly and simultaneously applied at all supports.

Although a significant amount of expertise was accumulated during phase I, the

assumptions made regarding the excitation (longitudinal and simultaneously acting) limited the extent to which this problem modeled a realistic situation. A structure's response to an earthquake is based on the simultaneous action of three components of ground motion: two in the horizontal plane, and one in the vertical direction. The structural response depends on the incidence angle (the angle between the ground motion components and the structural axes). Additionally, the excitation is expected to vary at each of the supports due to the length of these structures.

A phase II problem was developed to extend the problem to consider these issues. In this problem, the ground acceleration may be applied in any arbitrary direction using the two horizontal components of the historical earthquake with a specified incidence angle. Multi-support excitation is also considered in this phase of the study. Here, the prescribed ground motion is assumed to be identical at each support, although it is not applied simultaneously. It is assumed that bent/pier1 undergoes a specified ground motion, and the motion at the other three supports is identical to this motion but delayed based on the distance between adjacent supports and the speed of a typical earthquake **(Caicedo et al., 2002)**.

The problems have been prepared to provide a testbed for the development of effective strategies for the control of long-span bridges. To evaluate the proposed control strategies in terms that are meaningful for cable-stayed bridges, appropriate evaluation criteria and control design constraints are specified within the problem statement. Additionally, an alternate model of the bridge is developed for evaluating the robustness of the designs. This model includes the effects of snow loads on the bridge deck.

The problems are available for downloading on the benchmark web site *<http://wusceel.cive.wustl.edu./quake/>* in the form of a set of MATLAB® **(Mathworks, 1997a)** equations. A sample active control design is included. Designers/researchers participating in this benchmark study will define the devices, sensors, and control algorithm used, and evaluate them in the context of their proposed control strategies. These strategies may be passive, active, semi-active, or a combination thereof.

5.2.1 Benchmark Cable-stayed Bridge

The cable-stayed bridge used for this benchmark study is the Bill Emerson Memorial Bridge spanning the Mississippi River (on Missouri 74 – Illinois 146) near Cape

Girardeau, Missouri, designed by the HNTB Corporation **(Hague, 1997)**. The bridge is currently under construction and is scheduled to be completed in 2003. As shown in **Figure 5-1**, the bridge is composed of two towers, 128 cables, and 12 additional piers in the approach bridge from the Illinois side. It has a total length of 1205.8 m. The main span is 350.6 m in length, the side spans are 142.7 m in length, and the approach on the Illinois side is 570 m.

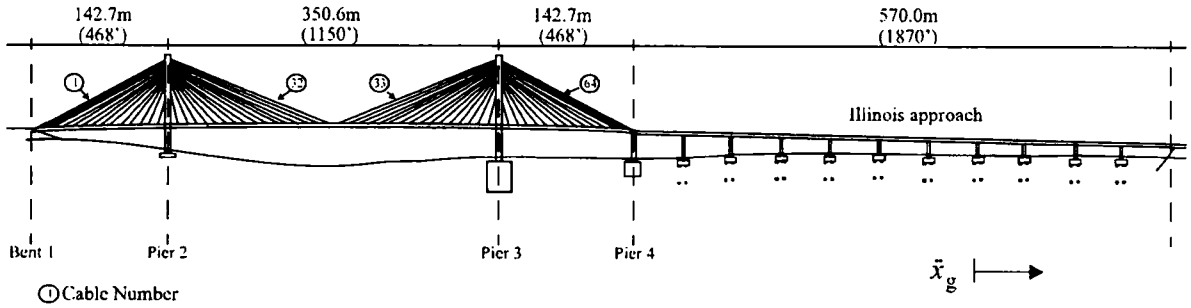

Figure 5-1. Drawing of the Bill Emerson Memorial Bridge

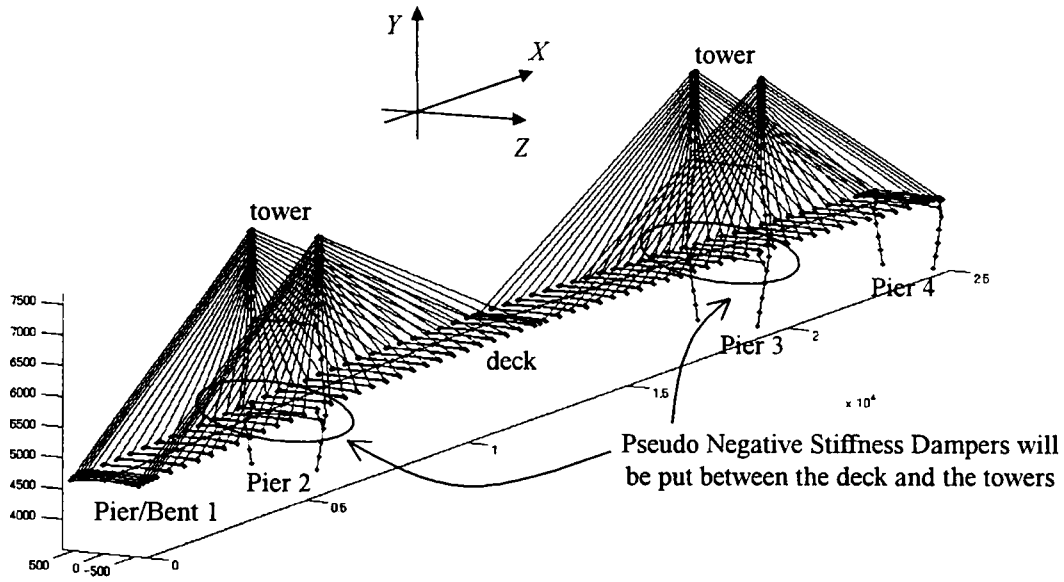

Figure 5-2. Bill Emerson Memorial Bridge Finite Element Model

5.2.2 Evaluation Model

Based on the description of the Bill Emerson Memorial Bridge, a three dimensional finite element model of the bridge was developed in MATLAB® **(Mathworks, 1997a)**.

The finite element model is shown in **Figure 5-2** The first ten undamped frequencies (shown as natural period in bracket) of the evaluation model are 0.2899 (3.45 s), 0.3699 (2.70 s), 0.4683 (2.14 s), 0.5158 (1.94 s), 0.5812 (1.72 s), 0.6490 (1.54 s), 0.6687 (1.50 s), 0.6970 (1.44 s), 0.7102 (1.41 s), and 0.7203 Hz (1.39 s). To make it possible for designers/researchers to place devices acting longitudinally between the deck and the tower, a modified evaluation model is formed in which the connections between the tower and the deck are disconnected. If a designer/researcher specifies devices at these nodes, the second model will be formed as the evaluation model, and the control devices should connect the deck to the tower. The frequencies of this second model are much lower than those of the nominal bridge model. The first ten frequencies of this second model are 0.1618 (6.18 s), 0.2666 (3.75 s), 0.3723 (2.69 s), 0.4545 (2.20 s), 0.5015 (1.99 s), 0.5650 (1.77 s), 0.6187 (1.61 s), 0.6486 (1.54 s), 0.6965 (1.43 s), and 0.7094 Hz (1.41 s). Note that the uncontrolled structure used as the basis of comparison for the controlled system, corresponds to the former model in which the deck-tower connections are fixed.

5.2.3 Evaluation Criteria

For cable-stayed bridges subjected to earthquake loading, critical responses are related to the structural integrity of the bridge rather than to serviceability issues. Thus, in evaluating the performance of each control algorithm, the shear forces and moments in the towers at key locations must be considered. Additionally, the tension in the cables should never approach zero, and should remain close to the nominal pretension.

A set of eighteen criteria have been developed to evaluate the capabilities of each control strategy **(Dyke et al., 2000)**. Because in the phase II the earthquake is assumed to have two horizontal components at a specified incidence angle, several of these criteria are evaluated in both the X (longitudinal) and Y (tranverse) directions. The first six evaluation criteria consider the ability of the controller to reduce peak responses, the second five criteria considered normed responses over the entire time record, and the last seven criteria consider the requirements of the control system itself. The evaluation criteria are summarized in **Table 5-1**.

Table 5-1. Evaluation Criteria

Criterion	Meaning
J_1	non-dimensionalized shear force at tower base
J_2	non-dimensionalized shear force at deck level
J_3	non-dimensionalized moment at tower base
J_4	non-dimensionalized moment at deck level
J_5	non-dimensionalized deviation of cable tension from nominal pretension
J_6	non-dimensionalized peak deck displacement at piers 1 and 4
J_7	non-dimensionalized normed shear force at tower base
J_8	non-dimensionalized normed shear force at deck level
J_9	non-dimensionalized normed moment at tower base
J_{10}	non-dimensionalized normed moment at deck level
J_{11}	non-dimensionalized normed deviation of cable tension from nominal pretension
J_{12}	non-dimensionalized force generated by control device(s)
J_{13}	non-dimensionalized stroke of control device(s)
J_{14}	non-dimensionalized instantaneous power required to control the bridge
J_{15}	non-dimensionalized total power force required to control the bridge
J_{16}	number of control devices
J_{17}	number of sensors
J_{18}	resources required to implement the control algorithm

For each control design, the evaluation criteria should be evaluated for each of three earthquake records provided in the benchmark problem: i) *El Centro*. The North-South component recorded at the Imperial Valley Irrigation District substation in El Centro, California, during the Imperial Valley, California earthquake of May, 18, 1940; ii) *Mexico City*. Recorded at the Galeta de Campos station with site Geology of Meta-Andesite Breccia in September 19, 1985; iii) *Gebze*. The North-South component recorded at the Gebze Tubitak Marmara Arastirma Merkezi on August 17, 1999. These three earthquakes are each at or below the design peak ground acceleration level for the bridge of 0.36 *g*'s. Ground accelerations and response spectra of the three earthquakes are shown in **Figures 5-3** to **5-5**.

For more detailed important summary of the benchmark problem statement, the readers may refer to **Appendix C:** Summary of Benchmark Problem Statement.

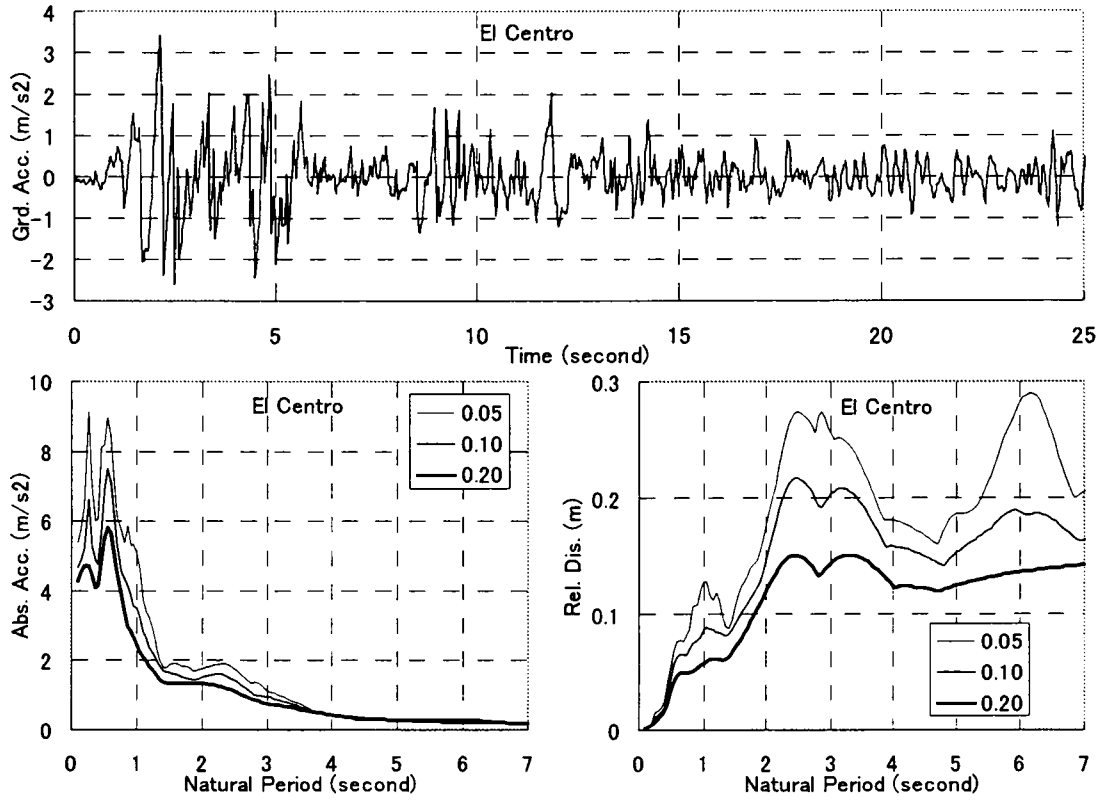

Figure 5-3. Ground Acceleration and Response Spectra for El Centro Earthquake

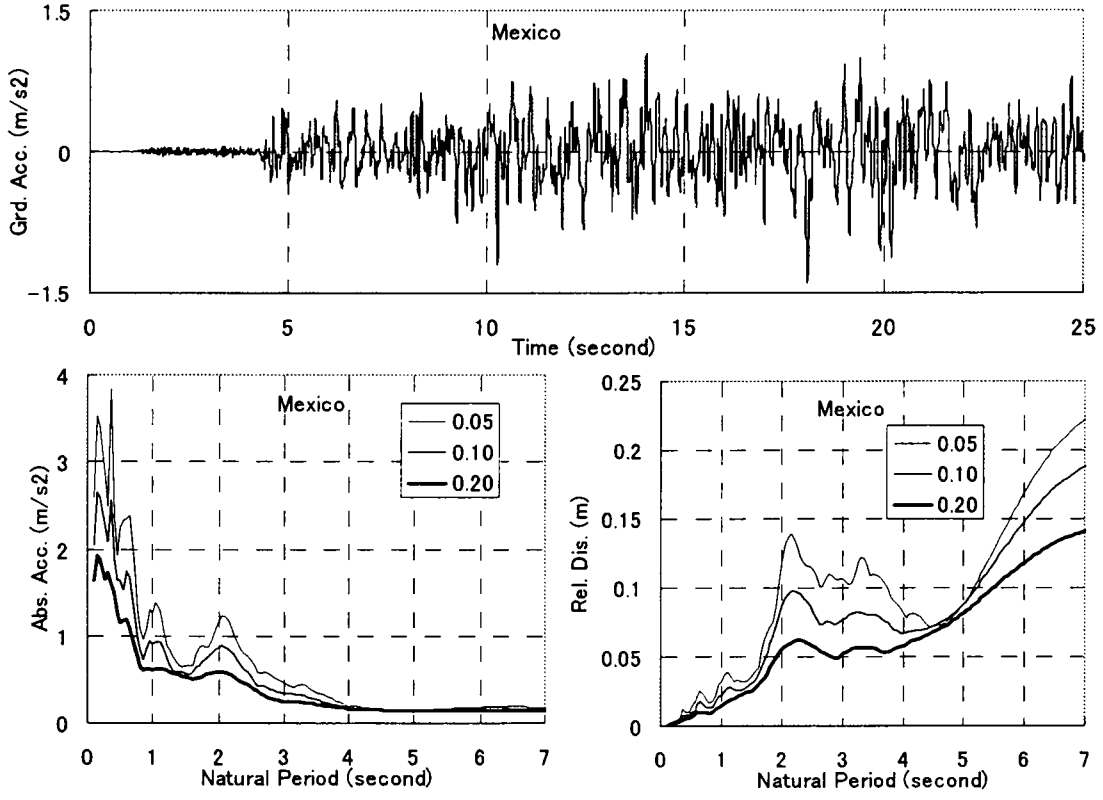

Figure 5-4. Ground Acceleration and Response Spectra for Mexico Earthquake

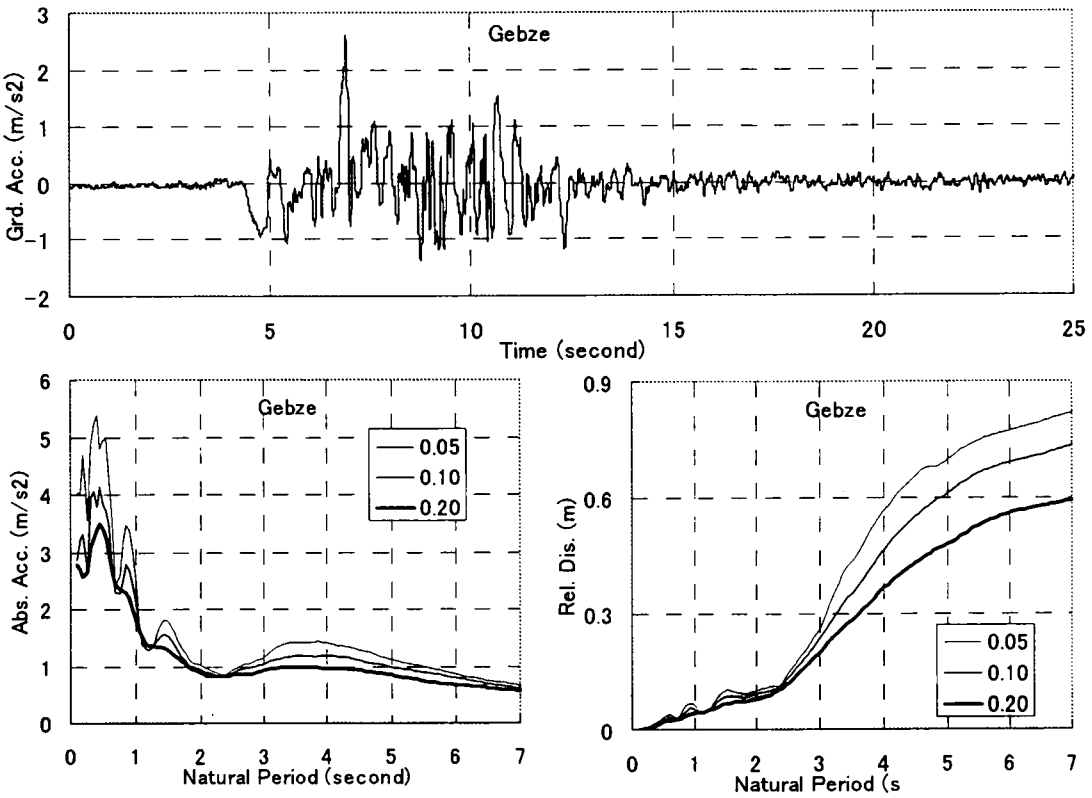

Figure 5-5. Ground Acceleration and Response Spectra for Gebze Earthquake

5.3 Application to Phase I Benchmark Problem

For the phase I of benchmark problem, the author will apply passive control system and pseudo negative control system. The pseudo negative stiffness control results will be compared to those of the passive system and those of active system, to show the effectiveness of pseudo negative stiffness control algorithm.

5.3.1 Passive Control System

The passive control system applied herein employs a total of 16 linear viscous dampers located between the deck the towers (eight between the deck and pier 2, and eight between the deck and pier 3; piers 2 and 3 are regarded as towers) and oriented to apply forces longitudinally. For simplicity and conservativeness, the damper force is a linear

function of piston velocity, then it is called linear viscous damper. The damper force is expressed in this equation,

$$F_d = C_d \times \dot{u} \tag{5-1}$$

where F_d is damper force, C_d is damping coefficient, and $\dot{u}$ is piston velocity.

It is important to check the appropriate damping coefficient related to the passive systems of this bridge. This can be done by altering the damping coefficient. The results are shown in **Figure 5-6** for total damping coefficient of 1000 to 7000 kN/m/s for four dampers. It is clear from the figure that increasing damping coefficient of the passive damper will decrease the deck displacement, although the relation is not linear, or in other words, rapid decrease is obtained when increasing damping coefficient at relatively small damping coefficient, and slow decrease at large damping coefficient. On the other hand, increasing damping coefficient will mainly decrease the force responses (shear and moment) when relatively small damping coefficient is used, and then increase the responses when damping coefficient becomes relatively large. Therefore, it is assumed to be appropriate to use a moderate damping coefficient of 3000 kN/m/s for four dampers, or 750 kN/m/s for each damper. Seismic response reduction because of additional linear viscous dampers to the benchmark cable-stayed bridge is shown in **Table 5-2**.

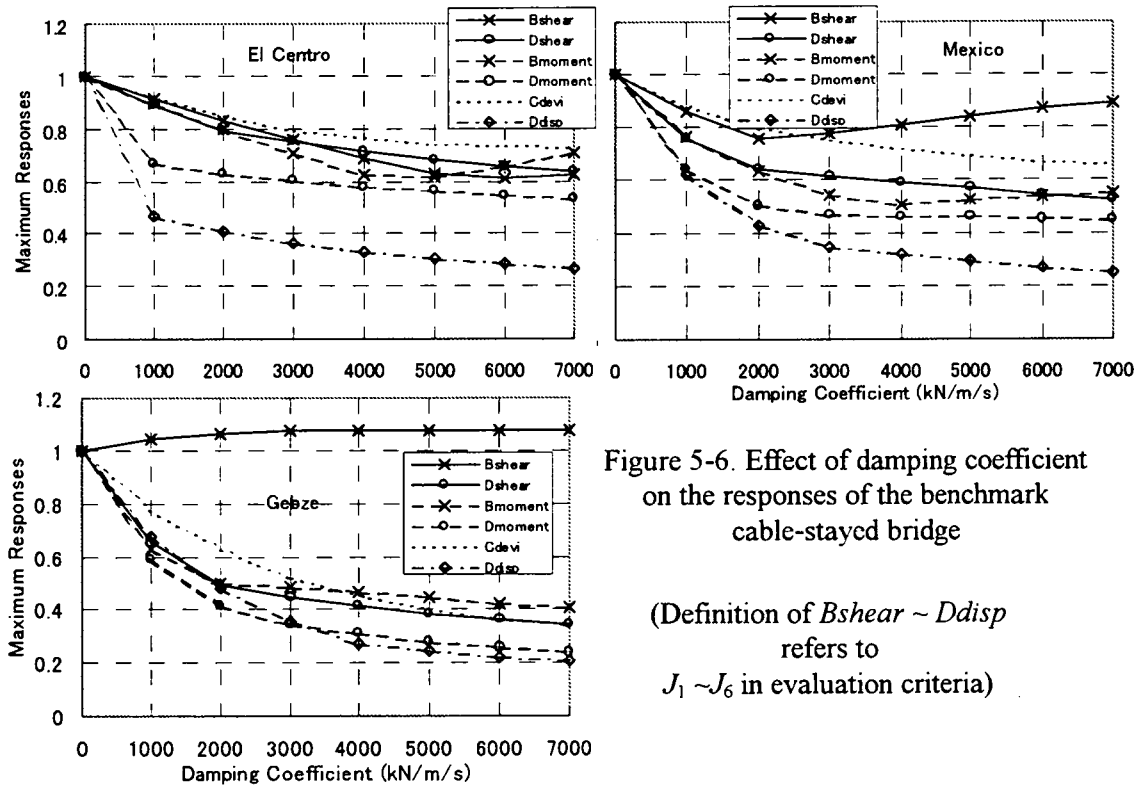

Figure 5-6. Effect of damping coefficient on the responses of the benchmark cable-stayed bridge

(Definition of *Bshear* ~ *Ddisp* refers to J_1 ~J_6 in evaluation criteria)

Table 5-2. Evaluation criteria for passive control (linear viscous dampers between the deck and the towers)

Evaluation Criteria	El Centro	Mexico	Gebze
J_1 (shear force at tower base)	0.346	0.430	0.435
J_2 (shear force at deck level)	1.020	1.129	1.022
J_3 (moment at tower base)	0.273	0.471	0.405
J_4 (moment at deck level)	0.513	0.552	1.278
J_5 (deviation of cable tension)	0.194	0.066	0.168
J_6 (deck displacement)	1.177	2.524	3.793
J_7 (normed shear force at tower base)	0.210	0.359	0.320
J_8 (normed shear force at deck level)	0.975	0.991	1.382
J_9 (normed moment at tower base)	0.243	0.385	0.479
J_{10} (normed moment at deck level)	0.805	1.080	1.845
J_{11} (normed deviation of cable tension)	0.025	0.009	0.017
J_{12} (force by control devices)	2.353e-3	0.922e-3	2.843e-3
J_{13} (stroke of control devices)	0.717	0.427	1.982
J_{16} (number of control devices)	16	16	16
J_{17} (number of sensors)	0	0	0

It is clear from the table that by applying only linear damper between the deck and the tower, the force response of the benchmark bridge can mainly be reduced. However, the evaluation criteria in Gebze columns shows significant increase in deck displacement response (the maximum deck displacement of the controlled bridge is 3.793 times that of uncontrolled bridge). This is because the controlled bridge uses only viscous dampers to replace the rigid connections between the deck and tower of the uncontrolled bridge.

To reduce the excessive displacement, it will be studied whether additional stiffness is also needed between the deck and the towers. It will be done by adding four elastic bearings parallel to the dampers: two bearings at pier 2 and two bearings at pier 3. This will give additional stiffness between the deck and the towers in the longitudinal direction to the bridge. The stiffness of one bearing is chosen within the range of 1000 kN/m and 8000 kN/m. The results are shown in **Figure 5-7**. From the figure, it was decided to use four bearings with stiffness of 8000 kN/m each, because the displacement response from Gebze earthquake can be reduced significantly. The results are shown in **Table 5-3**.

The study shows that disconnecting deck from the tower will result in excessive displacement response that dampers alone cannot effectively reduce it. Therefore, some stiffness is needed between the deck and the towers. The method for selecting appropriate amount of stiffness between the deck and tower has been discussed in **Chapter 4**,

Subchapter 4.4.

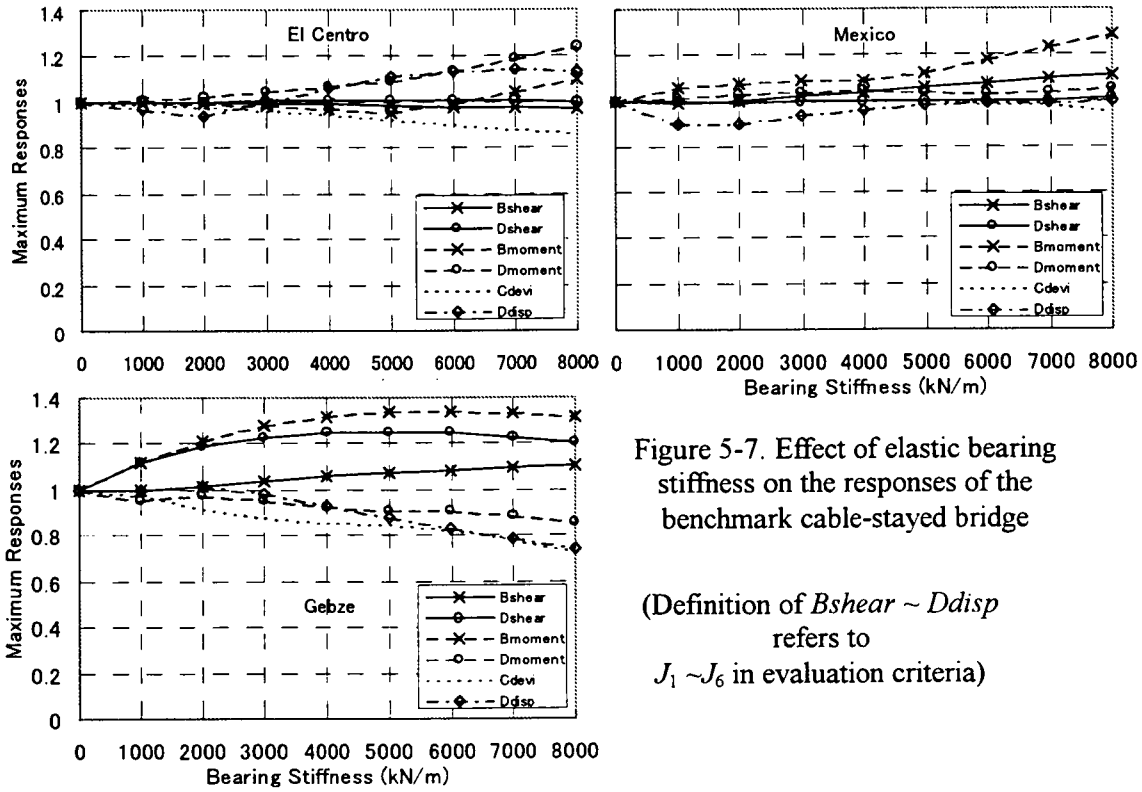

Figure 5-7. Effect of elastic bearing stiffness on the responses of the benchmark cable-stayed bridge

(Definition of *Bshear* ~ *Ddisp* refers to J_1 ~J_6 in evaluation criteria)

Table 5-3. Evaluation criteria for passive control (linear viscous dampers plus elastic bearings between the deck and towers)

Evaluation Criteria	El Centro	Mexico	Gebze
J_1 (shear force at tower base)	0.334	0.479	0.482
J_2 (shear force at deck level)	1.016	1.137	1.234
J_3 (moment at tower base)	0.300	0.607	0.532
J_4 (moment at deck level)	0.638	0.578	1.094
J_5 (deviation of cable tension)	0.167	0.063	0.123
J_6 (deck displacement)	1.340	2.511	2.798
J_7 (normed shear force at tower base)	0.227	0.405	0.412
J_8 (normed shear force at deck level)	0.989	1.015	1.220
J_9 (normed moment at tower base)	0.297	0.513	0.567
J_{10} (normed moment at deck level)	0.834	1.103	1.195
J_{11} (normed deviation of cable tension)	0.024	0.009	0.016
J_{12} (force by control devices)*	3.529e-3	1.471e-3	3.922e-3
J_{13} (stroke of control devices)	0.876	0.404	1.449
J_{16} (number of control devices)**	20	20	20
J_{17} (number of sensors)	0	0	0

Note: * Force by elastic bearings plus four dampers
** 16 linear viscous dampers plus 4 elastic bearings

5.3.2 Pseudo Negative Stiffness (PNS) Control System

The control system employs a total of 16 variable orifice oil dampers located between the deck and the towers (eight between the deck and pier2, and eight between the deck and pier3, piers2 and 3 are regarded as towers) and oriented to apply forces longitudinally. Displacement transducers are used for feedback to the control algorithm. Two displacement sensors are positioned between the deck and pier 2, and two between the deck and pier3, which make a total of four displacement sensors. All displacement measurements are obtained in the longitudinal direction to the bridge. For simplicity, the control devices act as ideal dampers, and damper dynamics and control-structure interaction is neglected.

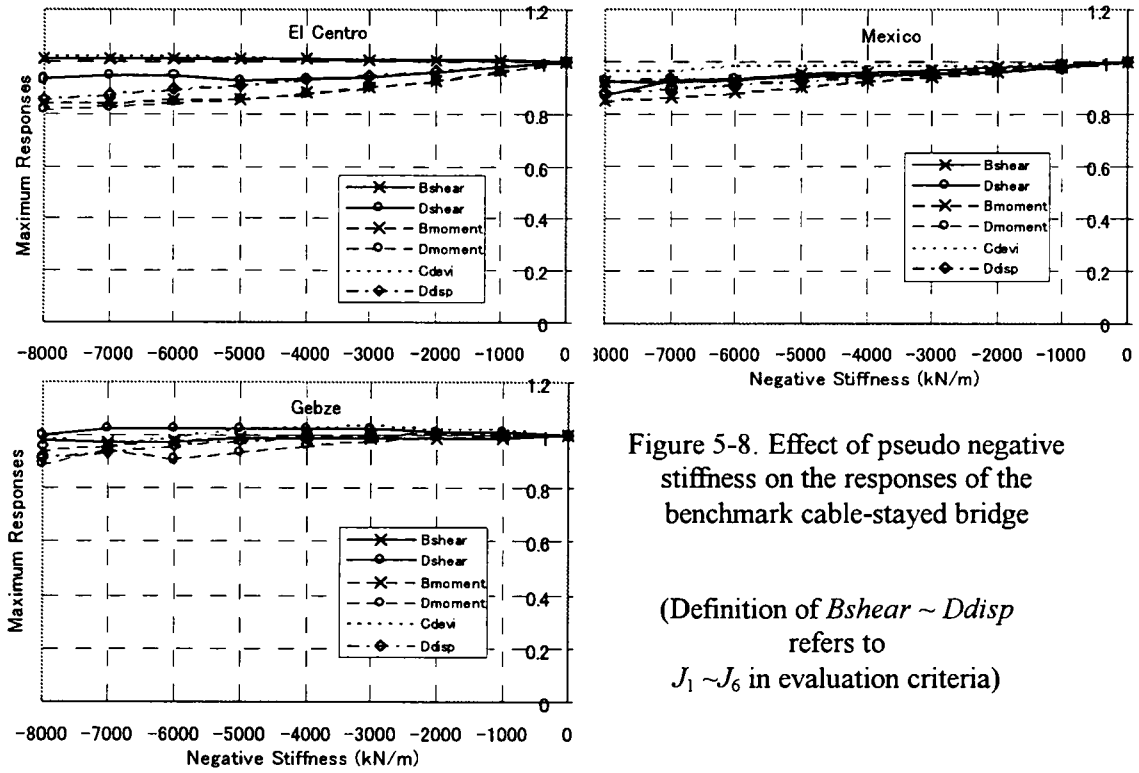

Figure 5-8. Effect of pseudo negative stiffness on the responses of the benchmark cable-stayed bridge

(Definition of *Bshear ~ Ddisp* refers to $J_1 \sim J_6$ in evaluation criteria)

The controller employs the pseudo-negative stiffness algorithm. The force command for the variable damper is the same as that specified in **Chapter 3**, **Equations (3-12)** and **(3-13)**. The two equations will be shown here for convenience as **Equations (5-2)** and **(5-3)**.

$$F_d = K_d u + C_d \dot{u} \tag{5-2}$$

$$f_D \begin{cases} F_d & \text{if } F_d \dot{u} > 0 \\ 0 & \text{if } F_d \dot{u} \le 0 \end{cases} \tag{5-3}$$

where u and $\dot{u}$ are piston displacement and velocity, respectively. f_D is the demand force to the variable damper.

In applying the pseudo-negative stiffness algorithm for controlling the variable dampers, the negative stiffness value (K_d) in **Equation (5-2)** is altered from –1000 kN/m to –8000 kN/m, with C_d equals to 3000 kN/m (the same with the one for passive system above). The effect of altering K_d on the response of the benchmark cable-stayed bridge is shown in **Figure 5-8**. Judging from the figure, K_d that has value of –8000 kN/m was chosen. The results are shown in **Table 5-4**. The variable dampers controlled by pseudo negative stiffness algorithm is then called PNS dampers in this dissertation.

Table 5-4. Evaluation criteria for PNS control (PNS dampers and elastic bearings between the deck and the towers)

Evaluation Criteria	El Centro	Mexico	Gebze
J_1 (shear force at tower base)	0.327	0.448	0.467
J_2 (shear force at deck level)	0.933	1.047	1.193
J_3 (moment at tower base)	0.248	0.504	0.491
J_4 (moment at deck level)	0.516	0.536	0.890
J_5 (deviation of cable tension)	0.175	0.060	0.116
J_6 (deck displacement)	1.110	2.178	2.476
J_7 (normed shear force at tower base)	0.213	0.375	0.366
J_8 (normed shear force at deck level)	0.907	0.913	1.127
J_9 (normed moment at tower base)	0.259	0.420	0.478
J_{10} (normed moment at deck level)	0.761	0.955	1.066
J_{11} (normed deviation of cable tension)	0.023	0.009	0.015
J_{12} (force by control devices)*	2.846e-3	1.116e-3	3.710e-3
J_{13} (stroke of control devices)	0.660	0.352	1.320
J_{16} (number of control devices)**	20	20	20
J_{17} (number of sensors)	4	4	4

Note: * Force by elastic bearings plus four PNS dampers
** 16 PNS dampers plus 4 elastic bearings

5.3.3 Comparison with Active Control System

Since results of active system in the benchmark problem by other participant is available **(Jung et al., 2001)**, it is interesting to be shown here for comparison. The active control

uses 24 actuators put between the deck and towers, the deck and abutment, and the deck and pier. The control algorithm is H_2/LQG. **Table 5-5** above shows the results of passive, semi-active, and active control of the benchmark control problem of cable-stayed bridges. The largest results among the three input earthquakes are shown.

The results show that pseudo negative stiffness control is significantly better than passive control and is comparable with active control. Even for some cases, such as tower base shear force, shear force at deck level, and deviation of cable tension, pseudo negative stiffness control is better than active control. Time history of the tower moment at base and the deck displacement is shown in **Figure 5-9**.

Table 5-5. Evaluation criteria for passive, PNS, and active controls (The largest among the three earthquakes)

Evaluation Criteria	Passive*	PNS Dampers**	Active***
J_1 (shear force at tower base)	0.482	0.467	0.498
J_2 (shear force at deck level)	1.234	1.193	1.197
J_3 (moment at tower base)	0.607	0.504	0.441
J_4 (moment at deck level)	1.094	0.890	0.865
J_5 (deviation of cable tension)	0.167	0.117	0.156
J_6 (deck displacement)	2.798	2.476	1.978
J_7 (normed shear force at tower base)	0.412	0.375	0.351
J_8 (normed shear force at deck level)	1.220	1.127	1.006
J_9 (normed moment at tower base)	0.567	0.478	0.327
J_{10} (normed moment at deck level)	1.195	1.066	0.844
J_{11} (normed deviation of cable tension)	0.024	0.023	0.015
J_{12} (force by control devices)	3.922e-3****	3.710e-3****	1.961e-3
J_{13} (stroke of control devices)	1.449	1.320	1.085
J_{16} (number of control devices)	20	20	24
J_{17} (number of sensors)	0	4	9

Note : * Linear viscous dampers and elastic bearings between the deck and towers
** PNS dampers and elastic bearings between the deck and towers
*** Actuators between the deck and all four piers
**** Total force of dampers plus elastic bearings

5.3.4 Device Hysteretic Loops and Earthquake Input Energy

Hysteresis loop of the passive system and pseudo negative stiffness control system is shown in **Figure 5-10**. **Figure 5-11** shows the combination of **Figure 5-10** with the elastic bearings at the deck-tower connections. It is clear from the **Figure 5-11** that the

area enclosed by the hysteresis loop of pseudo negative stiffness dampers is larger than that by passive linear viscous damper. Therefore, larger energy is absorbed by pseudo negative stiffness damper than that by linear viscous damper. This will result in lower earthquake input energy for the pseudo negative stiffness damper.

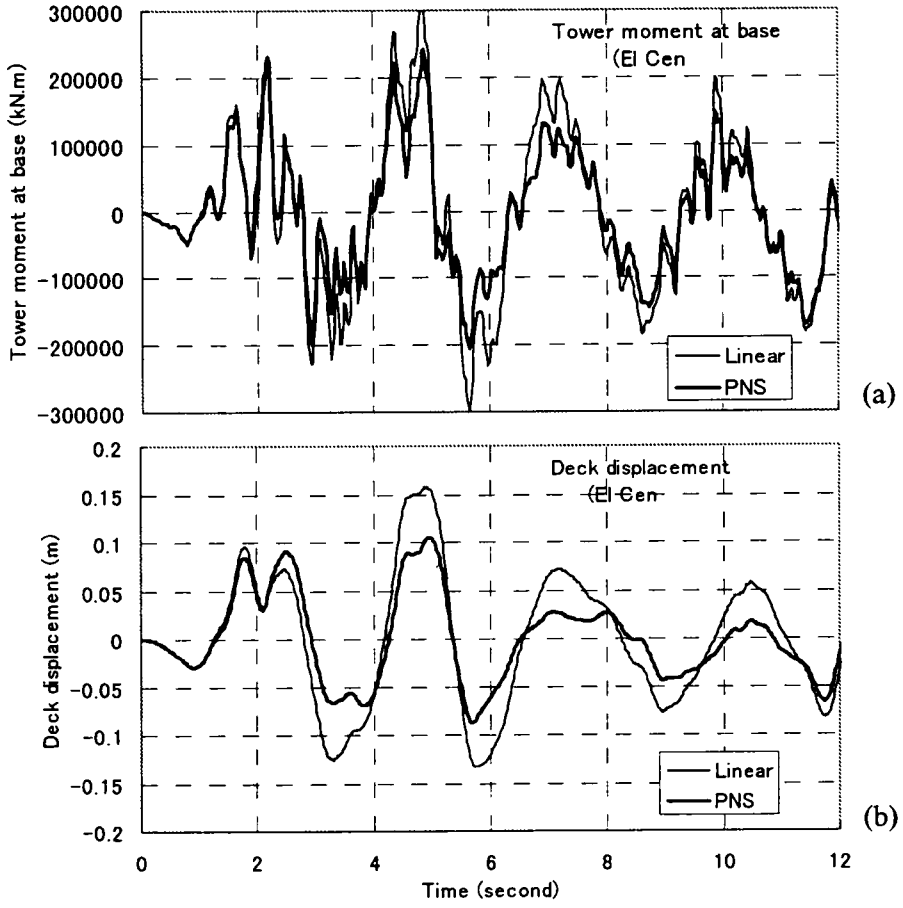

Figure 5-9. Time history of (a) tower 'pier2' moment at base and (b) deck displacement for El Centro earthquake

To calculate the earthquake input energy, since the mass matrix of the benchmark bridge is not directly available, it was decided to use the deck velocity response during the earthquakes. The reason for this is that for cable-stayed bridges, about 75% of the total mass is the deck mass **(Branco et al., 2000; Iemura and Pradono, 2002b)**, therefore it is assumed to be appropriate to use deck velocity and to use the deck mass to calculate the input energy based on the equation below **(Chopra, 1995)**.

$$E_I(t) = -\int_0^t m\ddot{u}_g(t)\dot{u}(t)dt \tag{5-4}$$

Equation (5-4) shows the earthquake input energy into the bridge calculated based on deck velocity, where m is the deck mass, $\dot{u}(t)$ is the deck relative velocity at time t, and $\ddot{u}_g$ is the ground acceleration, respectively. **Figure 5-12** shows the difference in earthquake input energy between the two systems. It is clear from the figure that earthquake input energy is smaller for pseudo negative stiffness damper.

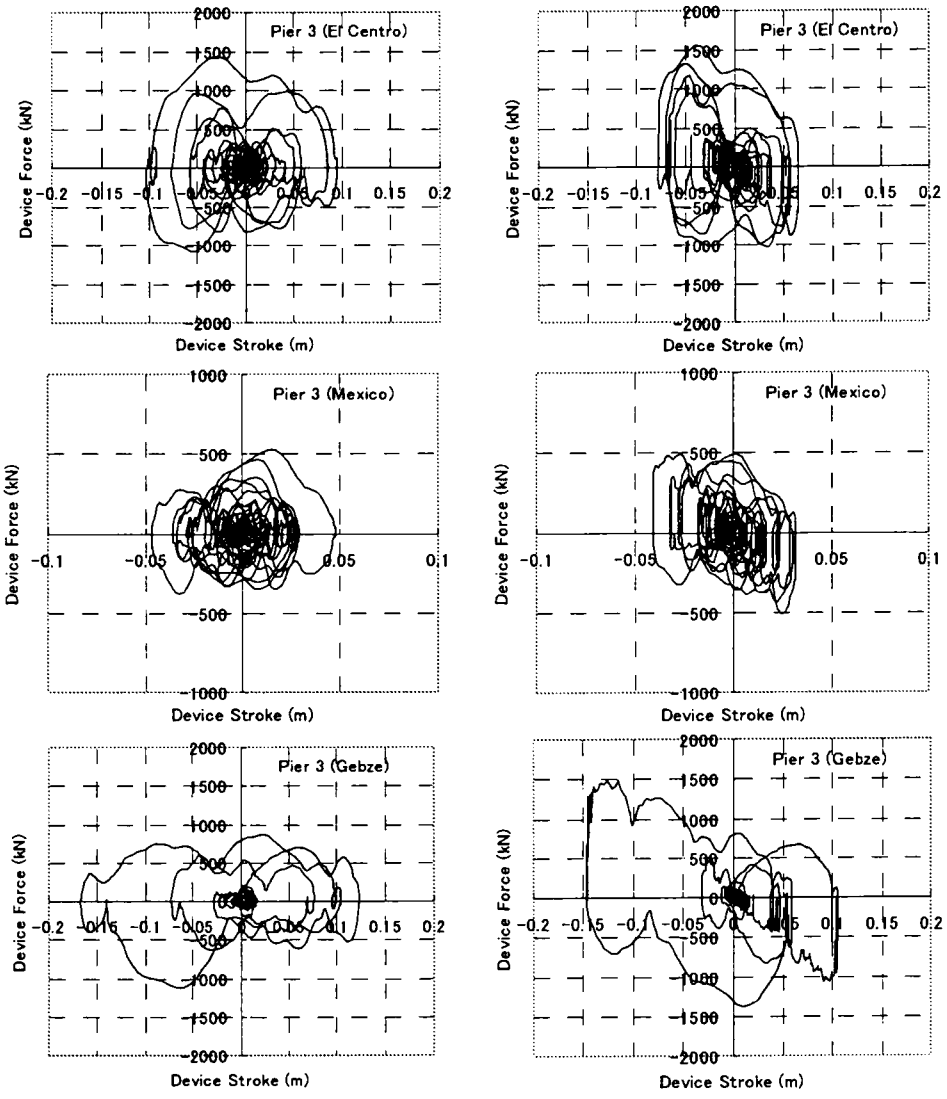

Figure 5-10. Damper hysteresis loops (left) passive system; (right) PNS system

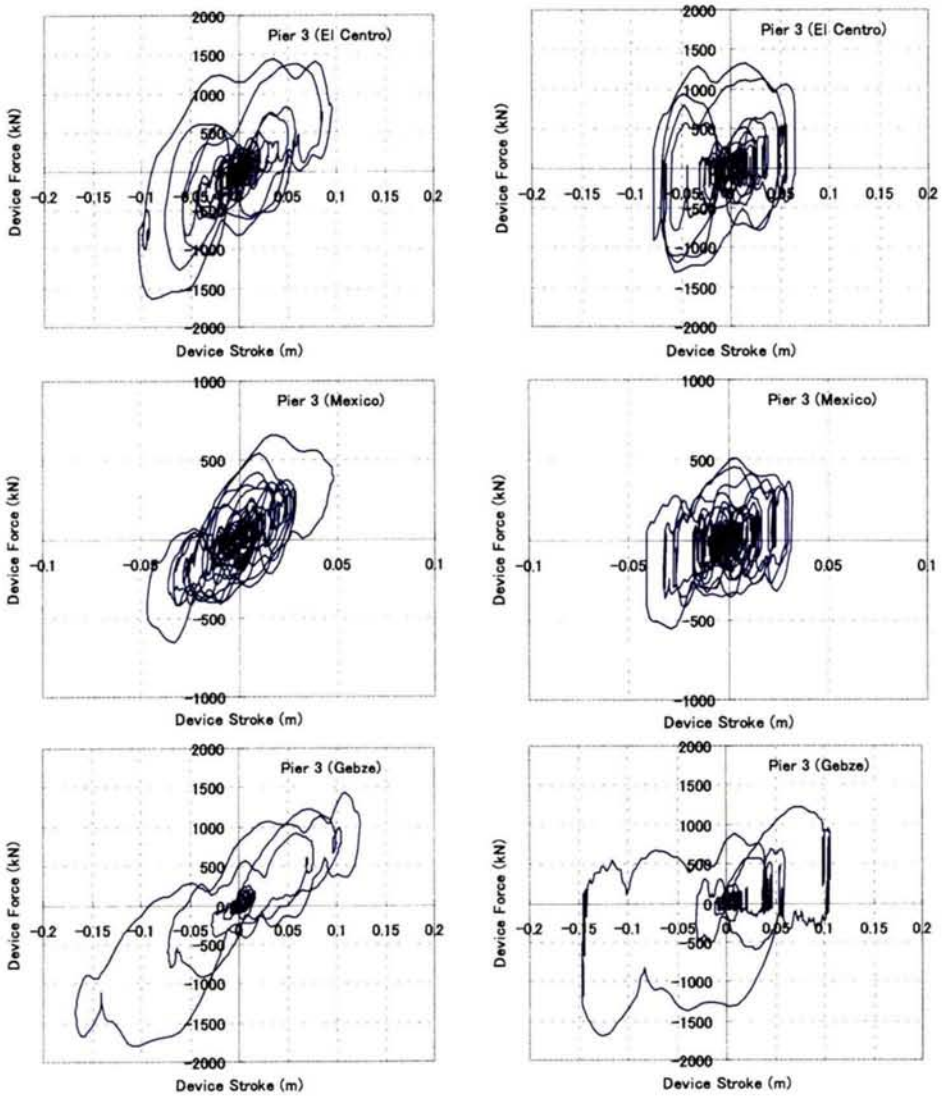

Figure 5-11. Damper+Bearing hysteresis loops (left) passive system; (right) PNS system

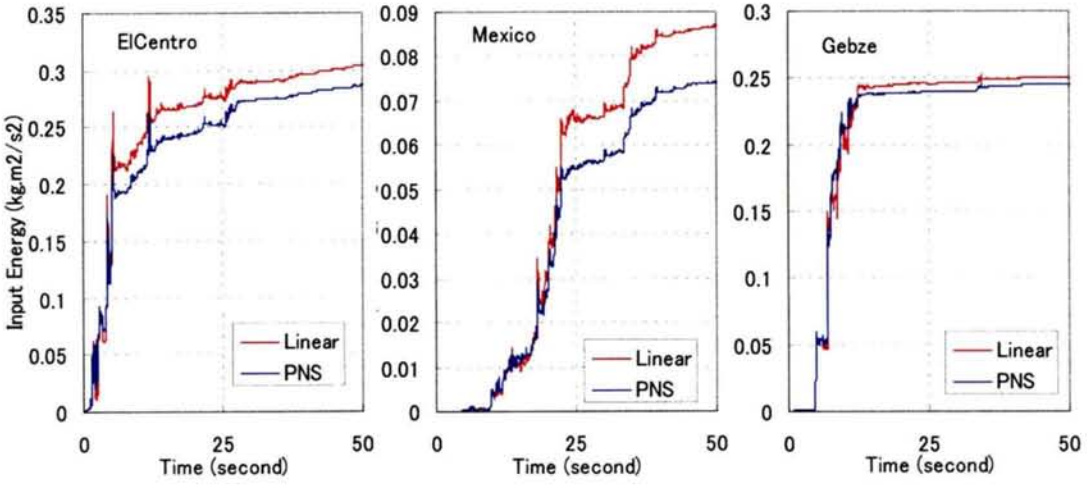

Figure 5-12. Earthquake input energy into the bridge

5.4 Application to Phase II Benchmark Problem

Phase II benchmark problem includes the issues of multi-support excitation, incidence angle, and control robustness. Passive control system and pseudo negative control system will be applied. Comparisons are made for the results of passive, pseudo negative stiffness, and active controls, to show the effectiveness of the pseudo negative stiffness control algorithms.

5.4.1 Passive Control System

The passive control system employs a total of 16 linear viscous dampers located between the deck and the towers (eight between the deck and pier2, and eight between the deck and pier3; piers2 and 3 are regarded as towers) and oriented to apply forces longitudinally. For simplicity, the damper force is linearly proportional to the piston velocity.

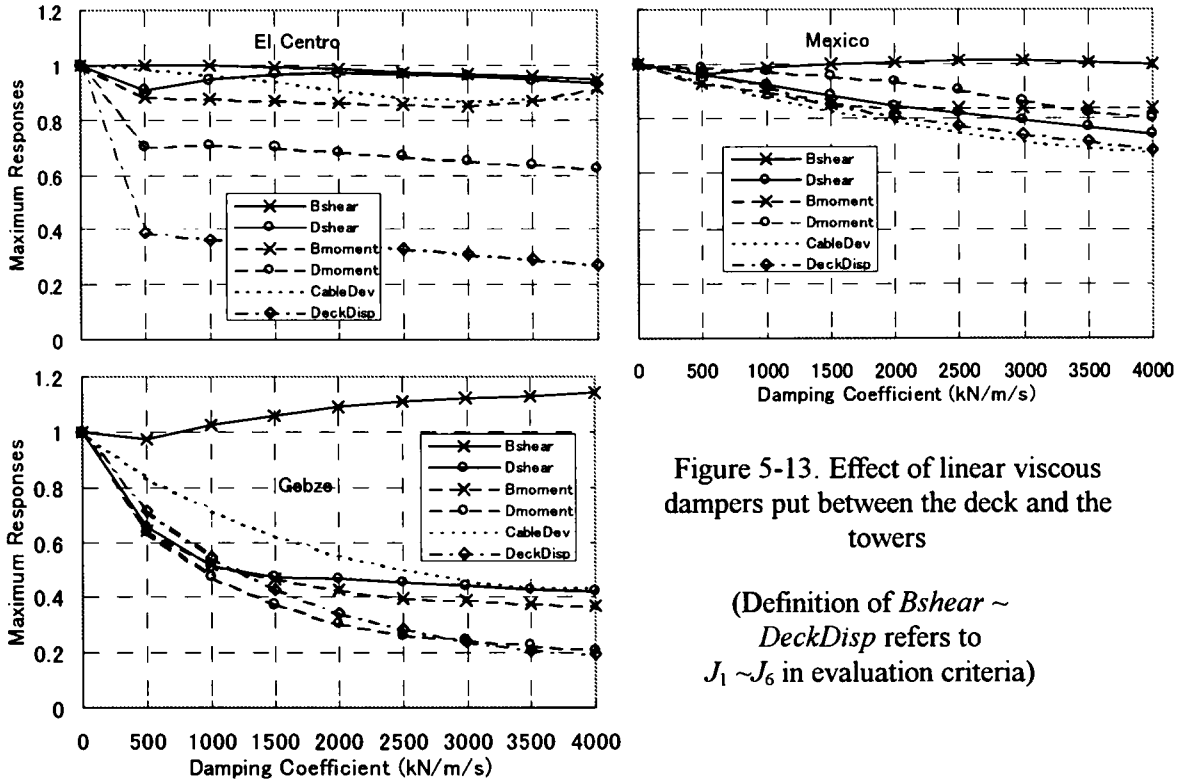

Figure 5-13. Effect of linear viscous dampers put between the deck and the towers

(Definition of *Bshear* ~ *DeckDisp* refers to J_1 ~J_6 in evaluation criteria)

It is important to check the appropriate damping coefficient related to this passive systems of the bridge. This can be done by altering the coefficient. The results are shown

in **Figure 5-13** for total damping coefficient of zero to 4000 kN/m/s for four dampers.

It is clear from the figure that increasing damping coefficient of the viscous damper will decrease the deck displacement, although the relation is not linear. On the other hand, increasing damping coefficient may increase the seismic induced force (for example tower base shear for Gebze input earthquake). Therefore, a damping coefficient of 2000 kN/m/s per four dampers is assumed to be appropriate. The evaluation criteria based on these additional viscous dampers is shown in **Table 5-6**.

Table 5-6. Evaluation criteria based on linear viscous dampers put between the deck and the towers

Evaluation Criteria	El Centro	Mexico	Gebze
J_{1x} (shear force at tower base(X))	0.323	0.365	0.385
J_{1z} (shear force at tower base(Z))	1.014	1.108	1.035
J_{2x} (shear force at deck level(X))	0.920	0.989	1.085
J_{2z} (shear force at deck level(Z))	0.962	0.999	0.995
J_{3x} (moment at tower base(X))	0.235	0.314	0.441
J_{3z} (moment at tower base(Z))	1.096	1.070	1.040
J_{4x} (moment at deck level(X))	0.549	0.810	1.300
J_{4z} (moment at deck level(Z))	1.009	0.993	0.999
J_5 (deviation of cable tension)	0.247	0.131	0.225
J_6 (deck displacement)	1.075	1.710	4.865
J_{7x} (normed shear force at tower base(X))	0.226	0.254	0.272
J_{7z} (normed shear force at tower base(Z))	1.002	1.048	1.042
J_{8x} (normed shear force at deck level(X))	0.899	0.933	1.145
J_{8z} (normed shear force at deck level(Z))	0.978	0.997	0.990
J_{9x} (normed moment at tower base(X))	0.231	0.275	0.463
J_{9z} (normed moment at tower base(Z))	0.997	1.045	1.031
J_{10x} (normed moment at deck level(X))	0.703	0.870	1.473
J_{10z} (normed moment at deck level(Z))	1.002	1.004	1.002
J_{11} (normed deviation of cable tension)	0.027	0.017	0.022
J_{12x} (force by control devices(X))	1.597e-3	0.983e-3	2.077e-3
J_{12z} (force by control devices(Z))	0.000e+0	0.000e+0	0.000e+0
J_{13x} (stroke of control devices(X))	0.531	0.754	2.072
J_{13z} (stroke of control devices(Z))	0.000	0.000	0.000
J_{16} (number of control devices)	16	16	16
J_{17} (number of sensors)	0	0	0

From the table, Gebze earthquake results in large displacement response. To reduce the excessive displacement, elastic bearings between the deck and the towers are added to the above viscous dampers in the longitudinal direction. It will be checked how much stiffness is needed between the deck and the towers. The stiffness of one bearing is varied from 1000 kN/m to 8000 kN/m. The results are shown in **Figure 5-14**. From the figure, it was decided to use four bearings with stiffness of 8000 kN/m each, because the displacement response of Gebze earthquake can be reduced significantly. The evaluation

criteria based on additional damping and stiffness between the deck and the towers are shown in **Table 5-7** (at 'passive' columns).

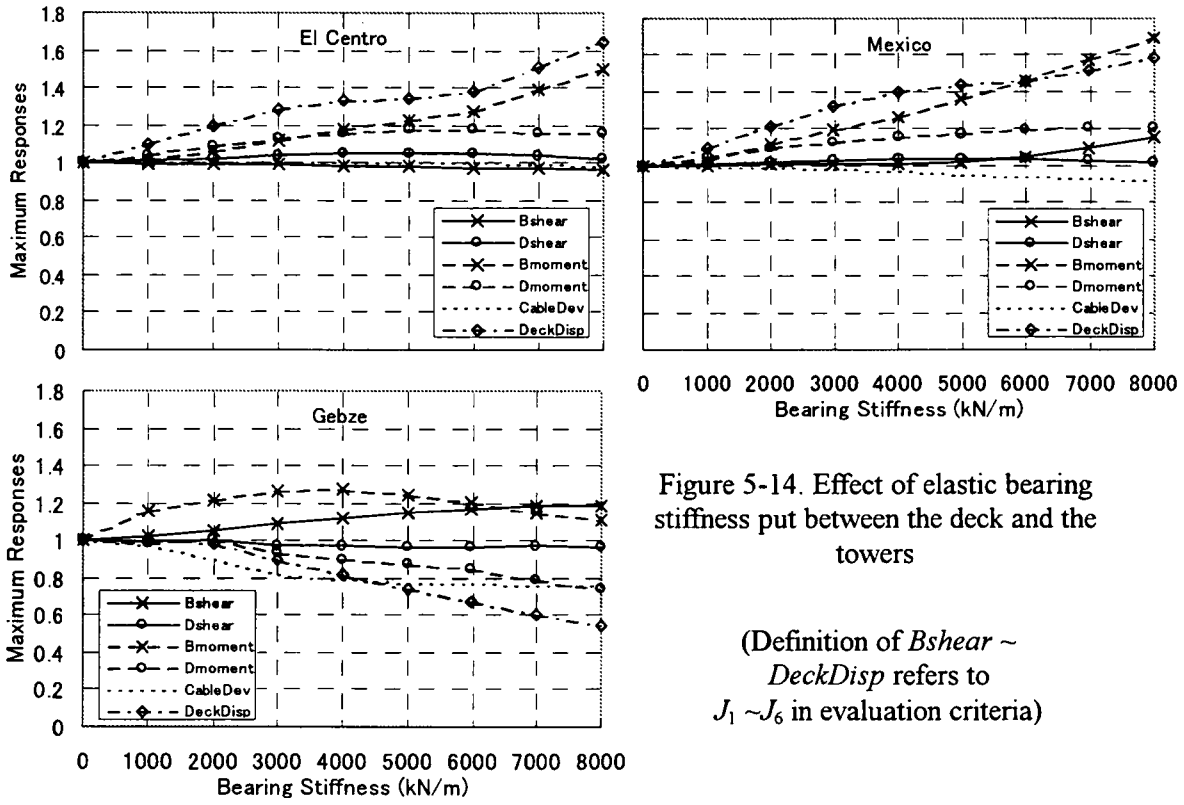

Figure 5-14. Effect of elastic bearing stiffness put between the deck and the towers

(Definition of *Bshear* ~ *DeckDisp* refers to J_1 ~J_6 in evaluation criteria)

5.4.2 Pseudo Negative Stiffness Control System

The pseudo negative stiffness (PNS) control system employs a total of 16 variable dampers located between the deck the towers (eight between the deck and pier2, and eight between the deck and pier3, piers2 and 3 are regarded as towers) and oriented to apply forces longitudinally. Elastic bearings used for the passive system is also applied herein. Displacement transducers are used for feedback to the control algorithm. Two displacement sensors are positioned between the deck and pier 2, and two between the deck and pier 3, which make a total of four displacement sensors. All displacement measurements are obtained in the longitudinal direction to the bridge. For simplicity, the control devices act as ideal dampers, and damper dynamics and control-structure interaction is neglected.

The negative stiffness value (K_d) in **Equation (5-2)** to control the variable damper is chosen as –8000 kN/m, because K_d that equals negative of the existing stiffness (in this

case bearing stiffness) gives the smallest damping plus elastic force. The damping coefficient C_d is set to be the same with the passive viscous damping case, that is 2000 kN/m/s.

Table 5-7. Evaluation criteria based on passive and PNS controls

Evaluation Criteria	ElCentro		Mexico		Gebze	
	passive*	pns**	passive*	pns**	passive*	pns**
J_{1x} (shear at tower base(X))	**0.311**	0.324	0.423	**0.367**	0.458	**0.425**
J_{1z} (shear at tower base(Z))	1.023	1.016	1.107	1.106	1.033	1.033
J_{2x} (shear at deck level(X))	0.943	**0.922**	1.008	**0.967**	1.047	**0.948**
J_{2z} (shear at deck level(Z))	0.964	0.965	0.995	0.994	0.991	0.995
J_{3x} (moment at tower base(X))	0.353	**0.261**	0.530	**0.411**	**0.488**	0.505
J_{3z} (moment at tower base(Z))	1.092	1.104	1.071	1.066	1.036	1.043
J_{4x} (moment at deck level(X))	0.635	**0.540**	0.971	**0.890**	0.959	**0.833**
J_{4z} (moment at deck level(Z))	1.009	1.007	0.993	0.992	1.000	1.000
J_5 (deviation of cable tension)	0.244	**0.218**	**0.120**	0.121	**0.171**	0.184
J_6 (deck displacement)	1.768	**1.139**	2.715	**2.038**	2.654	**2.605**
J_{7x} (nor. shear @tower base(X))	0.249	**0.232**	0.330	**0.288**	0.360	**0.314**
J_{7z} (nor. shear @tower base(Z))	1.007	0.998	1.047	1.044	1.041	1.034
J_{8x} (nor. shear @deck level(X))	0.911	**0.861**	1.076	**0.914**	1.001	**0.931**
J_{8z} (nor. shear @deck level(Z))	0.977	0.978	0.998	0.997	0.990	0.989
J_{9x} (nor. mom. @tower base(X))	0.298	**0.244**	0.474	**0.326**	0.509	**0.422**
J_{9z} (nor. mom. at tower base(Z))	1.001	0.995	1.045	1.041	1.031	1.026
J_{10x} (nor. mom. @deck level(X))	0.730	**0.666**	1.091	**0.869**	0.858	**0.767**
J_{10z} (nor. mom. @deck level(Z))	1.001	1.001	1.004	1.004	1.002	1.001
J_{11} (nor. deviation of cbl tension)	**0.024**	0.025	0.017	**0.016**	**0.015**	0.016
J_{12x} (force by devices(X))***	3.235e-3	**2.412e-3**	2.451e-3	**1.882e-3**	3.137e-3	**2.627e-3**
J_{12z} (force by devices(Z))***	0.000e+0	0.000e+0	0.000e+0	0.000e+0	0.000e+0	0.000e+0
J_{13x} (stroke of devices(X))	0.883	**0.583**	1.308	**0.942**	1.036	1.036
J_{13z} (stroke of devices(Z))	0.000	0.000	0.000	0.000	0.000	0.000
J_{16} (number of devices)****	20	20	20	20	20	20
J_{17} (number of sensors)	**0**	4	**0**	4	**0**	4

Note : * Linear viscous dampers and elastic bearings between the deck and towers

** PNS dampers and elastic bearings between the deck and towers

*** Force by four dampers plus an elastic bearing

**** 16 dampers plus four elastic bearings

Bold number shows that this type of control is better than the other one.

The evaluation criteria based on the pseudo negative stiffness control system are shown in **Table 5-7** (at 'pns' columns). It is clear from the table that pseudo negative stiffness control is significantly better than passive control. Hysteretic loop of the passive system and pseudo negative stiffness control system is shown in **Figure 5-15**. **Figure 5-16** shows the combination of **Figure 5-15** with the elastic bearings at the deck-tower connections. It

is clear from **Figure 5-16** that the area enclosed by the hysteretic loop of pseudo negative stiffness dampers plus elastic bearings is larger than that by passive linear viscous damper plus elastic bearings. Therefore, larger energy is absorbed by pseudo negative stiffness damper than that by linear viscous damper.

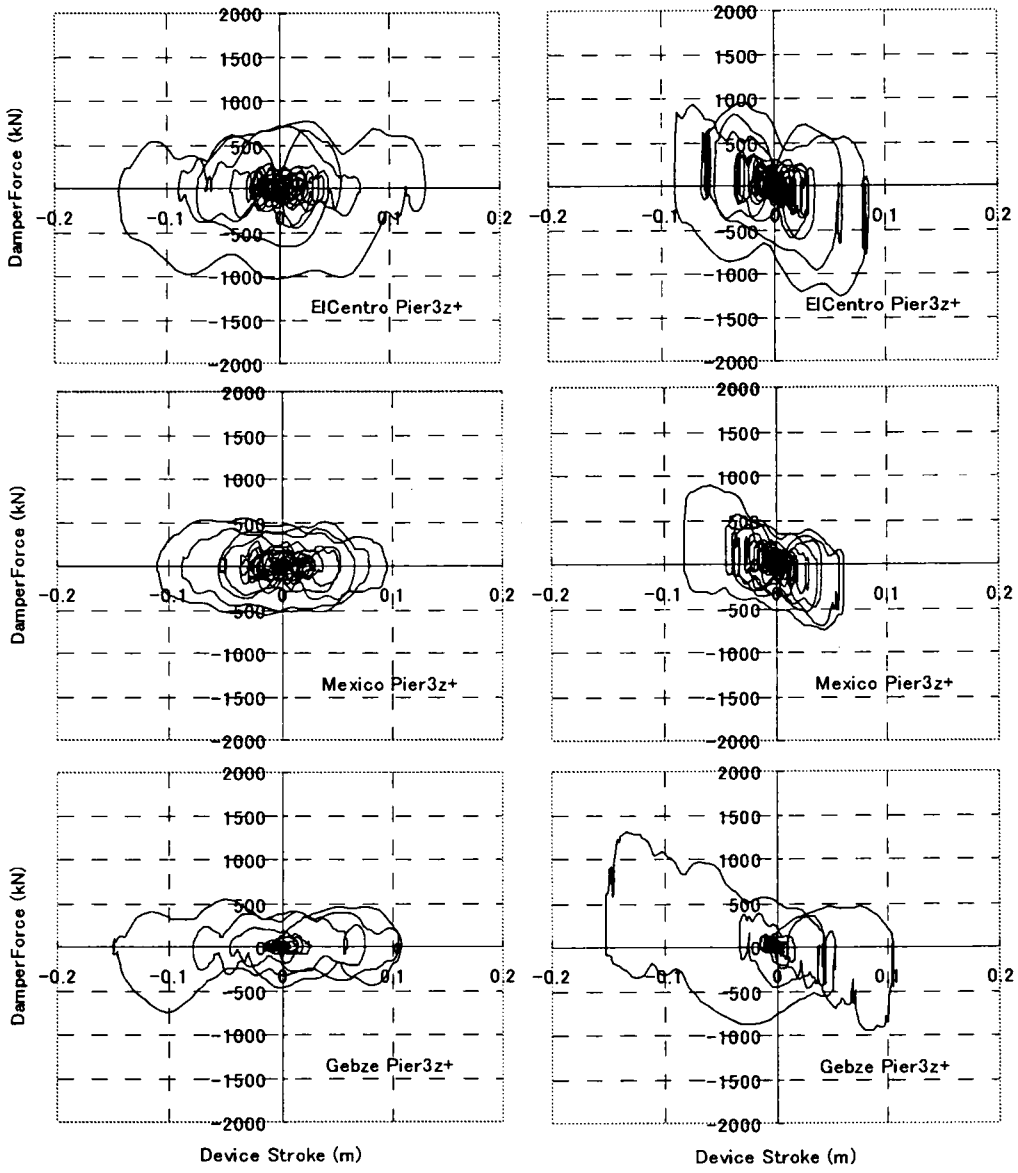

Figure 5-15. Damper hysteretic loops at Pier3
(left) passive system; (right) pseudo negative stiffness system

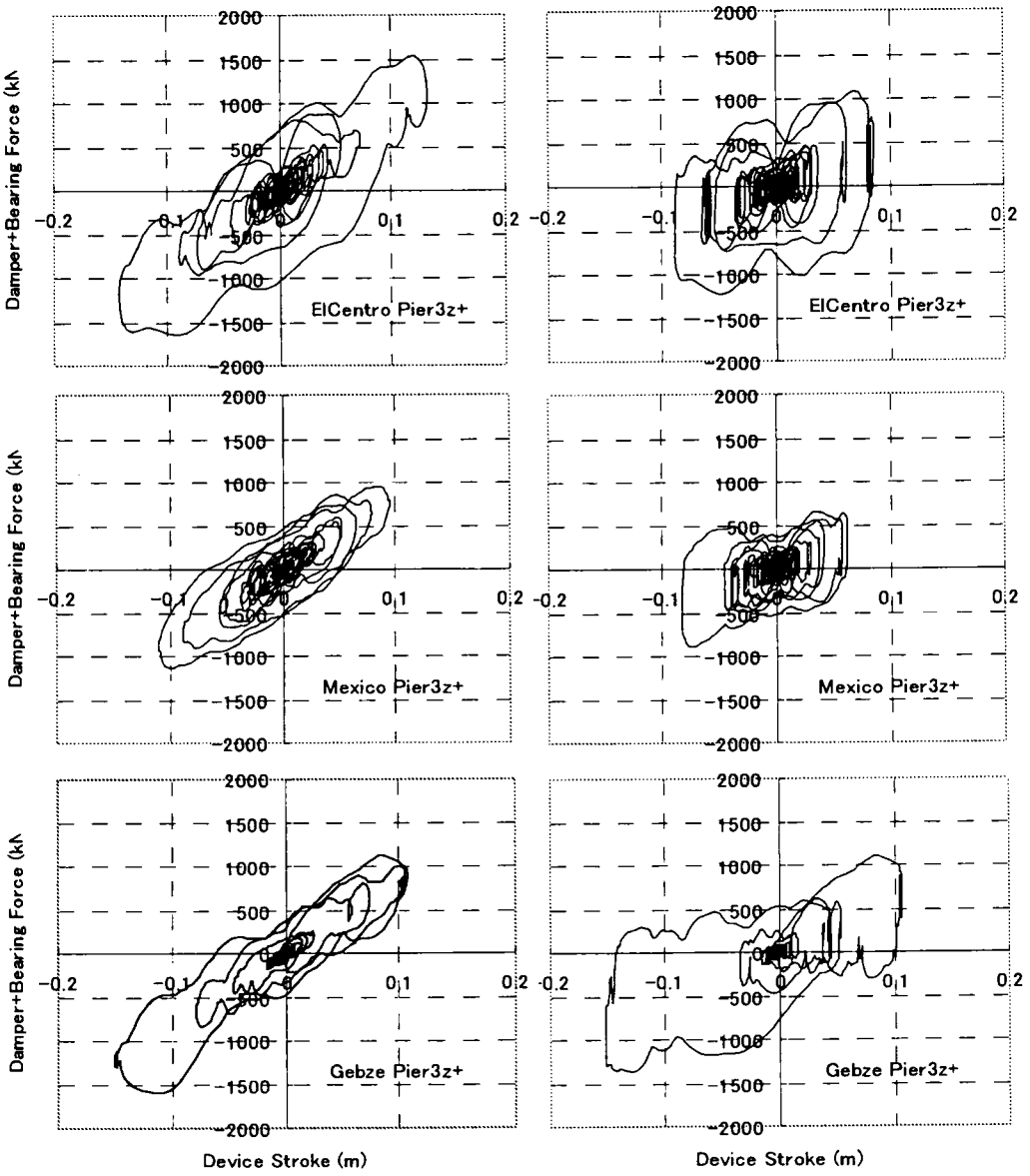

Figure 5-16. Damper+Bearing hysteretic loops at Pier3
(left) passive system; (right) pseudo negative stiffness system

5.4.3 Comparison with Active Control Results

Since the benchmark problem contains sample active control, it is interesting to be shown herein. The control uses 24 actuators put between the deck and towers, the deck and abutment, and the deck and pier **(Caicedo et al., 2002)**. **Table 5-8** shows the results of active control of the benchmark control problem of cable-stayed bridges. Comparison of the results between pseudo negative stiffness control and active control shows that pseudo negative stiffness control can achieve the potential of active control. Italics

numbers in the table shows that pseudo negative stiffness control has better performance than active control in reducing seismic responses, such as in shear at tower base, normed shear at tower base, normed shear at deck level, force and stroke of control devices, number of devices, and number of sensors. **Figures 5-17** and **5-18** show the time history of tower moment at base and deck displacement, respectively. It is clear from the figures that pseudo negative stiffness control is significantly better than passive control and is comparable to active control for this type of bridges.

Table 5-8. Evaluation criteria based on sample active control

Evaluation Criteria	El Centro	Mexico	Gebze
J_{1x} (shear force at tower base(X))	*0.331*	*0.415*	*0.474*
J_{1z} (shear force at tower base(Z))	1.022	1.117	1.037
J_{2x} (shear force at deck level(X))	0.810	0.828	0.941
J_{2z} (shear force at deck level(Z))	0.967	0.998	0.994
J_{3x} (moment at tower base(X))	*0.324*	0.396	0.456
J_{3z} (moment at tower base(Z))	1.097	1.079	1.046
J_{4x} (moment at deck level(X))	*0.612*	0.766	*0.955*
J_{4z} (moment at deck level(Z))	1.009	0.992	1.001
J_5 (deviation of cable tension)	*0.248*	*0.121*	0.182
J_6 (deck displacement)	1.028	1.783	2.403
J_{7x} (normed shear force at tower base(X))	*0.267*	*0.327*	*0.320*
J_{7z} (normed shear force at tower base(Z))	1.014	1.056	1.053
J_{8x} (normed shear force at deck level(X))	*0.869*	*0.964*	*0.956*
J_{8z} (normed shear force at deck level(Z))	0.978	0.996	0.991
J_{9x} (normed moment at tower base(X))	*0.248*	0.319	0.400
J_{9z} (normed moment at tower base(Z))	1.006	1.053	1.039
J_{10x} (normed moment at deck level(X))	0.636	0.793	0.780
J_{10z} (normed moment at deck level(Z))	1.002	1.004	1.003
J_{11} (normed deviation of cable tension)	0.023	0.015	0.015
J_{12x} (force by control devices(X))	*2.663e-3*	1.675e-3	*2.829e-3*
J_{12z} (force by control devices(Z))	0.000e+0	0.000e+0	0.000e+0
J_{13x} (stroke of control devices(X))	*0.630*	*0.971*	*1.048*
J_{13z} (stroke of control devices(Z))	0.000	0.000	0.000
J_{16} (number of control devices)*	*24*	*24*	*24*
J_{17} (number of sensors)**	*18*	*18*	*18*

Note : *16 Actuators between the deck and towers, four between the deck and abutment, and four between the deck and pier
** 14 accelerometers and four displacement transducers
Italics number shows that PNScontrol produces lower number

5.4.4 The Effects of Snow Loads

The benchmark problem has an alternate model to evaluate the robust performance of the proposed control design, that is the effects of snow loads on the model. The amount of the snow increases the mass of the bridge by approximately 3.5%. The maximum variation in

the frequencies is 4.38%. Again, simulation of the model was carried out for the proposed control design with snow loads. The results are shown in **Table 5-9**. It is also clear from the table that the pseudo negative stiffness control method can perform better than passive control when snow load is considered.

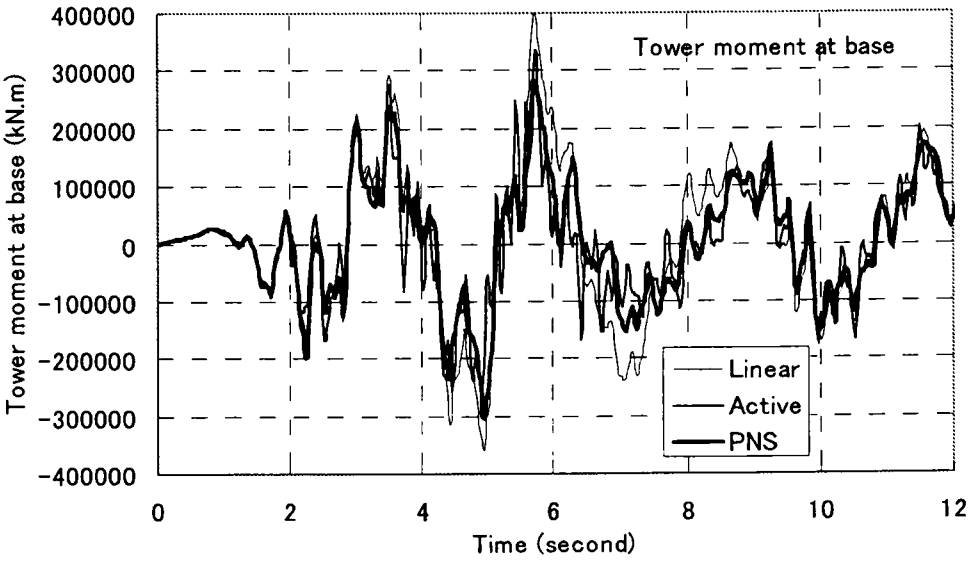

Figure 5-17. Time history of tower (pier2) moment at base, for El Centro earthquake, incidence angle 15°, no snow loads

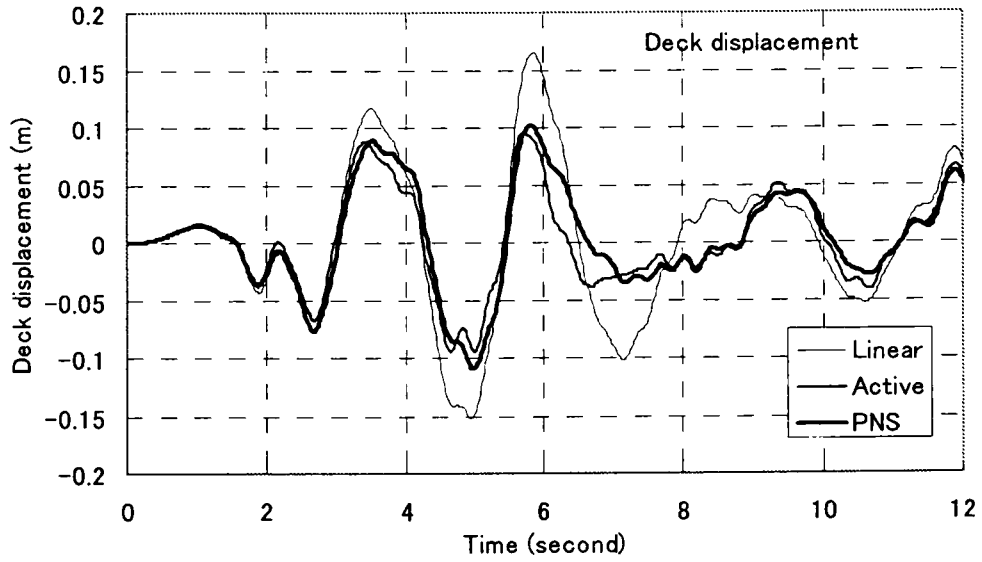

Figure 5-18. Time history of deck displacement at bent/pier1, for El Centro earthquake, incidence angle 15°, no snow loads

Table 5-9. Evaluation criteria based on passive and PNS controls (*with snow load*)

Evaluation Criteria	ElCentro		Mexico		Gebze	
	passive*	pns**	passive*	pns**	passive*	pns**
J_{1x} (shear at tower base(X))	**0.357**	0.365	0.469	**0.424**	0.469	**0.436**
J_{1z} (shear at tower base(Z))	1.023	1.020	1.106	1.103	1.034	1.034
J_{2x} (shear at deck level(X))	0.988	**0.976**	1.035	**0.968**	1.066	**0.958**
J_{2z} (shear at deck level(Z))	0.964	0.961	0.998	0.992	0.991	0.996
J_{3x} (moment at tower base(X))	0.338	**0.287**	0.539	**0.438**	0.527	0.527
J_{3z} (moment at tower base(Z))	1.091	1.094	1.084	1.082	1.036	1.042
J_{4x} (moment at deck level(X))	0.661	**0.564**	0.988	**0.893**	1.025	**0.861**
J_{4z} (moment at deck level(Z))	1.009	1.010	0.993	0.992	1.000	1.000
J_5 (deviation of cable tension)	0.243	**0.220**	**0.121**	0.122	**0.175**	0.187
J_6 (deck displacement)	1.752	**1.158**	2.651	**2.020**	2.933	**2.842**
J_{7x} (nor. shear @tower base(X))	0.293	**0.276**	0.387	**0.345**	0.385	**0.326**
J_{7z} (nor. shear @tower base(Z))	1.007	0.998	1.047	1.044	1.041	1.035
J_{8x} (nor. shear @deck level(X))	0.940	**0.875**	1.102	**0.929**	1.033	**0.942**
J_{8z} (nor. shear @deck level(Z))	0.978	0.979	0.999	0.998	0.990	0.989
J_{9x} (nor. mom. @tower base(X))	0.318	**0.262**	0.495	**0.348**	0.552	**0.444**
J_{9z} (nor. mom. at tower base(Z))	1.001	0.995	1.045	1.041	1.031	1.026
J_{10x} (nor. mom. @deck level(X))	0.766	**0.684**	1.115	**0.883**	0.923	**0.801**
J_{10z} (nor. mom. @deck level(Z))	1.002	1.002	1.004	1.004	1.002	1.002
J_{11} (nor. deviation of cbl tension)	0.025	0.025	0.017	**0.016**	0.015	0.015
J_{12x} (force by devices(X))***	3.272e-3	**2.398e-3**	2.463e-3	**1.956e-3**	**3.359e-3**	3.376e-3
J_{12z} (force by devices(Z))***	0.000e+0	0.000e+0	0.000e+0	0.000e+0	0.000e+0	0.000e+0
J_{13x} (stroke of devices(X))	0.871	**0.641**	1.279	**0.980**	1.153	**1.115**
J_{13z} (stroke of devices(Z))	0.000	0.000	0.000	0.000	0.000	0.000
J_{16} (number of devices)****	20	20	20	20	20	20
J_{17} (number of sensors)	**0**	4	**0**	4	**0**	4

Note : * Linear viscous dampers and elastic bearings between the deck and towers
** Pseudo negative stiffness dampers and elastic bearings between the deck and towers
*** Force by four dampers plus an elastic bearing
**** 16 dampers plus four elastic bearings
Bold number shows that this type of control is better than the other one.

5.4.5 The Effects of Incidence Angle

The above results were made for the incidence angle (the angle between the horizontal ground motion components and the structural axes) of 15°. The benchmark problem has two cases: 15° and 45° of incidence angles. Simulation of the proposed control by using 45° of incidence angle was also carried out and the results are shown in **Table 5-10**. It is clear from the table pseudo negative stiffness control is also effective when the incidence angle is 45°.

Table 5-10. Evaluation criteria based on passive and PNS controls (*incidence angle 45°*)

Evaluation Criteria	ElCentro		Mexico		Gebze	
	passive*	pns**	passive*	pns**	passive*	pns**
J_{1x} (shear at tower base(X))	**0.381**	0.394	0.433	**0.386**	**0.426**	0.444
J_{1z} (shear at tower base(Z))	0.988	0.995	1.023	1.021	0.994	0.999
J_{2x} (shear at deck level(X))	0.787	**0.736**	1.022	**0.991**	1.009	**0.793**
J_{2z} (shear at deck level(Z))	0.984	0.985	0.973	0.977	0.988	0.992
J_{3x} (moment at tower base(X))	0.435	**0.336**	0.557	**0.453**	0.568	**0.542**
J_{3z} (moment at tower base(Z))	0.978	0.977	1.015	1.002	0.989	0.993
J_{4x} (moment at deck level(X))	0.708	**0.578**	0.878	**0.833**	0.905	**0.722**
J_{4z} (moment at deck level(Z))	0.996	0.997	1.001	1.003	1.002	1.000
J_5 (deviation of cable tension)	0.265	**0.246**	0.128	**0.127**	**0.180**	0.183
J_6 (deck displacement)	1.803	**1.377**	3.148	**2.445**	3.164	**2.984**
J_{7x} (nor. shear @tower base(X))	0.264	**0.243**	0.364	**0.314**	0.412	**0.358**
J_{7z} (nor. shear @tower base(Z))	0.975	0.968	0.996	0.993	1.017	1.013
J_{8x} (nor. shear @deck level(X))	0.921	**0.844**	1.104	**0.935**	1.015	**0.907**
J_{8z} (nor. shear @deck level(Z))	0.991	0.992	0.971	0.972	1.000	0.999
J_{9x} (nor. mom. @tower base(X))	0.335	**0.265**	0.524	**0.357**	0.603	**0.495**
J_{9z} (nor. mom. at tower base(Z))	0.981	0.977	0.992	0.990	1.016	1.012
J_{10x} (nor. mom. @deck level(X))	0.816	**0.724**	1.152	**0.918**	1.002	**0.894**
J_{10z} (nor. mom. @deck level(Z))	1.003	1.003	1.003	1.003	1.004	1.002
J_{11} (nor. deviation of cbl tension)	0.025	0.025	0.017	**0.016**	0.017	0.017
J_{12x} (force by devices(X))***	3.218e-3	**2.173e-3**	2.463e-3	**1.949e-3**	2.984e-3	**2.683e-3**
J_{12z} (force by devices(Z))***	0.000e+0	0.000e+0	0.000e+0	0.000e+0	0.000e+0	0.000e+0
J_{13x} (stroke of devices(X))	0.800	**0.620**	1.229	**0.948**	1.257	**1.204**
J_{13z} (stroke of devices(Z))	0.000	0.000	0.000	0.000	0.000	0.000
J_{16} (number of devices)****	20	20	20	20	20	20
J_{17} (number of sensors)	**0**	4	**0**	4	**0**	4

Note : * Linear viscous dampers and elastic bearings between the deck and towers
** Pseudo negative stiffness dampers and elastic bearings between the deck and towers
*** Force by four dampers plus an elastic bearing
**** 16 dampers plus four elastic bearings
Bold number shows that this type of control is better than the other one.

5.7 Summary

This chapter presents the application of pseudo negative stiffness control on the benchmark cable-stayed bridge phase I and phase II. Benchmark control problems allow researchers to apply various control strategies, such as passive, active, semi-active, or combination thereof, to cable-stayed bridges, and to compare results directly in terms of a specified set of performance objectives. The benchmark cable-stayed bridge considers the issues of different earthquake types, three dimensionality, multi-support excitations, incidence angle, and control robustness.

The results show that by applying pseudo negative stiffness control, the response of the

benchmark bridge can be significantly reduced. The results are significantly better than those by passive control and comparable to those by active control.

Chapter 6

Conclusions

A newly developed pseudo negative stiffness control method has been presented and the application of this method for seismic safety enhancement of cable-stayed bridges has been thoroughly studied.

The objective of the research is to study the efficacy of pseudo negative stiffness control in reducing seismic responses of cable-stayed bridges. The applications of this control method to a typical cable-stayed bridge and the benchmark control problem of cable-stayed bridges are studied and the results are compared to those by passively and actively controlled cable-stayed bridges.

General view of seismic safety enhancement of civil structures is outlined in **Chapter 1**, pointing out the extreme importance of controlling structures under severe seismic attack. The traditional ductility design method is capable of avoiding structural collapse under very severe earthquakes, however, once the structural responses goes deeply into plastic range, structures may not be operational nor repairable. For higher reliability of structures even under a very severe earthquake motion, structural control techniques which effectively reduce seismic force to structures shall be developed.

Chapter 2 presents the application of structural control technologies for seismic response reduction of cable-stayed bridges. Cable-stayed bridges, which are increasing in popularity among bridge engineers, have very small structural damping. Therefore, the application of structural control technologies for seismic response reduction of a cable-stayed bridge is needed to absorb large seismic energy and reduce the response amplitudes.

The application of passive control devices can solve many problem of seismic design

for cable-stayed bridges. They are well known to many civil engineers, practical, economical, and robust. However, for a wider-frequency range and also for the transient vibration, active control is more effective in seismic response reduction.

The application of active control to a cable-stayed bridge was also presented in this chapter. Nevertheless, active control needs a large amount of external energy supply. Therefore, the application of semi-active control which solves the energy problem of fully active was presented. By using significantly small external energy supply, appropriately implemented semi-active systems perform significantly better than passive devices and have the potential to achieve the majority of the performance of fully active systems.

Recognizing that commonly applied semi-active control still uses large amount of sensors placed throughout the structure and complicated control algorithm that is potential to be the sources of errors and uncertainties, newly developed and simple pseudo negative stiffness control is presented in **Chapter 3**, pointing out its advantage over passive and commonly semi-active control. Experimental results using pseudo negative stiffness control is also shown for practical reference. The clear advantage of pseudo negative stiffness hysteretic loop over linear viscous damper hysteretic loop is analytically and graphically shown.

Seismic response spectrum for a single degree of freedom system employing linear viscous damper and pseudo negative stiffness damper is compared for better understanding on how the pseudo negative stiffness control performs better than linear viscous damper under seismic excitation. The response spectrum shows that pseudo negative stiffness control results in significantly lower absolute acceleration and relative velocity than that by linear viscous damper for similar relative displacement response. Moreover, the earthquake input energy is significantly lower for the pseudo negative stiffness control than that by linear viscous damper.

The application of passive and pseudo negative stiffness control to seismic retrofit of a cable-stayed bridge was presented in **Chapter 4**. For better relation with real case, the cable-stayed bridge is modeled from the Tempozan Bridge of Osaka, Japan, built in 1988 as part of Hanshin Expressway. Very high ground motion (level II design) is required in the new bridge design specification set in 1996 in Japan. Hence seismic safety of cable-stayed bridges built before the present specification has to be reviewed and seismic retrofit has to be done, if it is necessary. The results show that significant increase in seismic responses of the bridge in the longitudinal and transversal direction was found

when the existing bridge was simulated with new design earthquakes. On the contrary, by applying passive control for seismic retrofit of the bridge, significantly lower seismic responses were obtained so that seismic safety of the bridge could be enhanced.

The effect of soil-structure interaction has also been studied and the results show that the introduction of flexible support at the foundation makes the movement of the damper, installed between the deck and the tower, reduced. This reduction in movement results in lower structural damping ratio.

The effect of three dimensionality was also studied. The results shows that in the lateral or transversal direction, three dimensional model cannot be represented by any two dimensional model. However, for longitudinal direction, the results of two dimensional model agrees well with those of three dimensional model. Therefore, for studying the effects of earthquakes on the longitudinal direction, two-dimensional model is deemed appropriate.

The effect of connecting the deck ends to adjacent structures is also studied. It is found that the effect is favorable to the cable-stayed bridge during earthquake attack. By connecting to adjacent structures (piers, abutment, etc), seismic induced responses in the cable-stayed bridge is significantly reduced. Therefore, for the rest of the study, the deck ends were not connected to any other structures, for conservativeness.

When the pseudo negative stiffness control algorithm was applied to the cable-stayed bridge, the results is significantly better than that by viscous damper in seismic response reductions. Moreover, although cable-stayed bridges are complex in nature, the hysteretic loop produced by variable damper plus elastic bearings installed between the deck and towers could approach that of rigid-perfectly plastic force-deformation characteristics which has large damping ratio, so that the seismic response could be reduced significantly better than that by linear viscous dampers.

In order to further study the effectiveness of pseudo negative stiffness control for seismic safety enhancement of cable-stayed bridges, **Chapter 5** shows the application of this control strategy to the benchmark cable-stayed bridge. The benchmark cable-stayed bridge considers the issues of different earthquake types, three dimensionality, multi-support excitations, incidence angle, and control robustness. Benchmark control problems allow researchers to apply various control strategies, such as passive, active, semi-active, or combination thereof, to cable-stayed bridges, and to compare results directly in terms of a specified set of performance objectives. The results show that by

applying pseudo negative stiffness control, the response of the benchmark bridge can be significantly reduced. The results are significantly better than those by passive control and comparable to those by active control.

References

ABAQUS (1998), Hibbitt, Karlsson & Sorensen Inc., Pawtucket, RI.

Abdel-Ghaffar, A. M. (1991) Cable-stayed Bridges Under Seismic Action. *Cable-stayed Bridges: Recent Developments and Their Future*, Editor: M. Ito, Elsevier Science Publishers.

AIJ (1995) *Preliminary Reconnaissance Report of the 1995 Hyogoken-Nanbu Earthquake, English Edition*, Architectural Institute of Japan (AIJ), April

Blakeley, R., Charleson, A., Hitchcock, H., Megget, L., Priestley, M. J. N., Sharpe, R., and Skinner, R. (1979) Recommendations for the Design and Construction of Base Isolated Structures, *Bulletin of New Zealand National Society For Earthquake Engineering*, Waikanae, New Zealand, 12(2), 136-157.

Bowles, J. E. (1982) *Foundation Analysis and Design*. 3rd ed., McGraw-Hill Book Company, pp. 66.

Branco, F. A., Mendes, P. M., and Guerreiro, L. M. C. (2000) Special studies for Vasco da Gama bridge. *ASCE, Journal of Bridge Engineering*, Vol. 5, No. 3, August.

Caicedo, J. M., Dyke, S. J., Moon, S. J., Bergman, L. A., Turan, G., and Hague, S. (2002) *Phase II Benchmark Control Problem for Seismic Response of Cable-stayed Bridges, (http://wusceel.cive.wustl.edu/quake/)*.

Caicedo, J. M., Dyke, S. J., Turan, G., and Bergman, L. A. (2000) Comparison of Modeling Techniques for Dynamic Analysis of a Cable-stayed Bridge, *Proceedings of the Engineering Mechanics Conference*, ASCE, Austin, Texas, May 21-23.

Caughey, T. K. (1993) Musings on Structural Control, *Proc. International Workshop on Structural Control*, Hawaii, pp. 65-75.

Caughey, T. K. (1998) The Benchmark Problem, *Earthquake Engineering and Structural Dynamics*, Vol. 27, pp. 1125.

Chopra, A. K. (1995) *Dynamics of Structures, Theory and Applications to Earthquake Engineering*, Prentice Hall.

Dyke, S. J., Spencer, B F., Sain, M. K., and Carlson, J. D. (1996a) A New Semi-active Control Device for Seismic Response Reduction, *Proc. 11th ASCE Engineering*

Mechanics Spec. Conference, Ft. Lauder-dale, Florida.

Dyke, S. J., Spencer, B F., Sain, M. K., and Carlson, J. D. (1996b) Seismic Response Reduction using Magnetorheological Dampers, *Proc. IFAC World Congress*, San Francisco, California.

Dyke, S. J., Spencer, B F., Sain, M. K., and Carlson, J. D. (1996c) Modeling and Control of Magnetorheological Dampers for Seismic Response Reduction, *Smart Materials and Structures*, Vol. 5, pp. 565-575.

Dyke, S. J., Spencer, B F., Sain, M. K., and Carlson, J. D. (1997) On the Efficacy of Magnetorheological Dampers for Seismic Response Reduction, *Proc. DETC'97, ASME Design Engineering Technical Conferences*, Sacramento, California, September 14-17.

Dyke, S. J., Caicedo, J. M., Turan, G., Bergman, L. A., and Hague, S. (2003) Phase I Benchmark Control Problem for Seismic Response of Cable-stayed Bridges, *Journal of Structural Engineering*, ASCE. (in press)

Dyke, S. J., Turan, G., Caicedo, J. M., Bergman, L. A., and Hague, S. (2000) Benchmark Control Problem for Seismic Response of Cable-stayed Bridges, (*http://wusceel.cive.wustl.edu/quake/*).

EERI (1995) *The Hyogo-Ken Nanbu Earthquake 17 January, 1995, Preliminary Reconnaissance Report*, Editors: Craig D. Comartin, Marjorie Greene, and Susan K. Tubbesing, Earthquake Engineering Research Institute (EERI), February.

Gavin, H. P. and Aldemir, U. (2001) Behavior and Response of Auto-adaptive Seismic Isolation, *Proc. 3rd U.S.-Japan Workshop in Urban Earthquake Disaster Mitigation*, Editors: S. Otani and M. A. Sozen, Seattle, WA, August 15-16, pp. 120-128.

Hague, S. (1997) Composite Design for Long Span Bridges, *Proceedings of the XV ASCE Structure Congress*, Portland, Oregon.

Hall, J. F. (1999) Discussion, The Role of Damping in Seismic Isolation, *J. Earthquake Engineering and Structural Dynamics*, 28, 1717-1720

Hanshin Highway Public Corporation (1992) *Tempozan Bridge, Structure and Construction Data*. (in Japanese)

He, W.L., Agrawal, A.K., and Mahmoud, K. (2001) Control of Seismically Excited Cable-stayed Bridge using Resetting Semiactive Stiffness Dampers. *Journal of Bridge Engineering*, Vol. 6, No. 6, November/December.

Housner, G.W., Bergman, L.A., Caughey, T.K., Chassiakos, A.G., Claus, R.O., Masri, S.F.,

Skelton, R.E., Soong, T.T., Spencer, B.F., Yao, J.T.P. (1997) Structural Control: Past, Present, and Future. *Journal of Engineering Mechanics*, Vol. 123, No. 9, September.

Iemura, H. (1999) From Ductility Demand to Vibration Control Aseismic Design, *Proceedings of the 12th KKNN Seminar/Workshop on Civil Engineering*, KAIST, Taejon, Korea, August 20-22.

Iemura, H., Adachi, Y., Okashiro, S., and Mizutani, T. (2001a) Application of Structural Control Technologies to Seismic Retrofit of a Cable-Stayed Bridge. *Proc. IABSE Conference*, Seoul, June.

Iemura, H., Igarashi, A., and Nakata, N. (2001b) Semi-active Control of Full-scale Structures using Variable Joint Damper System. *The Fourteenth KKNN Symposium on Civil Engineering*, Kyoto, Japan, November 5-7.

Iemura, H., Igarashi, A., and Nakata, N. (2002) Semi-active Optimal Control Test of Full-scale Structural Steel Frames with the Variable Joint Damper System, *Proc. 3rd World Conf. on Struct. Control*, Como, Italy. (in press)

Iemura, H. and Pradono, M. H. (2001) Seismic Retrofit of a Cable-stayed Bridge with Dynamic Response Control Device. *The Fourteenth KKNN Symposium on Civil Engineering*, Kyoto, Japan, November 5-7.

Iemura, H. and Pradono, M. H. (2002a) Structural Control, *Earthquake Engineering Handbook*, Editors: Wai-Fah Chen and Charles Scawthorn, CRC Press, Chapter 19, pp. 19-1 to 19-29.

Iemura, H. and Pradono, M. H. (2002b) Passive and Semi-active Seismic Response Control of a Cable-stayed Bridge, *Journal of Structural Control*, John Wiley and Sons, Vol. 9, pp. 189-204, December.

Iemura, H. and Pradono, M. H. (2002c) Seismic Response Control of a Cable-stayed Bridge with Passive and Semi-active Control Technologies, *Proc. 3rd World Conf. on Struct. Control*, Como, Italy. (in press)

Japan Roadway Association (1996) *The Seismic Design Specification*.

Jung, H-J, Spencer, B.F., Lee, I-W. (2001) Benchmark Control Problem for Seismically Excited Cable-stayed Bridges using Smart Damping Strategies. *Proc. IABSE Conference*, Seoul, June.

Kamagata, S. and Kobori, T. (1994) Autonomous Adaptive Control of Active Variable Stiffness System for Seismic Ground Motion, *Proc. 1st World Conference on Structural Control*, Los Angeles, CA, TA4, pp. 33-42

Kawashima, K. and Unjoh, S. (1991) Seismic Behavior of Cable-stayed Bridges. *Cable-Stayed Bridges: Recent Developments and Their Future*, Editor: M. Ito, Elsevier Science Publishers.

Kelly, J. M. (1999) The Role of Damping in Seismic Isolation, *J. Earthquake Engineering and Structural Dynamics*, 28, 3-20.

Kurata, N., Kobori, T., Takahashi, M., Niwa, N. and Midorikawa, H. (1999) Actual seismic response controlled building with semi-active damper system, *Earthquake Engrg. and Struct. Dyn.*, 28, 1427-1447.

Kwakernaak, H. and Sivan, R. (1972) *Linear Optimal Control Systems*, Wiley, New York, NY.

MathWorks (1997a) *MATLAB The Language of Technical Computing*. The Math Works Inc., 24 Prime Park Way, Natick, MA 01760-1500.

MathWorks (1997b) *SIMULINK Dynamic System Simulation for MATLAB*. The Math Works Inc., 24 Prime Park Way, Natick, MA 01760-1500.

McClamroch, N. H. and Gavin, H. P. (1995) Closed Loop Structural Control Using Electrorheological Dampers, *Proc. American Control Conference*, Seattle, Washington, pp. 4173-4177.

Mukai, Y., Tachibana, E., and Inoue, Y. (1994) Experimental Study of Active Fin System for Wind-induced Structural Vibration, *Proc. 1st World Conference on Structural Control*, pp. WP2-52 to WP2-61.

Nazmy, A. S. and Abdel-Ghaffar, A. M. (1987) *Seismic Response Analysis of Cable-stayed Bridges Subjected to Uniform and Multiple-Support Excitations*, Report No. 87-SM-1, Department of Civil Engineering, Princeton University, Princeton, NJ 08544, May.

Ohtori, Y. and Spencer, B. F. (1999) A MATLAB-based Tool for Nonlinear Structural Analysis, *Proceedings of the 13th Engineering Mechanics Conference*, Baltimore, Maryland, June 13-16.

Patten, W. N. (1998) The I-35 Walnut Creek Bridge: An intelligent highway bridge via semi-active structural control, *Proc. 2nd World Conf. on Struct. Control*, 1, Kyoto, Japan, pp427-436.

Patten, W. N., He, Q., Kuo, C. C., Liu, L., and Sack, R. L. (1994a) Suppression of Vehicle Induced Bridge Vibration via Hydraulic Semi-active Vibration Dampers, *Proc. 1st World Conference on Structural Control*, Los Angeles, CA, FA1, pp. 3-38.

Patten, W. N., He, Q., Kuo, C. C., Liu, L., and Sack, R. L. (1994b) Seismic Structural Control via Hydraulic Semi-active Vibration Dampers, *Proc. 1st World Conference on Structural Control*, Los Angeles, CA, FA2, pp. 83-89.

Paulay, T. and Priestley, M. J. N. (1992) *Seismic Design of Reinforced Concrete and Masonry Buildings*, John Wiley & Sons, Inc., Toronto.

Prakash, V. and Powell, G. H. (1993) *Drain-2DX, Drain-3DX, and Drain-Building: Base Program Design Documentation*, Report No. UCB/SEMM-93/16, University of California, Berkeley, California, December.

Priestley, M. J. N., Seible, F., and Calvi, G. M. (1996) *Seismic Design and Retrofit of Bridges*, John Wiley and Sons, Inc., New York.

Rakicevic, Z. and Jurukovski, D. (2001) *Optimum Design of Passive Controlled Steel Frame Structures*, Report IZIIS 2001-59, Project 123/NIST, Skopje, December.

Reid, T. J. (1956) Free Vibration and Hysteretic Damping, *Journal Aero. Soc.*, Vol. 69, pp. 283.

Sage, A. P. and White, C. C. III (1977) *Optimum Systems Control*, 2nd edition, Prentice Hall, Englewood, Cliffs, NJ.

Scawthorn, C. (2002) Earthquakes: A Historical Perspective, *Earthquake Engineering Handbook*, Editors: Wai-Fah Chen and Charles Scawthorn, CRC Press, Chapter 1, pp. 1-1 to 1-66.

Schemmann, A. G., Smith, H. A., Bergman, L. A., and Dyke, S. J. (1998) Feasibility Study: Control of a Cable-stayed Bridge Model, Part I: Problem Definition, *Proc. 2nd World Conference on Structural Control*, Vol. 2, John Wiley and Sons, England, pp. 975-979, Kyoto, Japan, June 30 – July 2.

Session 10 – Benchmark Tests of Buildings (1998) *Proc. 2nd World Conference on Structural Control*, Kyoto, Japan, June 29-July 2, pp. 1349-1490.

Soong, T. T. (1990) *Active Structural Control, Theory and Practice*, Longman Scientific and Technical, England.

Special Issue: Benchmark Problems (1998) *Earthquake Engineering and Structural Dynamics*, Vol. 27, No.11.

Spencer, B. F., Christenson, R. E., and Dyke, S. J. (1999) Next Generation Benchmark Control Problem for Seismically Excited Buildings, (*http://www.nd.edu/~quake/*).

Spencer, B.F., Dyke, S.J., Sain, M.K., and Carlson, J.D. (1997) Phenomenological Model for Magnetorheological Dampers. *Journal of Engineering Mechanics*, Vol. 123, No. 3,

March.

Spencer, B. F. and Sain, M. K. (1997) Controlling Buildings: A New Frontier in Feedback, *Special Issue of the IEEE Control Systems Magazine on Emerging Technology*, Vol. 17, No. 6, pp. 19-35, December.

Spencer, B. F. and Soong, T. T. (1999) New Applications and Development of Active, Semi-active, and Hybrid Control Techniques for Seismic and Non-seismic Vibration in the USA. *Proceedings of International Post-SmiRT Conference Seminar on Seismic Isolation, Passive Energy Dissipation, and Active Control of Vibration of Structures*, Cheju, Korea, August 23-25.

Spencer, B. F., Suhardjo, J., and Sain, M. K. (1994) Frequency Domain Optimal Control Strategies for Aseismic Protection, *ASCE Journal of Engineering Mechanics*, Vol. 120, No. 1, pp. 135-159.

Sun, L. and Goto, Y. (1994) Applications of Fuzzy Theory to Variable Dampers for Bridge Vibration Control, *Proc. 1st World Conference on Structural Control*, Los Angeles, CA, WP1, pp. 31-40.

Wilson, J. and Gravelle, W. (1991) Modeling of a Cable-stayed Bridge for Dynamic Analysis, *Earthquake Engineering and Structural Dynamics*, Vol. 20, 707-721.

Yamada, Y., Shiraishi, N., Toki, K., Matsumoto, K., Matsuhashi, K., Kitazawa, M., and Ishizaki, H. (1991) Earthquake-resistant and Wind-resistant Design of the Higashi-Kobe Bridge, *Cable-stayed Bridges: Recent Developments and Their Future*, Editor: M. Ito, Elsevier Science Publishers.

Zhou, K., Doyle, J. C., and Glover, K. (1996) *Robust and Optimal Control*, Prentice-Hall, New Jersey.

Appendix A

MATLAB® Program for PNS Control Response Spectrum

It has been shown in **Chapter 3** that pseudo negative stiffness control response spectrum is significantly better than those by passive linear viscous damper. Programs to calculate the pseudo negative stiffness response spectrum in MATLAB® and SIMULINK® (**Mathworks, 1997a,b**) are shown herein.

A.1 MATLAB® Program

The MATLAB® program, called *M*-File, is shown herein.

```
%--------------------------------------
% <RespPNSKb.m>
% Calculates response spectrum using
% pseudo negative stiffness control.
%
% Mulyo Harris Pradono July 5th, 2002
%--------------------------------------

clear;

%-------------------------
% load input earthquake
%-------------------------
load Equake.dat -ascii;
inputeq = Equake;
clear Equake;
dt = 0.01;
N  = length(inputeq);
time = [0:dt:(N-1)*dt]';
zdd = [time inputeq];

%----------------------------
% sets of damping ratio
% represented by coefficient
```

```
%---------------------------
damp = [0.0 0.5 1.0]; % equivalent to h = 15.9, 32.95, & 53.4 %

%-----------------------------------------
% natural period is set from
% 0.2 (sec) to 7.0(sec) with 0.05(sec) step
%-----------------------------------------
T    = [0.2:0.05:7.0]';

%-------------------
% Loop calculations
%-------------------
for ii=1:length(T)
        for jj=1:length(damp);

                %----------------------------------------
        % create SDOF model from given parameters
        %----------------------------------------
        m =   1.0;
        k = 4*pi^2*m/T(ii)^2;

        %----------------------------------------
        % negative stiffness and damping coefficient
        %----------------------------------------
        K_ns  = -k;
        DmpCS = damp(1,jj)*sqrt(k*m);

        %---------------------------
        % simulation using SIMULINK
        %---------------------------
        sim('sdofrespns');

        %---------------------------------
        % Pick up important time histories
        %---------------------------------
        if T(ii) == 0.75
            Resp75dm(:,jj) = resp(:,1);
            Resp75am(:,jj) = resp(:,3);
        end

        if T(ii) == 6.30
            Respdm(:,jj) = resp(:,1);
            Respam(:,jj) = resp(:,3);
        end

                %-------------------------------
                % set maximum values to arrays
                %-------------------------------
                dm(ii,jj) = max(abs(resp(:,1)));
                vm(ii,jj) = max(abs(resp(:,2)));
                ien(ii,jj) =    (inputen(N,1));
                am(ii,jj) = max(abs(resp(:,3)));

                fprintf('T = %f(sec),  h = %f done.¥n',T(ii),DmpCS);

         end;
end;

%---------------------------------
% plot results
%---------------------------------
figure(1)
subplot(413),plot(T,dm),xlabel('Nat. Period (sec)'),ylabel('Disp. Spect.(cm)'),grid on,
axis([0 7 0 300]);
subplot(412),plot(T,vm),xlabel('Nat. Period (sec)'),ylabel('Vel. Spect.(kine)'),grid on,
axis([0 7 0 300]);
subplot(411),plot(T,am),xlabel('Nat. Period (sec)'),ylabel('Abs.Acc. Spect.(gal)'),grid on,
axis([0 7 0 1200]);
subplot(414),plot(T,ien),xlabel('Nat. Period (sec)'),ylabel('InputEn.Spect.(kg.gal.cm)'),grid on,
axis([0 7 0 6e8]);

%---------------------------------
% plot results
%---------------------------------
figure(2)
plot(Respdm(:,1),-Respam(:,1)),xlabel('Rel. Disp(cm)'),ylabel('Abs. Acc.(gal)'),grid on
```

```
title('T=6.30 sec., h=15.9%');

%---------------------------------
% plot results
%---------------------------------
figure(3)
plot(Respdm(:,2),-Respam(:,2)),xlabel('Rel. Disp(cm)'),ylabel('Abs. Acc.(gal)'),grid on
title('T=6.30 sec., h=32.9%');

%---------------------------------
% plot results
%---------------------------------
figure(4)
plot(Respdm(:,3),-Respam(:,3)),xlabel('Rel. Disp(cm)'),ylabel('Abs. Acc.(gal)'),grid on
title('T=6.30 sec., h=53.4%');

%---------------------------------
% plot results
%---------------------------------
figure(5)
plot(Resp75dm(:,1),-Resp75am(:,1)),xlabel('Rel. Disp(cm)'),ylabel('Abs. Acc.(gal)'),grid on
title('T=0.75 sec., h=15.9%');

%---------------------------------
% plot results
%---------------------------------
figure(6)
plot(Resp75dm(:,2),-Resp75am(:,2)),xlabel('Rel. Disp(cm)'),ylabel('Abs. Acc.(gal)'),grid on
title('T=0.75 sec., h=32.9%');

%---------------------------------
% plot results
%---------------------------------
figure(7)
plot(Resp75dm(:,3),-Resp75am(:,3)),xlabel('Rel. Disp(cm)'),ylabel('Abs. Acc.(gal)'),grid on
title('T=0.75 sec., h=53.4%');

%---------------------------------
% save results
%---------------------------------
Hasil = [T dm vm am ien];
save SpectData.dat Hasil -ascii
Hasil2 = [Respdm(:,1) Respam(:,1) Respdm(:,2) Respam(:,2) ...
          Respdm(:,3) Respam(:,3)];
save HystData.dat Hasil2 -ascii
Hasil3 = [Resp75dm(:,1) Resp75am(:,1) Resp75dm(:,2) Resp75am(:,2) ...
          Resp75dm(:,3) Resp75am(:,3)];
save HystData75.dat Hasil3 -ascii
```

A.2 SIMULINK® Blocks

The SIMULINK® blocks used to simulate single degree of freedom system with pseudo negative stiffness control algorithm for variable dampers are shown herein. **Figure A-1** shows the main blocks to calculate responses and input energy of a single degree of freedom system subjected to earthquake excitation. **Figure A-2** shows the contents of the block named "SDOF System" in **Figure A-1**. This block diagram is a common method for calculating SDOF responses. However, the uncommon one is the block "PNS Damper" whose content is shown in **Figure A-3**.

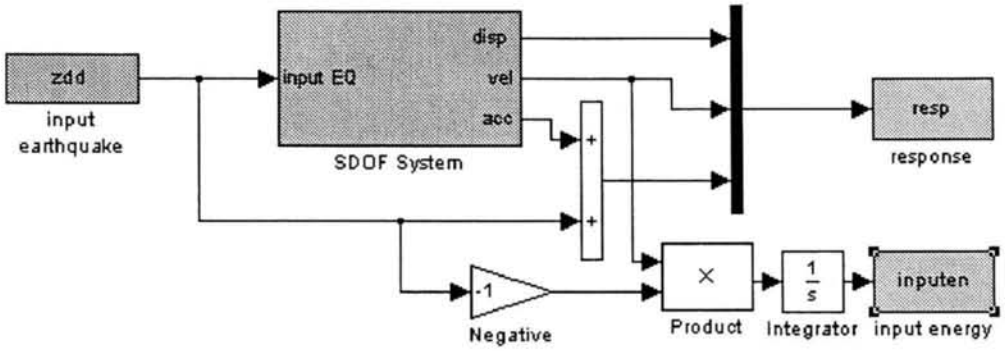

Figure A-1. SIMULINK block diagrams for calculating responses and input energy for a single degree of freedom system subjected to earthquake excitation

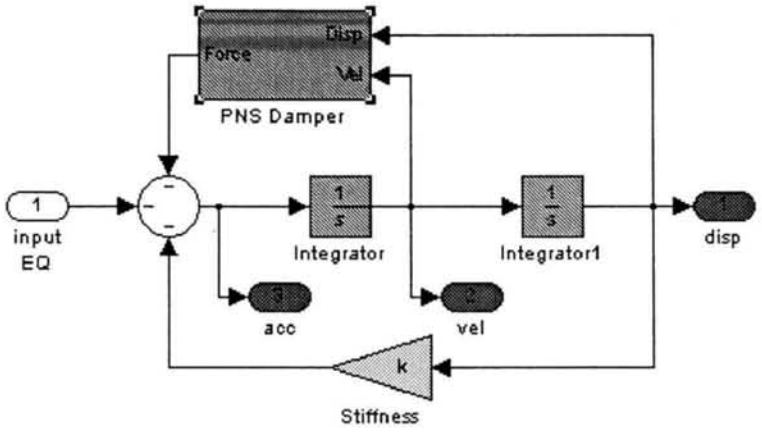

Figure A-2. Contents of the block named "SDOF System" in **Figure A-1**

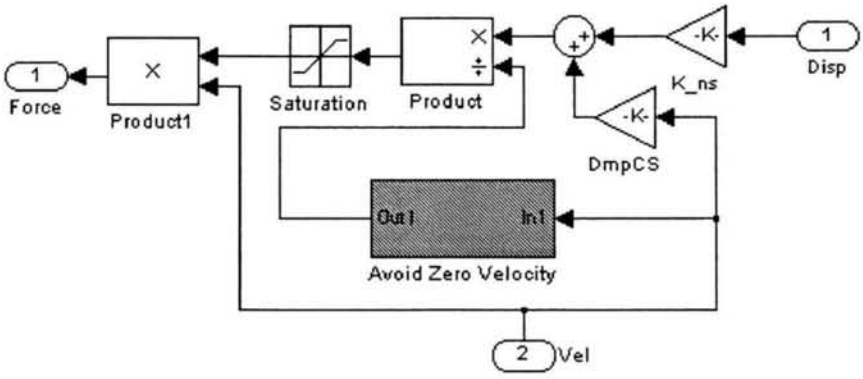

Figure A-3. Contents of the block named "PNS Damper" in **Figure A-2**

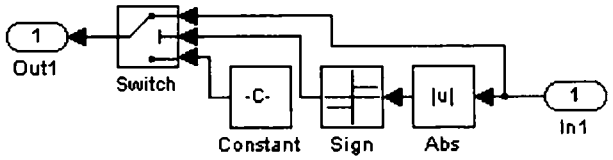

Figure A-4. Contents of the block named "Avoid Zero Velocity" in **Figure A-3**

Figure A-3 shows the block "Saturation" which saturates the maximum and minimum damping coefficient needed in order to cope with variable damper limitation. For information, zero velocity will cause mathematical problem when it used to divide the force in order to find the corresponding damping coefficient. Therefore, very small value is assigned when velocity is zero, which is all done in the block named "Avoid Zero Velocity". **Figure A-4** shows the content of the block.

Appendix B

Member Sectional Properties and Materials

Member sectional properties and materials are useful for calculation of finite element model properties which are used in **Chapter 4**.

B.1 Member Sectional Properties

The member sectional properties are shown in **Figure B-1** for the base of the tower. Other members' properties were calculated in the same way so that the whole finite element members have their corresponding data needed for simulations using commercial time history analysis **(Prakash and Powell, 1993)**.

B.2 Member Materials

Member materials are used to calculate the member stiffness and yield strength in order to check whether the new design earthquake cause the bridge to response beyond its elastic limit **(Chapter 4.3)**. **Figure B-2** shows the calculations needed.

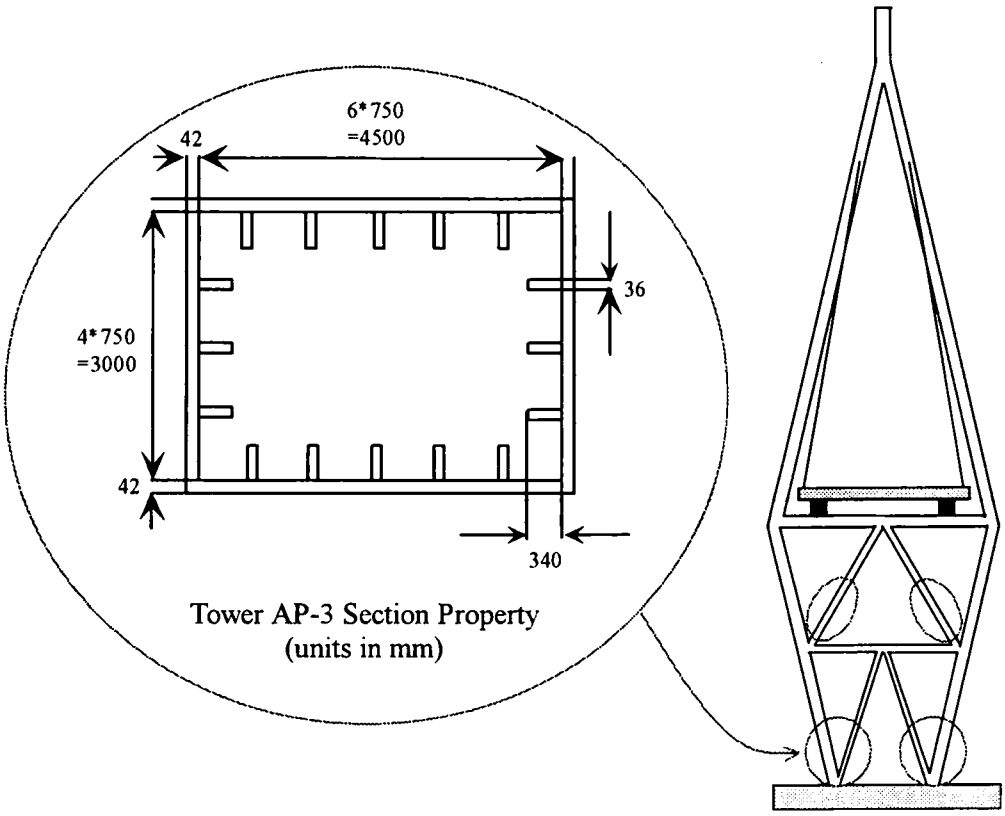

Figure B-1. Member sectional properties

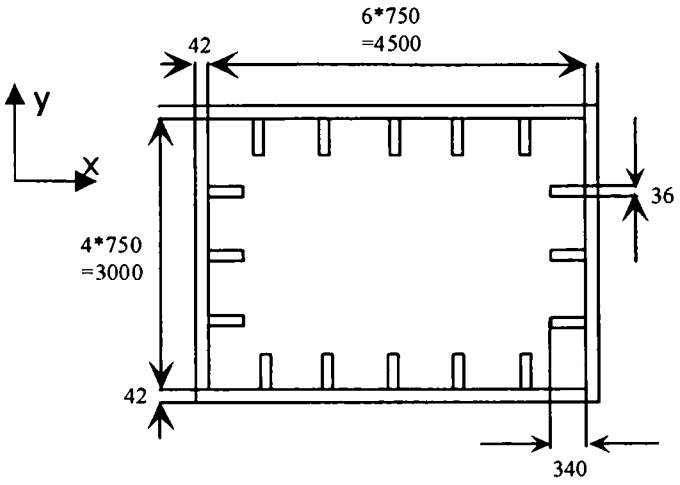

Base of Tower AP-3 Section Property

A = 0.863 m2
Ixx = 1.627 m4
Iyy = 2.443 m4
σy = 460 MPa

Static Gravity Analysis:
Ms = 52940 kN.m
Ss = 3210 kN
Fs = 118500 kN

$$M_y = \frac{I\sigma_y}{h}$$

$$\phi_y = \frac{M_y}{EI}$$

(a)

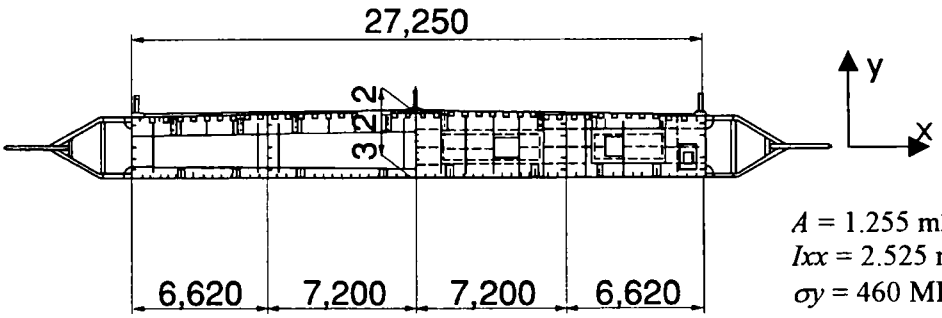

Deck Section Property
(mid-left position, see **Figure 4-4**)

A = 1.255 m2
Ixx = 2.525 m4
σy = 460 MPa

Static Gravity Analysis:
Ms = -37550 kN.m
Fs = 32120 kN

$$M_y = \frac{I\sigma_y}{h} \qquad \phi_y = \frac{M_y}{EI}$$

(b)

Cable Section Property
(top-left position, see **Figure 4-4**)

A = 0.02686 m2
σy = 1800 MPa

Fy = 34000 kN (ϕ=0.7)

Static Gravity Analysis:
Fs = 8257 kN

(c)

Figure B-2. Calculation of member elastic limit

Appendix C

Summary of the Benchmark Problem Statement

Chapter 5 has highlighted the important statements from the benchmark problem of cable-stayed bridges. More detail about the benchmark problem is presented herein.

C.1 Benchmark Cable-stayed Bridge

Introduction and figure of the benchmark bridge has been made in **Chapter 5**. Additional information will be presented.

The bridge has four lanes plus two narrower bicycle lanes, for a total width of 29.3 m. The deck is composed of steel beams and prestressed concrete slabs. Additionally, a concrete barrier is located in the center of the bridge, and a railing is located along the edges of the deck (**Figure C-1**).

The 128 cables are made of high-strength, low-relaxation steel. The smallest cable area is 28.5 cm^2 and the largest cable area is 76.3 cm^2. The H-shaped towers have a height of 102.4 m at pier 2 and 108.5 m at pier 3. Each tower support a total 64 cables. The towers are constructed of reinforced concrete. The cross section of each tower varies five times over the height of the tower, as shown in **Figure C-2**.

The finite element model, shown in **Figure 5-2** (in **Chapter 5**), has a total of 579 nodes, 420 rigid links, 162 beam elements, 134 nodal masses, and 128 cable elements. The towers are modeled using 50 nodes, 43 beam elements, and 74 rigid links. Constraints are applied to restrict the deck from moving in the lateral direction at piers 2, 3, and 4.

Boundary conditions restrict the motion at pier 1 to allow only longitudinal displacement (X) and rotations about Y and Z axes. The cables are modeled with truss elements. In the finite element model, the nominal tension is assigned to each cable. Note that the Illinois approach is not included in this model. Because the bearing at pier 4 does not restrict longitudinal motion and rotation about the X axis of the bridge, the Illinois approach was found to have a negligible effect on the dynamics of the cable-stayed portion of the bridge.

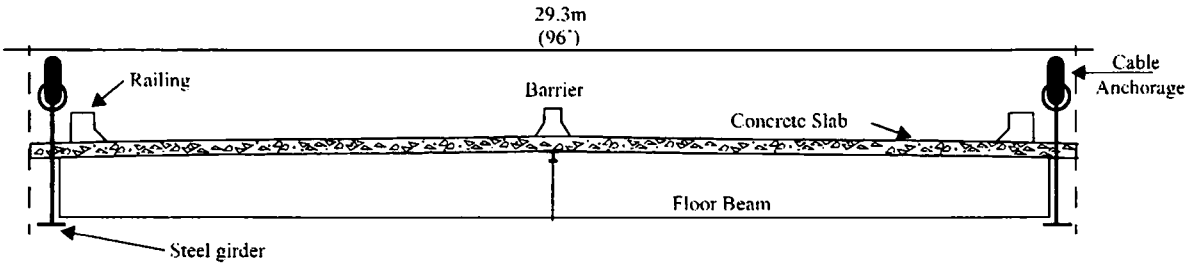

Figure C-1. Cross section of the bridge deck

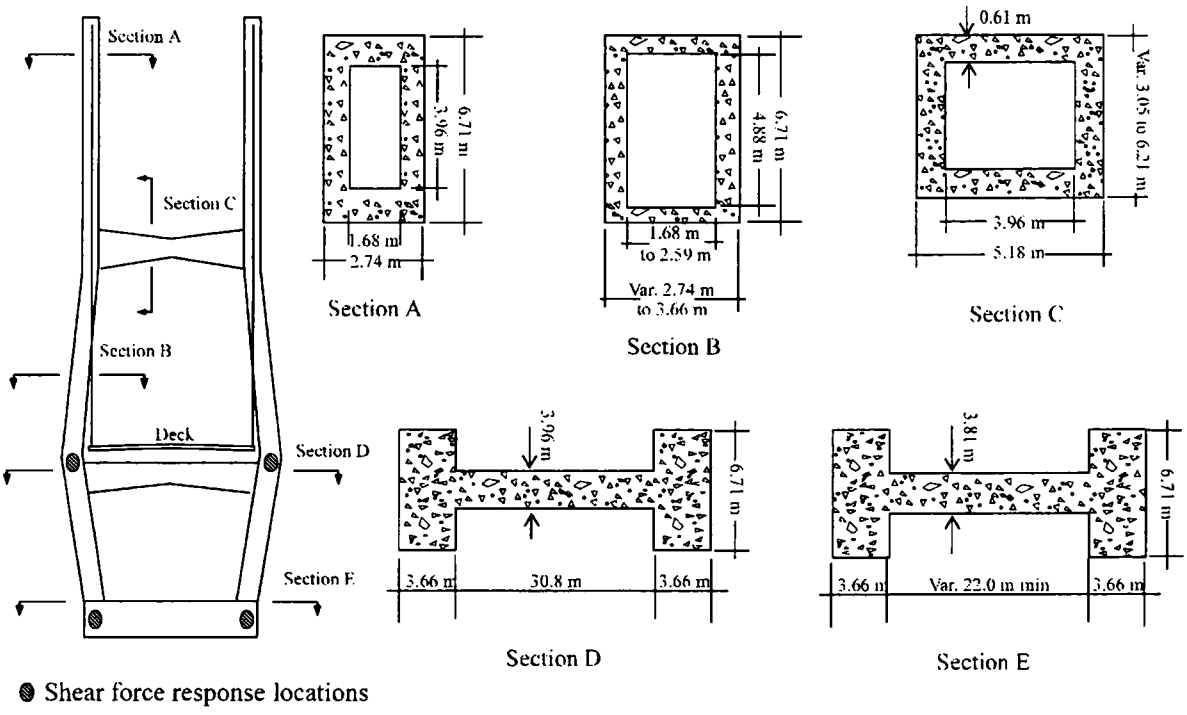

Figure C-2. Cross sections of the towers

C.2 Evaluation Model

A linear evaluation model is used in this benchmark study. However, the stiffness matrices used in this linear model are those of the structure determined through a nonlinear static analysis corresponding to the deformed state of the bridge with dead loads **(Wilson and Gravelle, 1991)**. Cable-stayed bridge exhibit nonlinear behavior due to variations of the catenary shape of the inclined cables, cable tensions that induced compression force in the deck and towers, and large displacements **(Caicedo et al., 2002)**. A nonlinear static analysis was performed using the commercial finite element program ABAQUS® **(1998)**, giving the model tangent stiffness matrix at the (deformed) equilibrium position, and the element mass and stiffness matrices are output to MATLAB® **(Mathworks, 1997a)** for assembly.

The deck was modeled using the method described by Wilson and Gravelle **(1991)**. In this approach, the deck is modeled as a central beam (the spine) which has no mass. Lumped masses are employed to model the mass of the deck, which are connected to the spine using rigid links **(Figure C-3)**. The masses are included to more realistically model the torsional response of the deck to lateral loads, and have been shown to be important in the modeling of this structure **(Caicedo et al., 2000)**.

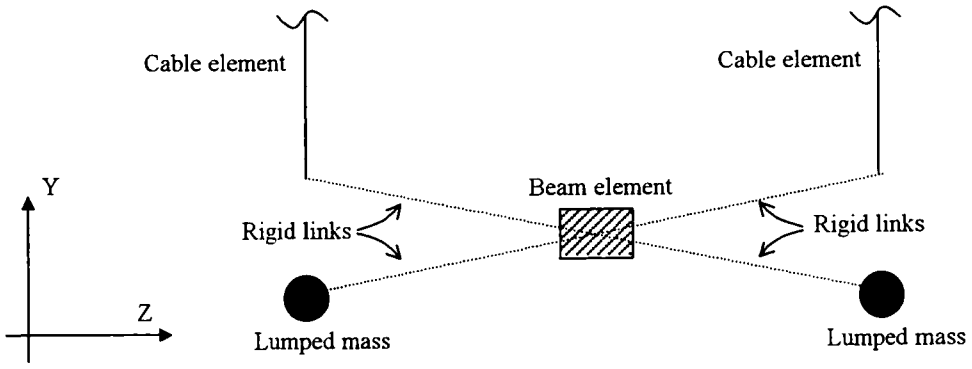

Figure C-3. Finite element modeling of the cross section of the deck

Because the mass moment of inertia of the main deck is different than the one induced by the lumped masses, it is necessary to make corrections to those quantities. In the calculation, the correction consists of finding the difference between the mass moment of inertia of the lumped masses and that of the actual deck section's mass moment of inertia.

This difference in the mass moment of inertia is added to the node at the center of the deck to achieve the correct value of mass moment of inertia in the sectional model.

The model resulting from the finite element formulation has a large number of degrees of freedom (909 DOF) and high frequency dynamics. Thus, some assumptions are made regarding the behavior of the bridge to make the model more manageable for dynamic simulation while retaining the fundamental behavior of the bridge. Application of the DOF reduction to the full model of the bridge resulted in 419 DOF reduced order model. The first 100 natural frequencies of the reduced model were compared and are in good agreement with those of the 909 DOF structure **(Caicedo et al., 2002)**.

An alternate model is also developed to evaluate the robust performance of the proposed control designs. To develop the alternate model, the effects of snow loads on the model are considered. Snow with a mass per length of 97.7 kg/m^2 is added to the deck, and its effect perturbs the mass matrix of the model **(Caicedo et al., 2002)**. This amount increases the mass of the bridge by approximately 3.5%. The maximum variation in the frequencies is 4.8%. The model is to be used to investigate the robustness of the control system with respect to the uncertainties in mass.

The linear model of the bridge system is simulated using a version of the analysis tool developed by Ohtori and Spencer **(1999)** for linear systems. This tool allows the user to implement the compiled C code from within the MATLAB® **(Mathworks, 1997a)** environment through SIMULINK® **(Mathworks, 1997b)** block to simulate the responses of a seismically excited structural system. This tool solved the incremental equations of motion using the Newmark-β method in combination with the pseudo force method. The program has been validated through a comparison with a commercial structural analysis program.

A representative sample of the mode shapes is shown in **Figure C-4**. This mode shape is for the model where connections between the deck and towers is rigid during large earthquake.

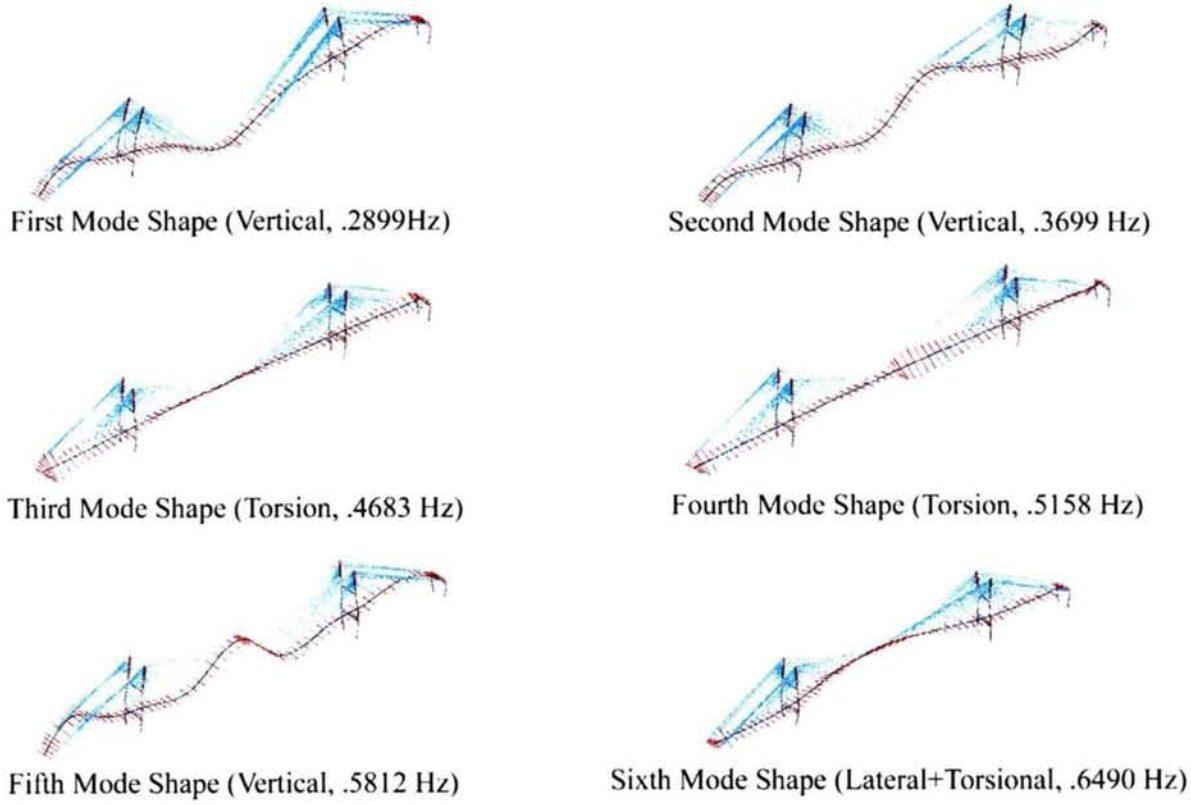

Figure C-4. Representative mode shapes of the bridge evaluation model

C.3 Control Design Problem Statement

As stated previously, the designer/researcher must define the sensors, devices, and algorithms to be used in his/her control strategy. These must be defined in specific forms to properly interface with the benchmark bridge. The sensors and control devices interface with the bridge model through measurement and connection outputs. The information can be inserted into the input/output file in terms of the node numbers.

Figure C-5 provides the SIMULINK® model used for evaluation of the proposed control strategies. The simulation consists of: 1) excitation sources, 2) bridge model, and 3) control model that includes sensors, controller and converters, and control devices.

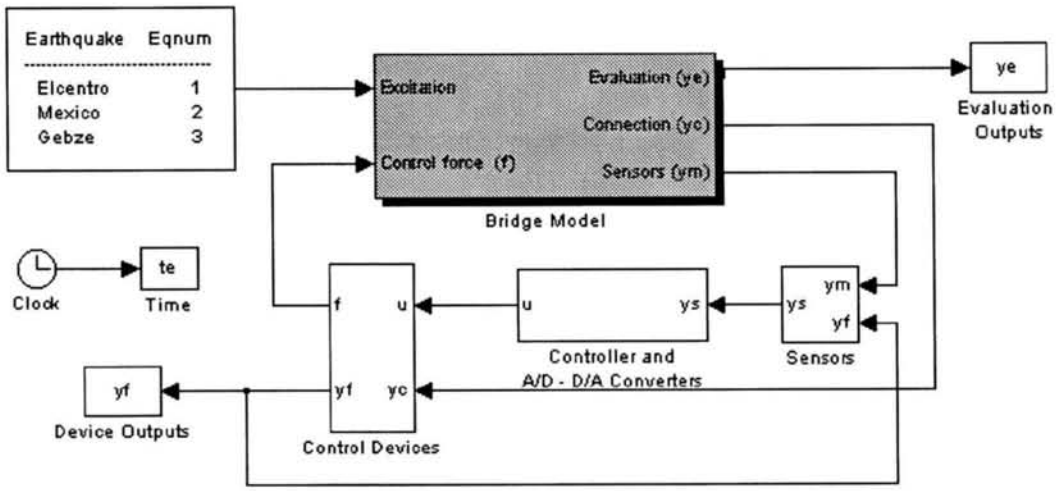

Figure C-5. SIMULINK model for benchmark cable-stayed bridge problem

A MATLAB®-based graphical user interface (GUI) tool has been developed to aid the researcher/designer in generating the input/output information for the evaluation model **(Dyke et al., 2000; Caicedo et al., 2002)**. The graphical user interface allows the user to select the node numbers defining the evaluation outputs, the connection outputs, and the measured outputs for use in each control strategy **(Figure C-6)**. The location of the control devices may also be specified within the GUI. Once the control system setup is specified, the user may choose to generate the evaluation model from within the GUI or from the MATLAB® command window directly.

To consider multi-support excitations, the prescribed ground motion is assumed to be identical at each support, although it is not simultaneous. Bent/pier1 is assumed to experience a specified ground motion, and the motion at the other three supports is delayed based on the distance between adjacent supports and the speed of the L-wave of a typical earthquake (3 km/sec) **(Caicedo et al., 2002)**. For each control design, the evaluation criteria should be evaluated for each specified excitation case: Case A) an incidence angle of 15° with arrival times of 0.00, 0.05, 0.16, and 0.20 seconds for bent/pier1, pier2, pier3, and pier4, respectively; and Case B) an incidence angle of 45° with arrival times of 0.00, 0.03, 0.12, and 0.15 seconds for bent/pier1, pier2, pier3, and pier4, respectively. The incidence angle is defined between the longitudinal direction of the bridge and the N-S wave of the earthquake. Researchers/designers may evaluate their control designs for additional incidence angles by modifying the input file.

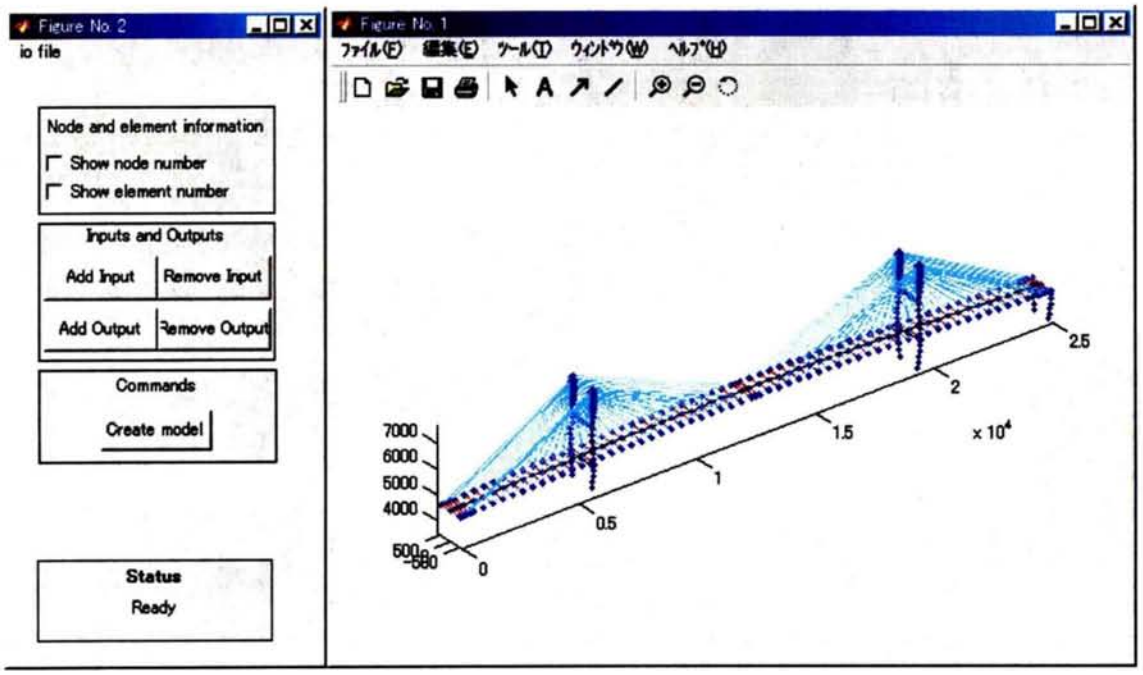

Figure C-6. Graphical User Interface (GUI)
for selecting sensors and control device locations

Appendix D

Data and Results of the Benchmark Cable-stayed Bridge

Chapter 5 has shown the efficacy of pseudo negative stiffness damper in reducing the responses of the benchmark cable-stayed bridges. More detail about the supporting data and the results are shown in this appendix.

D.1 Supporting Data

The supporting data are in MATLAB® and SIMULINK® program to apply the pseudo negative stiffness damper for the benchmark cable-stayed bridge. The original SIMULINK® block diagram provided in (**Dyke et al., 2000** and **Caicedo et al., 2002**) shown in **Figure D-1** has been modified by the author so that it can employee pseudo negative stiffness control (**Figure D-2**). As shown in the figure, the sample active control forces has been terminated in order that pseudo negative stiffness control force and additional elastic bearing forces can be inserted into the structure.

The first MATLAB® program, called "smp_io.m", specifies the locations of sensors, devices, and evaluation outputs that will be read by the SIMULINK® block diagrams. However, as the program has included displacement sensors model at the deck-tower connections, no further modification was done for this program file. The device connection models are also available between deck and towers, although there are more device connections at bent/pier1 and pier4. Evaluation outputs also needs no modification.

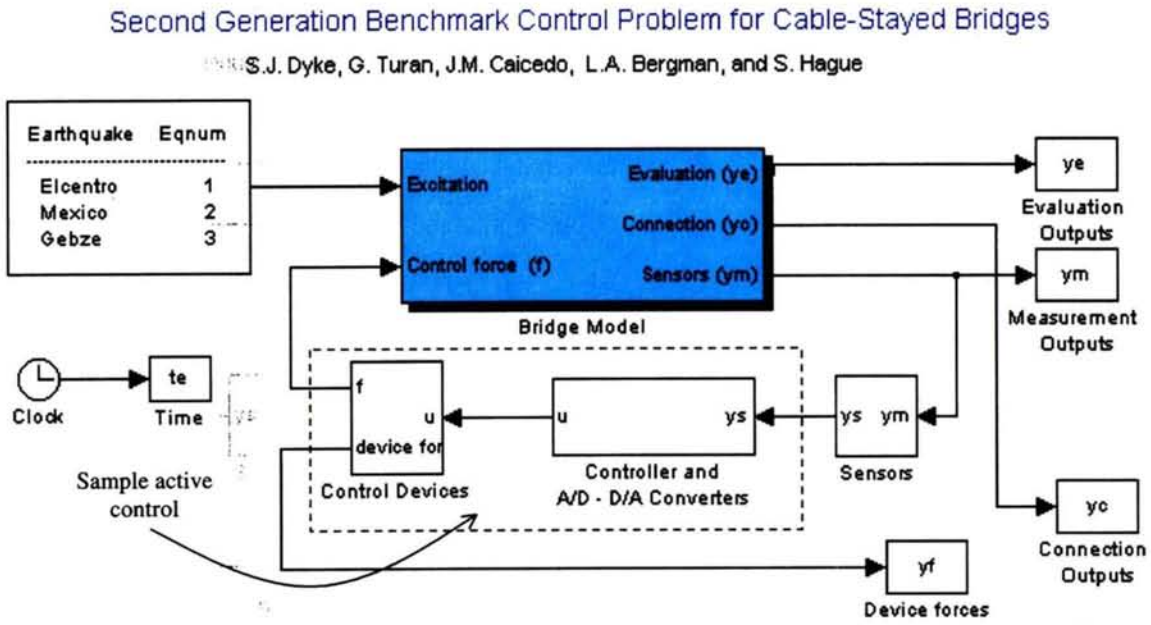

Figure D-1. Original SIMULINK block diagram in the benchmark problem with sample active control

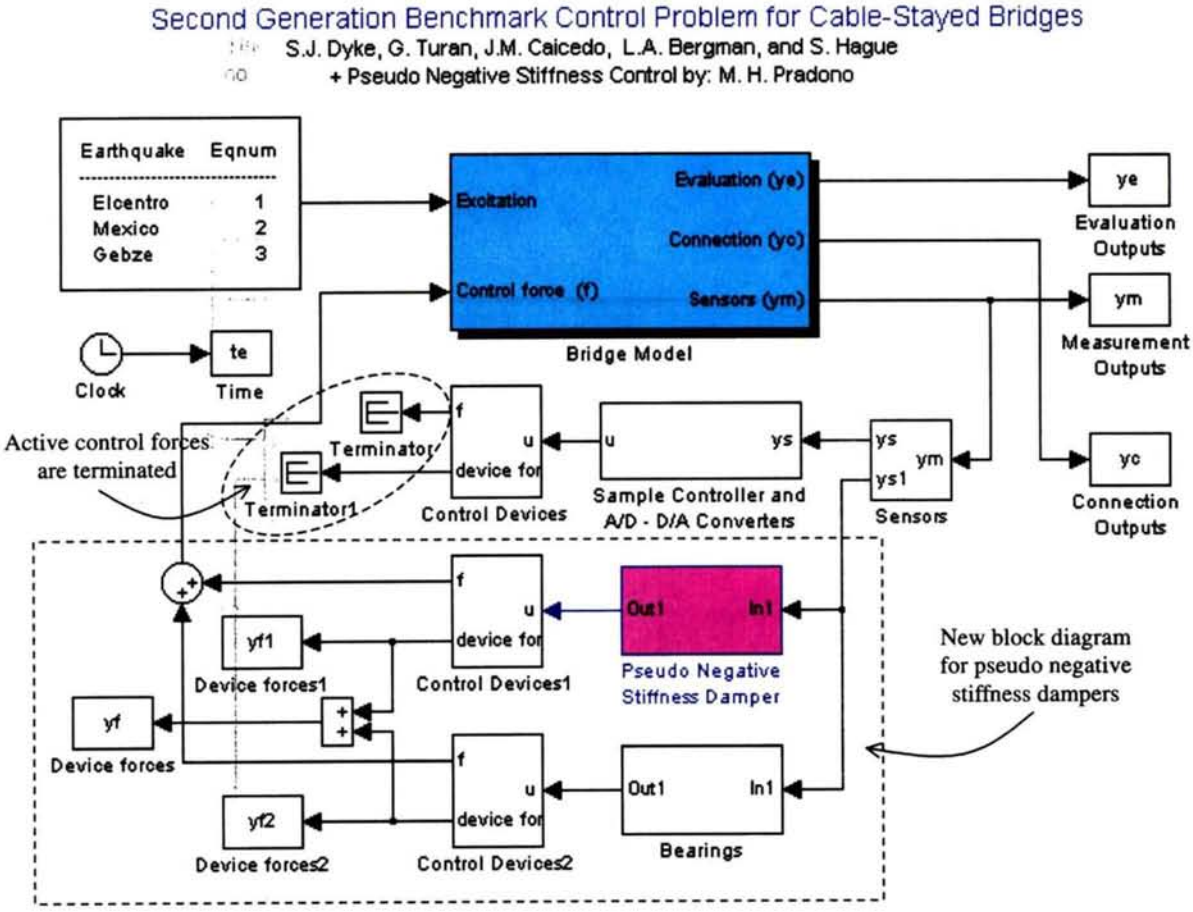

Figure D-2. Modified SIMULINK block diagram for application of pseudo negative stiffness damper

The block "Pseudo Negative Stiffness Damper" in **Figure D-2** contains blocks that are shown in **Figure D-3**. The input "In1" is the relative displacement (u_{dev}) between the deck and the tower at each device locations (shown in **Figure D-4**). The displacement is then differentiated to get relative velocity between the deck and the tower ($\dot{u}_{dev}$). After that, the procedure for manipulating these data to produce negative stiffness hysteretic loop (f_{Dc}) is shown in **Figure D-3**.

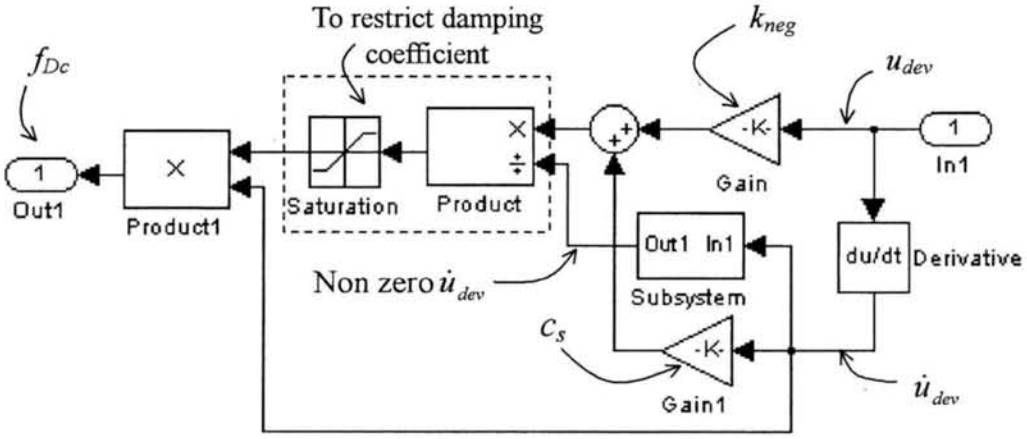

Figure D-3. Pseudo negative stiffness control in SIMULINK® diagram

Figure D-4 shows the typical device layout at the tower. Four viscous dampers are located between each of the following pairs of nodes on piers 2 and 3: (84, 313), (151,314), (118, 428), (185, 429). The dampers have a capacity of 2000 kN.

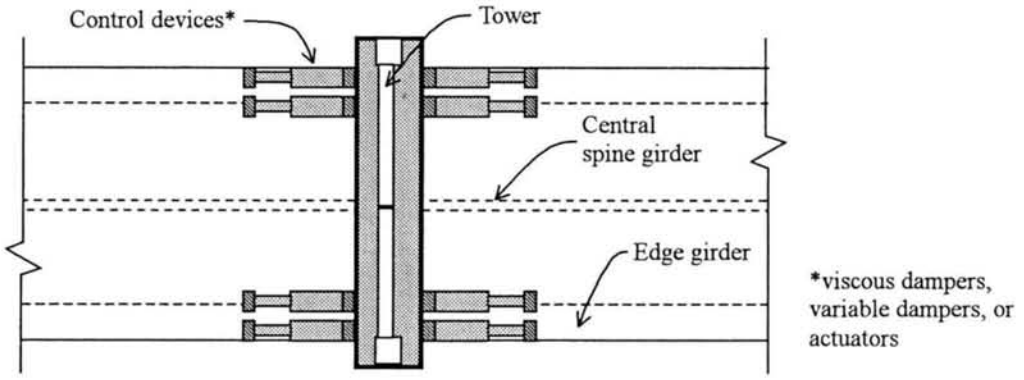

Figure D-4. Schematic of device implementation

D.2 Results

The results are about the hysteretic behavior of the variable dampers located at pier2 and pier3, to study the effect of incidence angle and multi-support excitations on the hysteretic behavior of dampers. Incidence angle is the angle between the ground motion direction and the longitudinal axis of the structure (**Figure D-5**).

The prescribed ground motion is assumed to be identical at each support, although it is not simultaneous. Bent1 is assumed to experience a specified ground motion, and the motion at the other three supports is delayed based on the distance between adjacent supports and the speed of the L-wave of a typical earthquake (3 km/sec). Incidence angle of 45° gives arrival times of 0, 0.03, 0.12, and 0.15 seconds at bent1, pier2, pier3, and pier4, respectively. Whereas 15° incidence angle gives arrival times of 0, 0.05, 0.16, and 0.20 seconds. Results are given for the device hysteretic loop at incidence angle of 45° (**Figures D-6** up to **D-17**). Then, for a different angle (15°), hysteretic loop for the devices are shown in **Figures D-18** up to **D-22**).

It is clear from the figures that the hysteretic loops are not identical in all locations because of multi-support excitation and incidence angle effects. However, these effects have insignificant influence on the effectiveness of pseudo negative stiffness dampers.

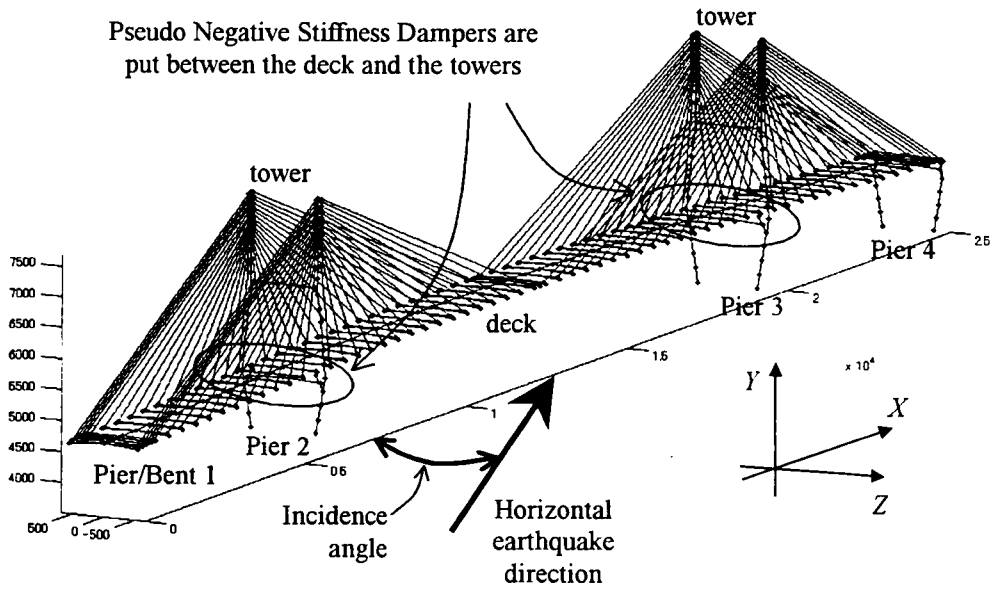

Figure D-5. Definition of incidence angle on benchmark bridge

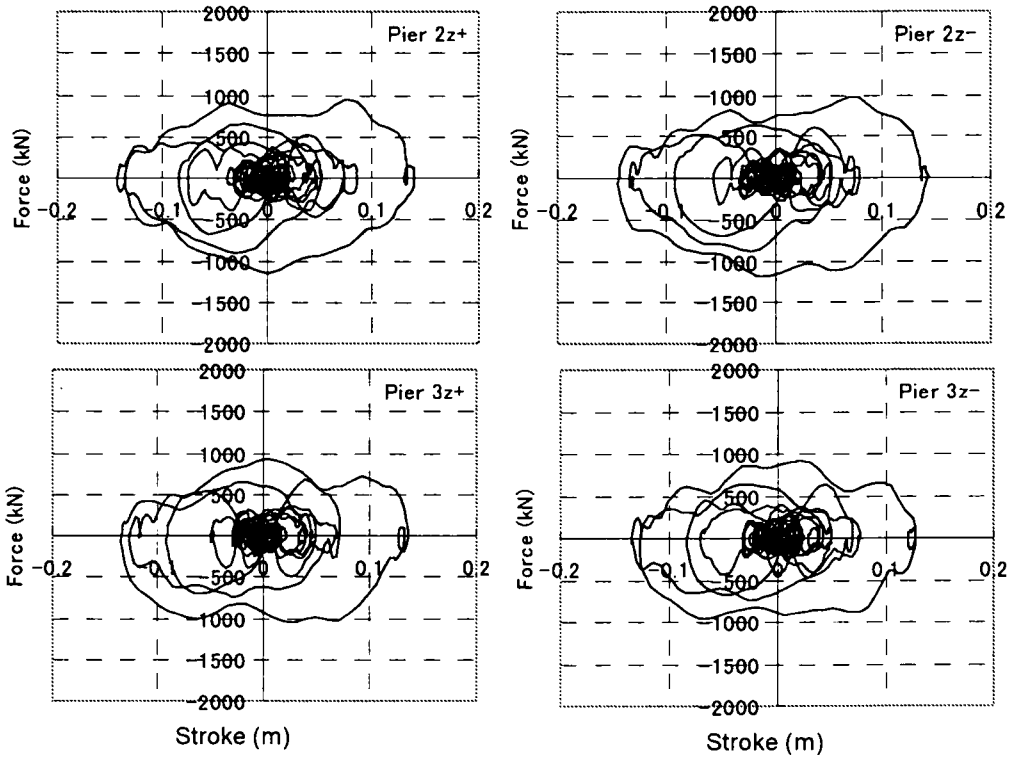

Figure D-6. Viscous damper hysteretic loop at pier2 and pier3
(El Centro, incidence angle 45°)

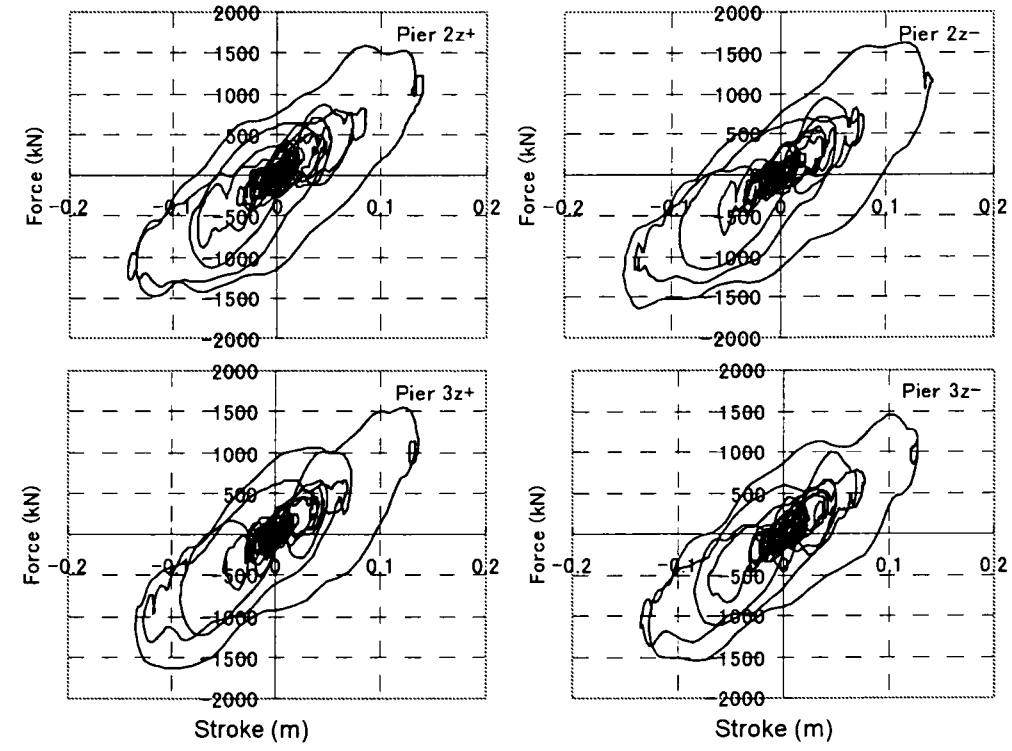

Figure D-7. Viscous damper plus bearing hysteretic loop at pier2 and pier3
(El Centro, incidence angle 45°)

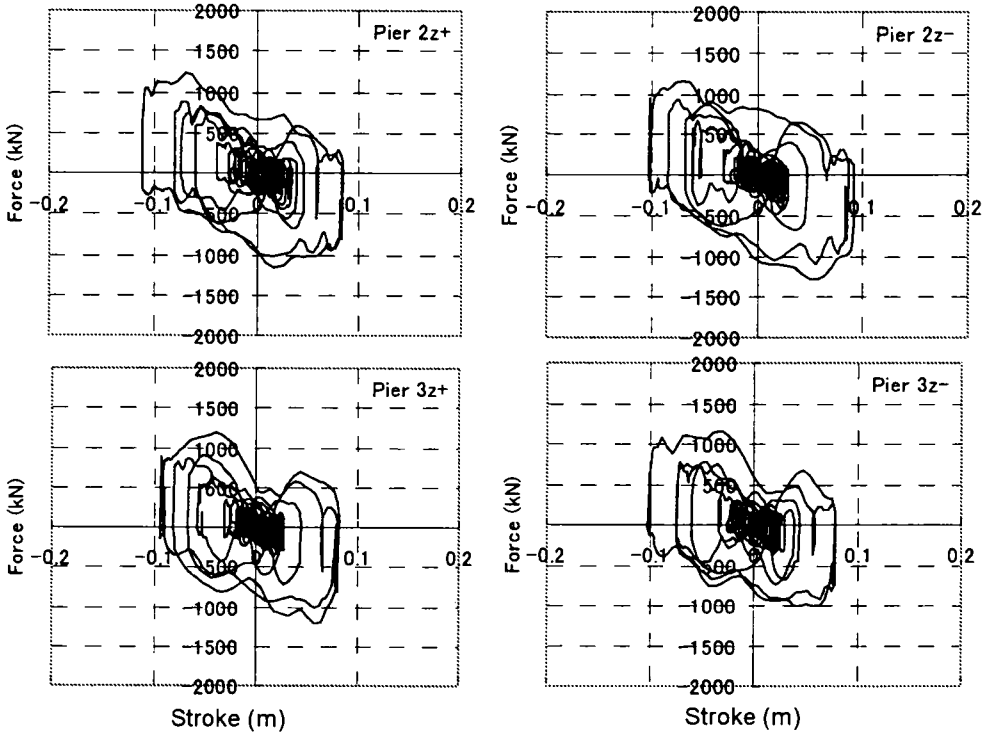

Figure D-8. PNS damper hysteretic loop at pier2 and pier3
(El Centro, incidence angle 45°)

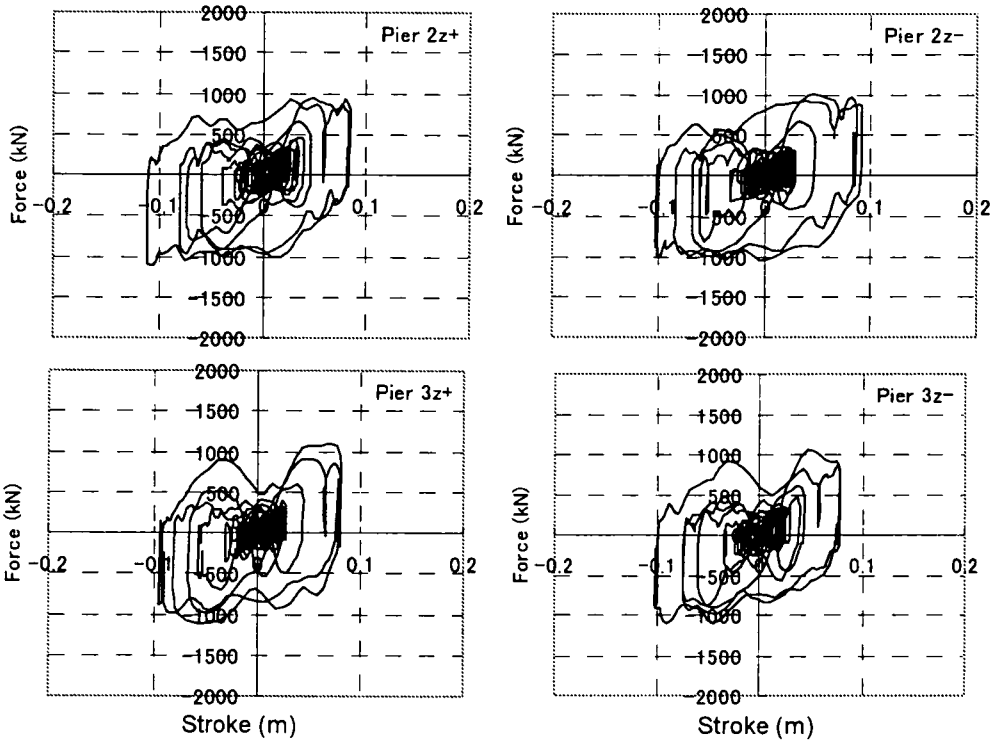

Figure D-9. PNS damper plus bearing hysteretic loop at pier2 and pier3
(El Centro, incidence angle 45°)

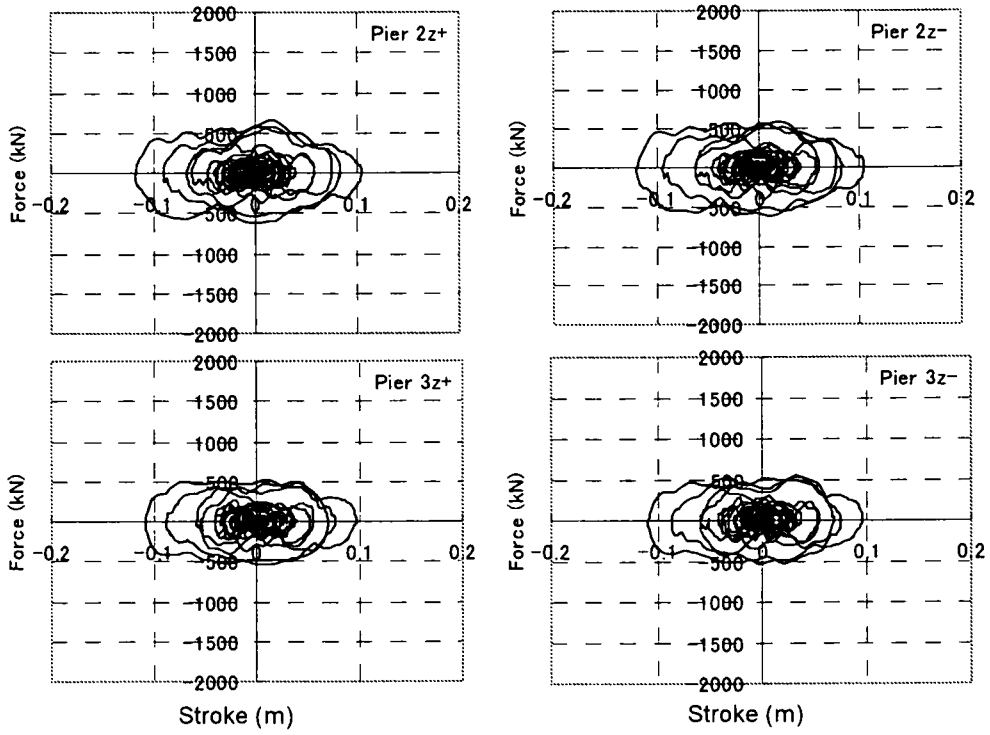

Figure D-10. Viscous damper hysteretic loop at pier2 and pier3 (Mexico, incidence angle 45°)

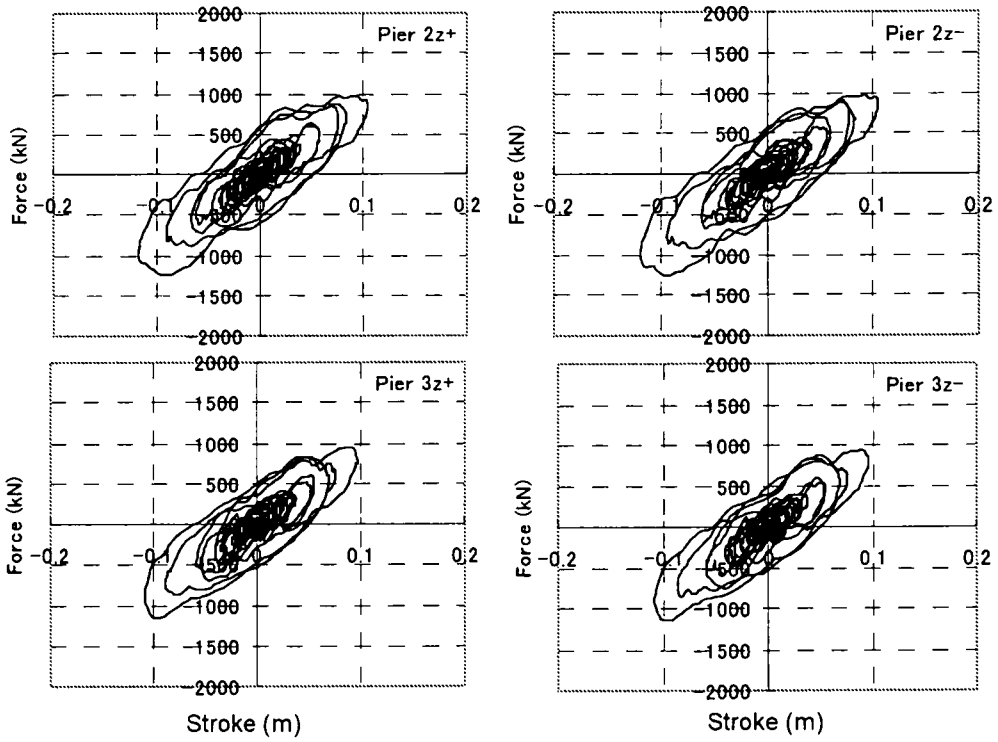

Figure D-11. Viscous damper plus bearing hysteretic loop at pier2 and pier3 (Mexico, incidence angle 45°)

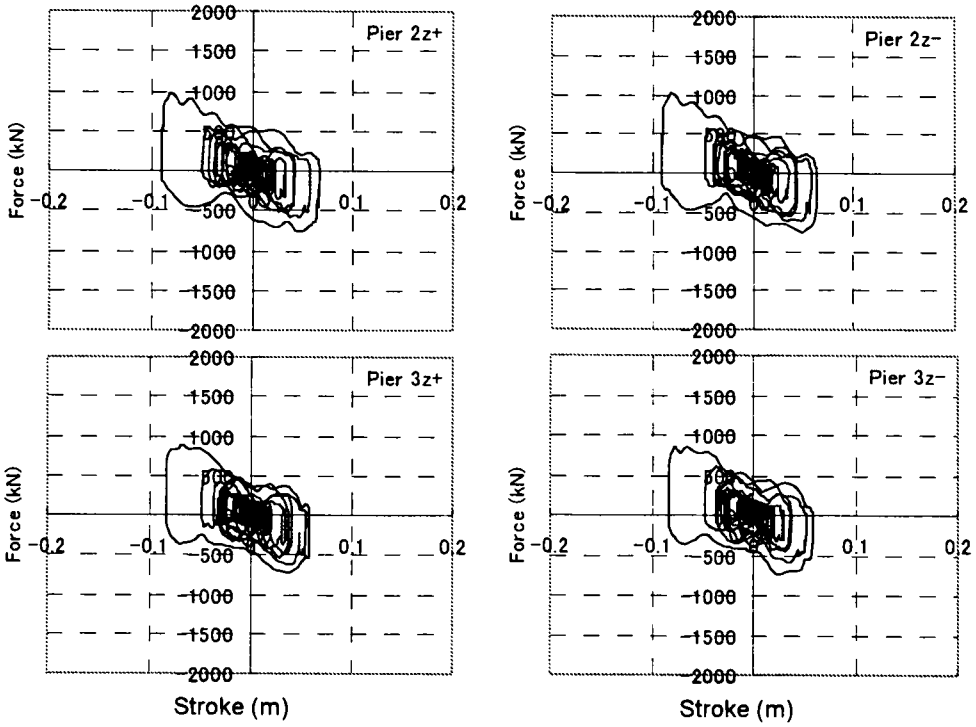

Figure D-12. PNS damper hysteretic loop at pier2 and pier3
(Mexico, incidence angle 45°)

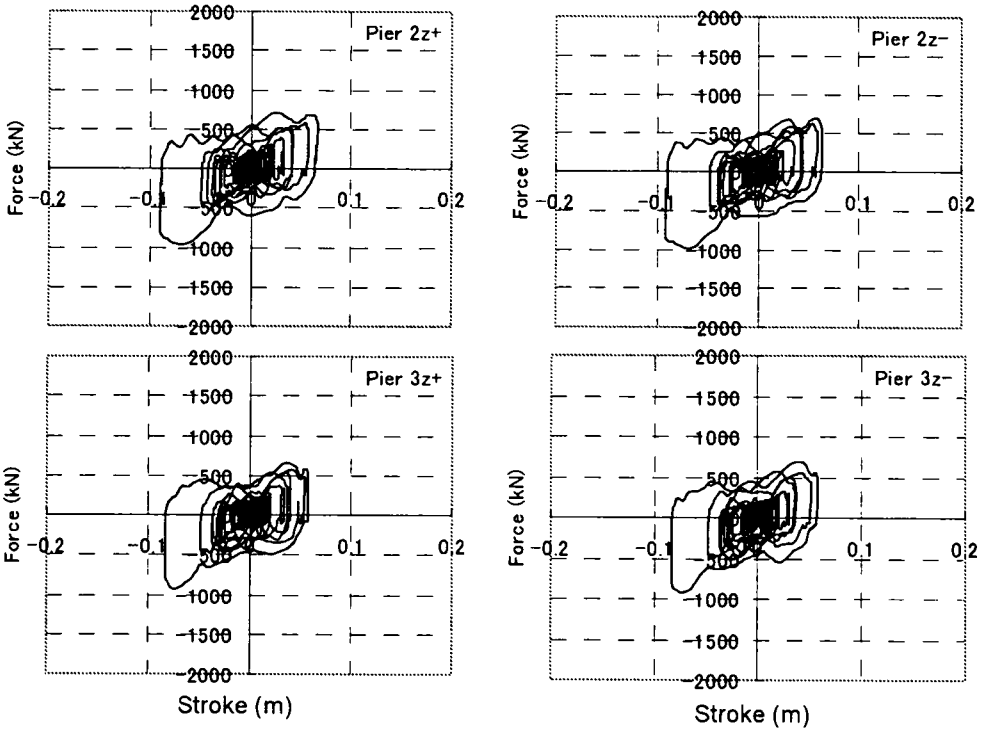

Figure D-13. PNS damper plus bearing hysteretic loop at pier2 and pier3
(Mexico, incidence angle 45°)

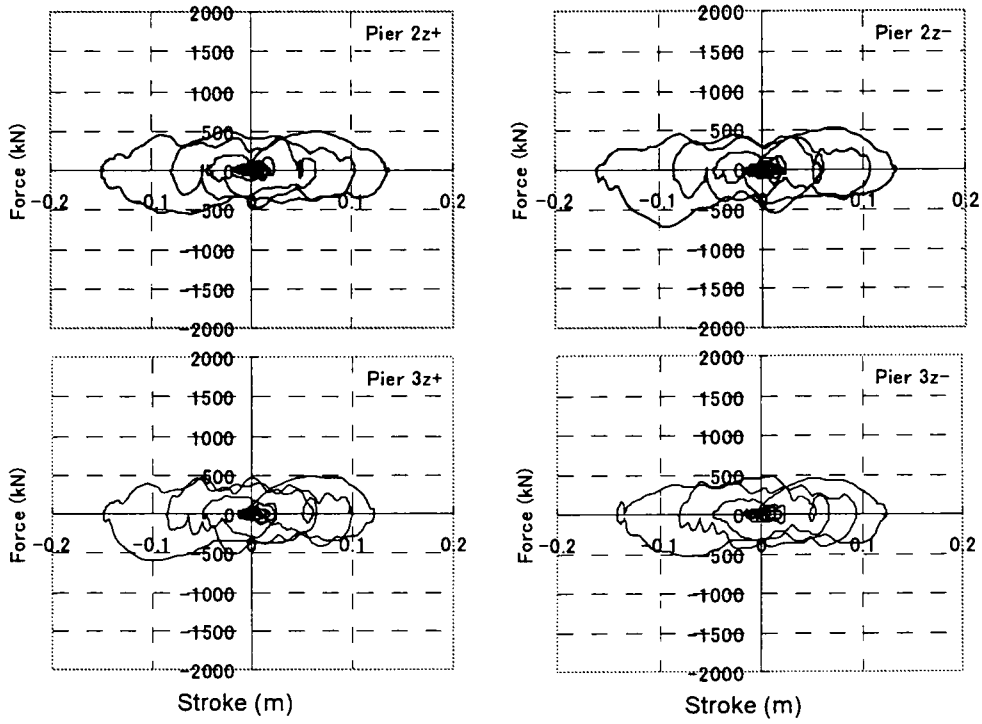

Figure D-14. Viscous damper hysteretic loop at pier2 and pier3
(Gebze, incidence angle 45°)

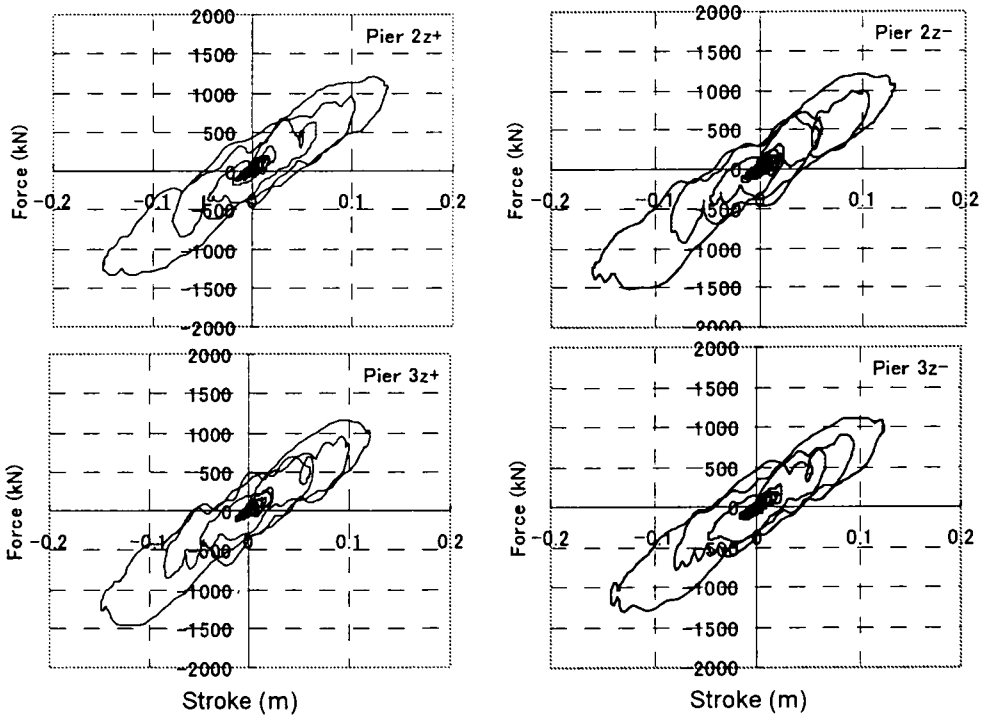

Figure D-15. Linear damper plus bearing hysteretic loop at pier2 and pier3
(Gebze, incidence angle 45°)

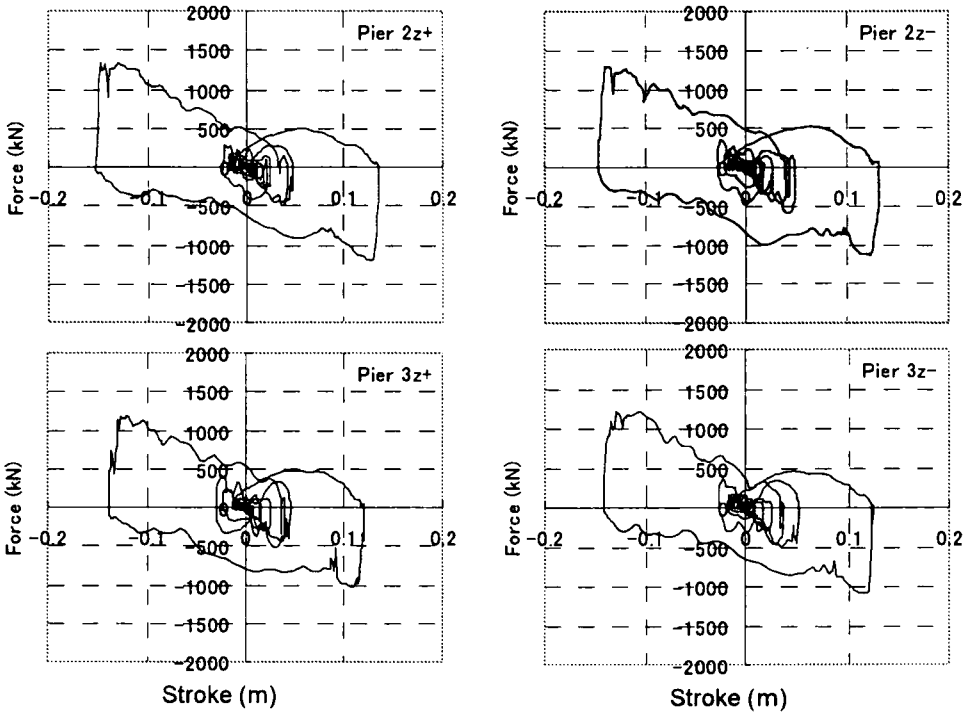

Figure D-16. PNS damper hysteretic loop at pier2 and pier3
(Gebze, incidence angle 45°)

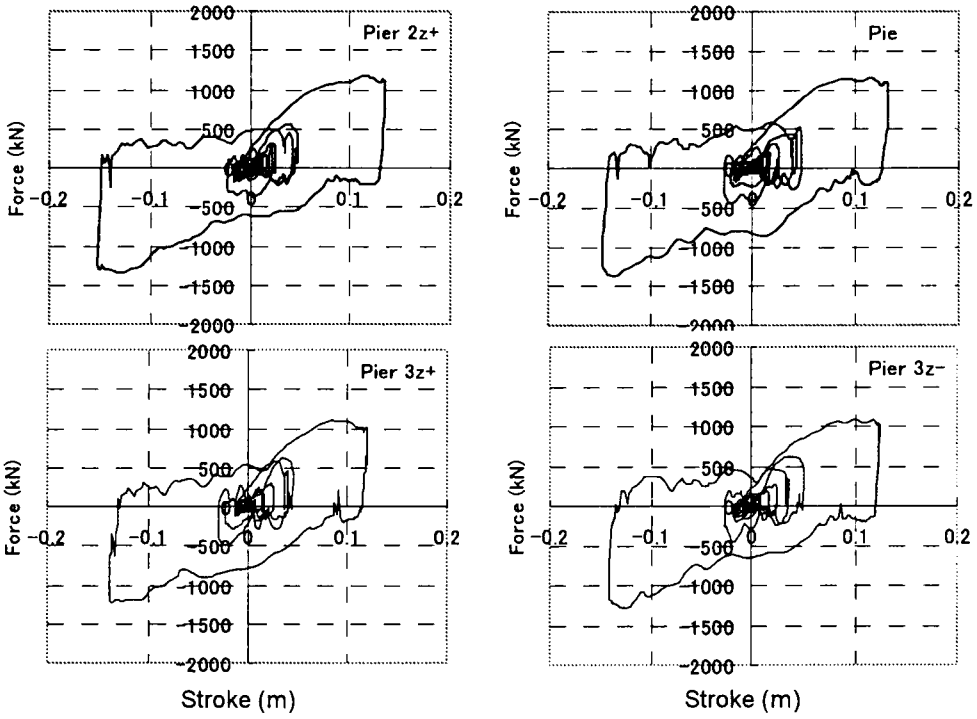

Figure D-17. PNS damper plus bearing hysteretic loop at pier2 and pier3
(Gebze, incidence angle 45°)

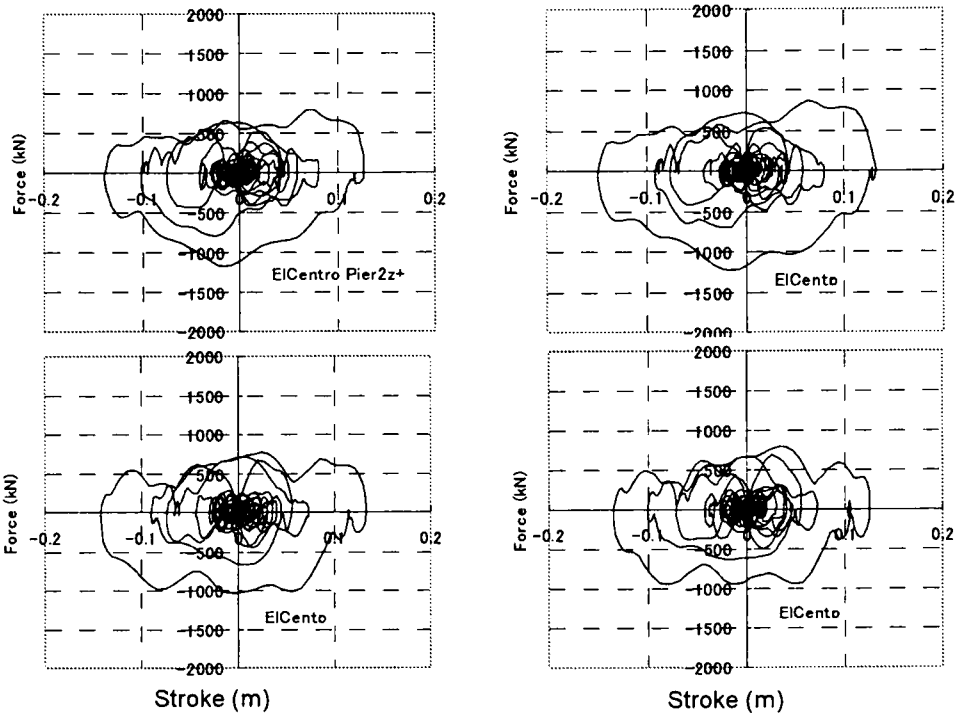

Figure D-18. Viscous damper hysteretic loop at pier2 and pier3
(El Centro, incidence angle 15°)

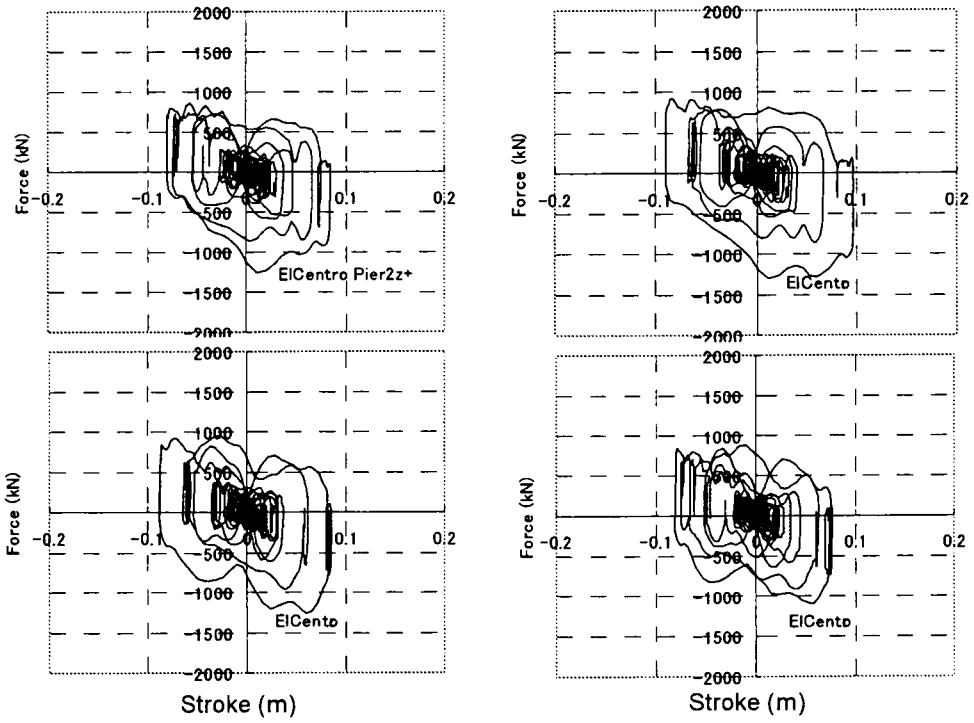

Figure D-19. PNS damper hysteretic loop at pier2 and pier3
(El Centro, incidence angle 15°)

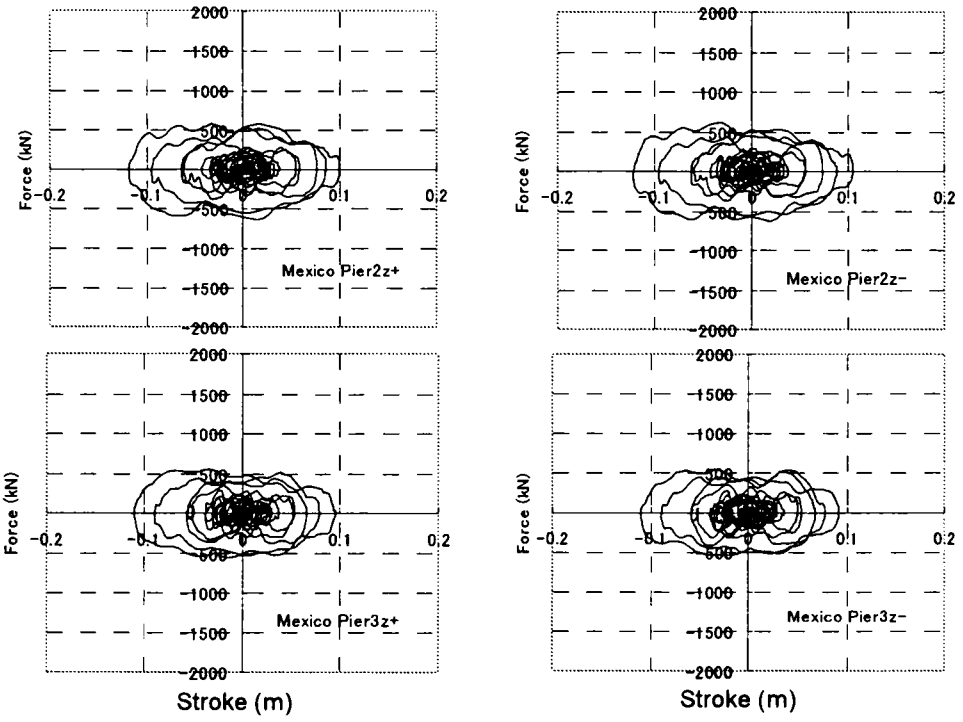

Figure D-20. Viscous damper hysteretic loop at pier2 and pier3
(Mexico, incidence angle 15°)

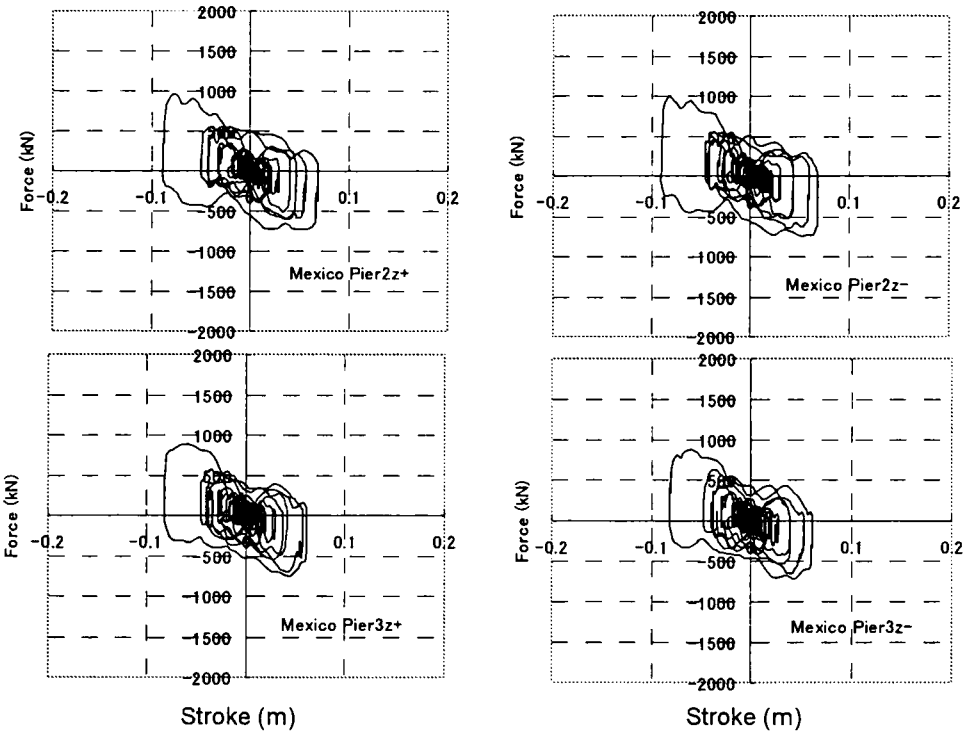

Figure D-21. PNS damper hysteretic loop at pier2 and pier3
(Mexico, incidence angle 15°)

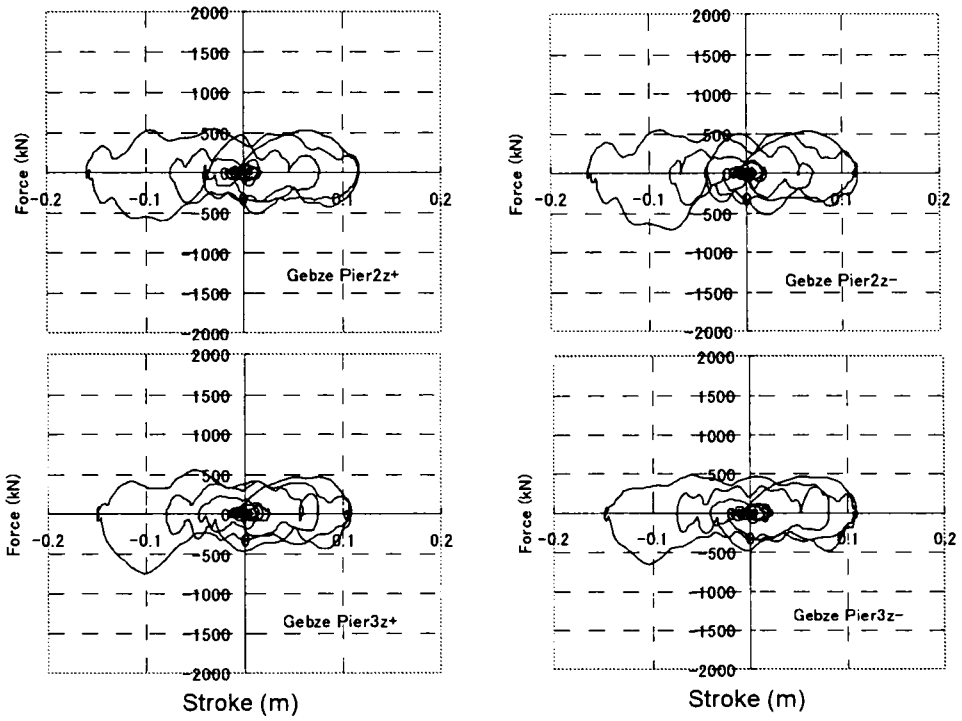

Figure D-22. Viscous damper hysteretic loop at pier2 and pier3
(Gebze, incidence angle 15°)

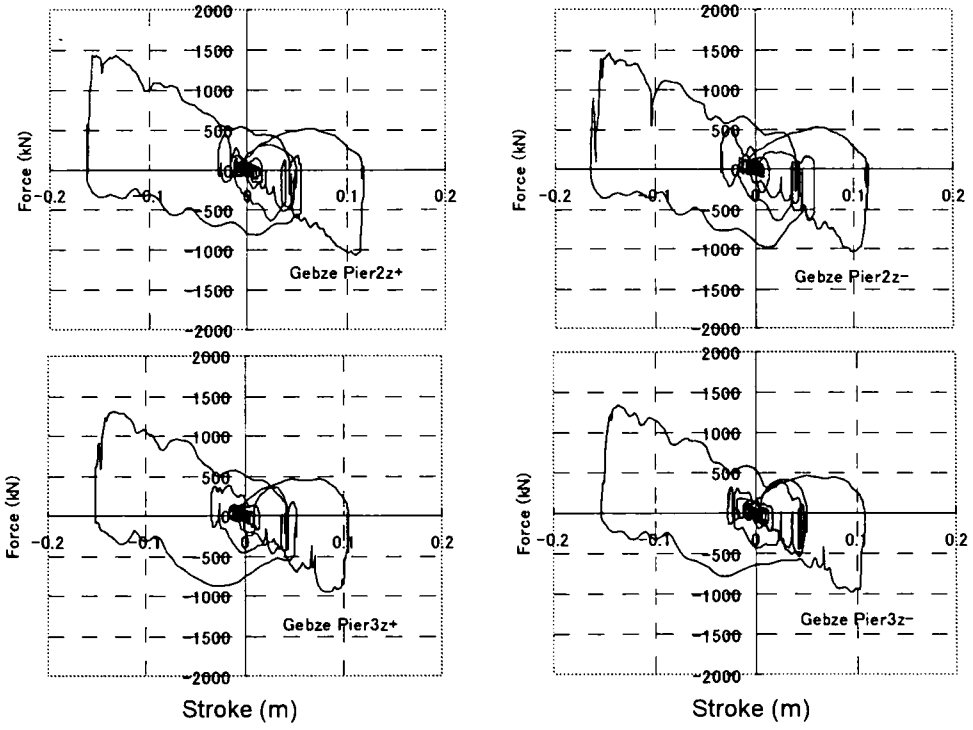

Figure D-23. PNS damper hysteretic loop at pier2 and pier3
(Gebze, incidence angle 15°)

Appendix E

Pseudo Negative Stiffness Control using Variable Damping Device

This appendix discusses about generating negative stiffness hysteretic loop using variable orifice oil damper under general excitation.

E.1 Performance Test

Performance test were conducted on a variable orifice oil damper with constant opening ratio subjected to sinusoidal input **(Iemura et al., 2001; Iemura et al., 2002)**. The tests are combination of opening ratio and frequency.

The specification of variable damper is shown in **Table E-1**. The system configuration of the variable damper and the photograph are shown in **Figure E-1**. It is a semi-active hydraulic-type damper which consists of three parts. (i) Dynamic damper part comprises a cylinder in which oil is installed, double rod to apply forces, by-pass pipe which contains flow control valve, and accumulator which keeps line pressure in by-pass pipe constant. Opening ratio of the flow control valve can be changed by electric power based on signal from control PC. By changing it, quantity of flow through valve can be adjusted and pressure loss is varied. This series of mechanism enables to generate the demanded force as close as possible. Because opening ratio can be changed in real time, this variable damper is regarded as real time control device. (ii) Controller part calculates the demanded force at the damper position at every time step on the basis of a control algorithm using the several system responses. It sends signal of the opening ratio of flow

control valve to dynamic damper part. (iii) Hydraulic unit part is used when oil will be put into cylinder.

Table E-1. Specification of Variable Damper

Rated load	Dynamic ± 50 kN
Maximum displacement	± 50 mm
Maximum velocity	20 kine
Control system	Electric hydraulic control system
Line pressure	210 kgf/cm^2
Servo valve	Direct acting type
Range of damping coefficient	200 – 800 kN.sec/m

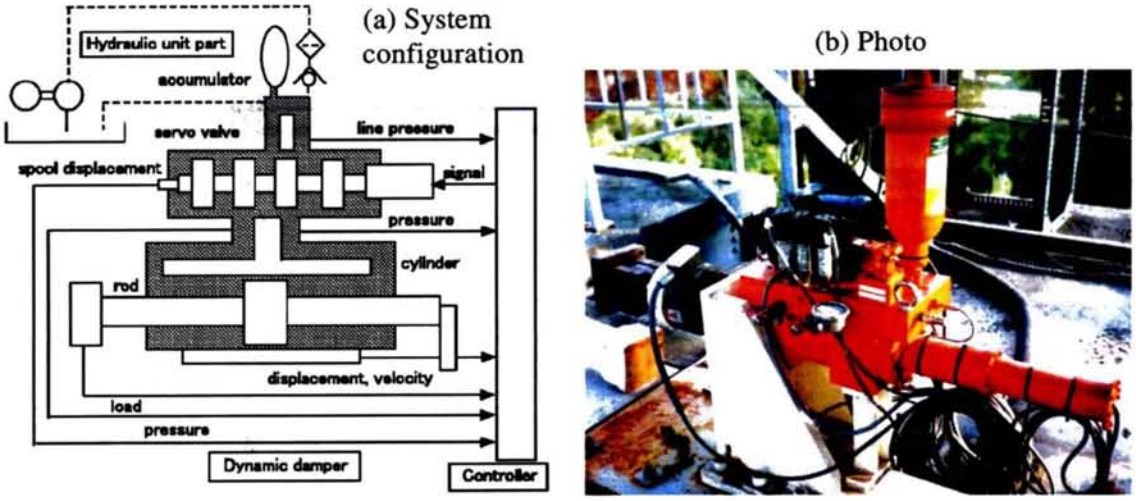

Figure E-1. Variable damping device

Seven response quantities of the variable damper are recorded. Relative displacement and relative velocity are measured by displacement sensor inside the damper. Damping force is measured by the load cell installed on the edge of the rod. Other measured responses are spool displacement to calculate the opening ratio, line pressure, and the pressures inside left and right parts of the cylinder.

According to the test results, in the case of same opening ratio, almost all the relationships between relative velocity and damping force show almost the same trace regardless of input frequency, though the scales are of course different. Some of the relationships between relative velocity $\dot{u}$ (or v_r in the figure) and damping force f_D in the test input 1.8 Hz are shown in **Figure E-2**.

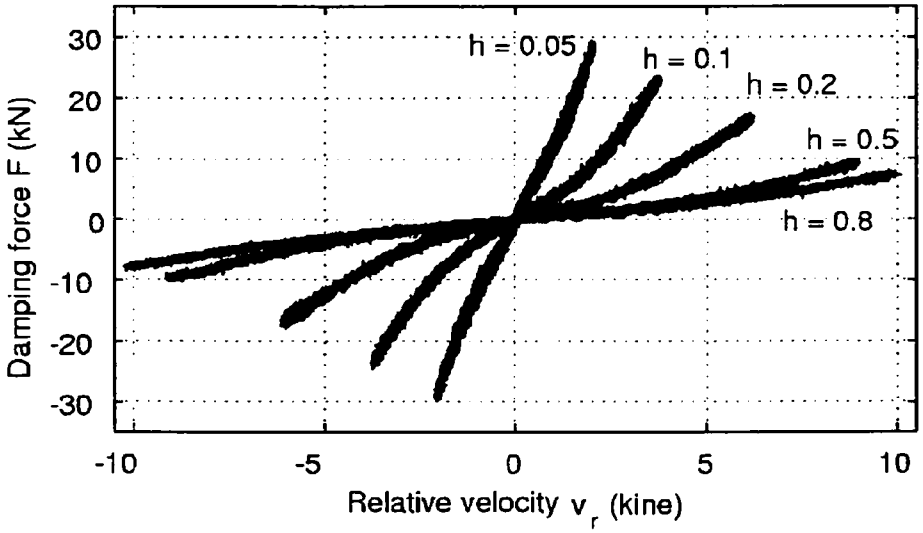

Figure E-2. Relationships between relative velocity and damping force in performance test of input 1.8 Hz

From the figure, it is considered that damping force of the variable damper is almost dependent on the square of relative velocity and that it is possible to neglect stiffness element in modeling the damper. The formula for damping device in general is as follow.

$$F(h,\dot{u}) = \mathrm{sgn}(\dot{u})\left[f(h)\dot{u}^2 + g(h)\right] \tag{E-1}$$

Where F, $\dot{u}$, and h are damping force, relative velocity, and opening ratio, respectively. Friction element is considered as $g(h)$. The function $f(h)$ and $g(h)$ are decided on the basis of the regression analysis of the test result with least-squares method. The results are shown in **Equation (E-2)**. **Figure E-3** shows that the regression curve for $f(h)$ almost corresponds to the test results of it.

$$f(h) = \frac{159.232}{h^2} + 307.2 \quad (\mathrm{kN.sec^2/m^2}), \qquad g(h) = 0.6 \quad (\mathrm{kN}) \tag{E-2}$$

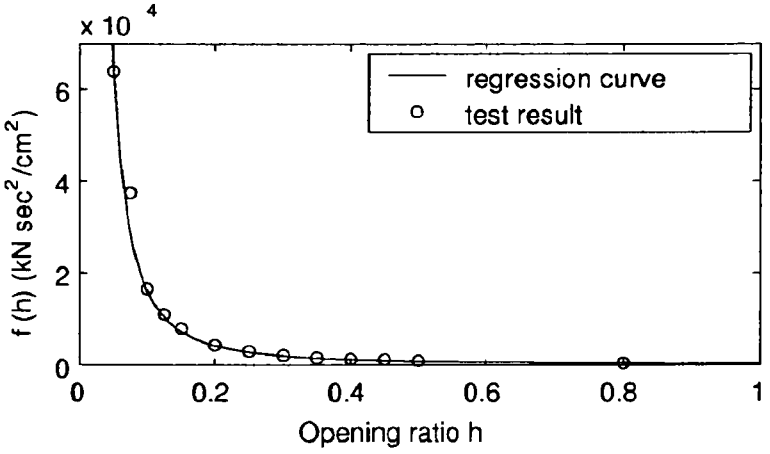

Figure E-3. Regression curve of the coefficient of the square of relative velocity

E.2 Damper Force under General Excitation

From the above results, the relationship among damping force f_D (unit kN), orifice opening ratio h, and piston velocity $\dot{u}$ (unit m/s) can be rewritten as in **Equation (E-1)**.

$$f_D = \mathrm{sgn}(\dot{u})\left\{\left(\frac{159.232}{h^2}+307.2\right)\dot{u}^2+0.6\right\}\ (\mathrm{kN}) \tag{E-1}$$

Relative displacement u and relative velocity $\dot{u}$ are measured by displacement sensor inside the damper. Controller part then calculates demand force F_d at damper position at every time step on the basis of **Equation (E-2)** using measured relative displacement u and relative velocity $\dot{u}$,

$$F_d = K_d u + C_d \dot{u} \tag{E-2}$$

where K_d is an arbitrary negative value (representing negative stiffness) and C_d is an arbitrary positive value (representing damping coefficient). How to choose these numbers is a subject discussed in **Chapter 3**.

Therefore, when the demand force is as shown above, opening ratio h that produces damping force f_D very close to the demand force F_d can then be calculated.

$$h \approx \sqrt{\frac{159.232}{\frac{\left(\frac{F_d}{\mathrm{sgn}(\dot{u})}-0.6\right)}{\dot{u}^2}-307.2}} \tag{E-3}$$

Opening ratio of the flow control valve can then be altered in a real time by electric power based on signal from the controller. However, opening ratio h can only be applied in the range of $h_{\min}$ (0.05) and $h_{\max}$ (0.80) because of the limitation of the oil damper.